Material and Surface Properties of Bio-Inspired Polydopamine and its Modified Polypyrrole Functional Nanocomposites

by

Wei Zhang

A thesis

presented to the University of Waterloo

in fulfillment of the

thesis requirement for the degree of

Doctor of Philosophy

in

Chemical Engineering

Waterloo, Ontario, Canada, 2015

AUTHOR'S DECLARATION

I hereby declare that this thesis consists of material all of which I authored or co-authored: see Statement of Contributions included in the thesis. This is a true copy of the thesis, including any required final revisions, as accepted by my examiners.

I understand that my thesis may be made electronically available to the public.

STATEMENT OF CONTRIBUTIONS

The research work described in Chapter 3 has been published in *Biomacromolecules*. **2013**, *14*, 394-405.

The research work described in Chapter 4 has been published in *Macromolecular Rapid Communication*. **2014**, *35*, 350-354.

The research work described in Chapter 5 has been published in *Advanced Functional Materials*. **2015**, *25*, 1588-1597.

The research work described in Chapter 6 has been submitted in *Advanced Functional Materials*. **2015**, submitted.

I am the first author of all these journal publications.

Abstract

Inspired by marine mussel adhesives, the dopamine (DA) polymerization process has been introduced as a versatile deposition method to coat almost all kinds of material surfaces and form a nanoscale polydopamine (PDA) thin film. Although the DA polymerization mechanism and the PDA structure have not been fully explored, PDA films have gained great interest for their promising applications, such as anti-corrosion coating, drug delivery, biosensing and nanocomposite functionalization. In this project, we started with the fundamental investigations of the surface, adhesion, friction and cracking properties of PDA thin films. A series of surface characterizations and mechanical tests were performed to reveal the static and dynamic properties of PDA films coated on glass, polydimethylsiloxane (PDMS) and epoxy substrates in both dry and wet conditions. The systematic studies of the PDA film provide insights into its stability, mechanical and adhesive properties; further investigations are focused on the effective transferring of this nano-material to functional devices and biocompatible coatings. To achieve this goal, we combined PDA with polypyrrole (PPy), which is one of the most extensively investigated electrically conductive polymers because of its economic preparation, long-term stability and good biocompatiablity. After being functionalized by PDA, the PPy morphology changed from globular to fibrous; the adhesion between PPy film and glass substrates was enhanced due to the PDA self-adhesion property and the use of proper DA/pyrrole (Py) ratios also improved PPy conductivity. All of these new features significantly improve PPy processability and broaden its potential applications. In order to understand the effect of DA on Py polymerization, we performed a detailed and systematic investigation using three types of bioinspired catechol derivatives simple catechol (CA), *L*-3,4-dihydroxyphenylalanine (DOPA) in addition to the dopamine and 2-pheny-lethylamine (PA) in the synthesis of PPy. These studies provided strong evidence that catechol modification can be applied as a general protocol to functionalize conducting

polymers to overcome their poor water dispersibility and low interfacial adhesion of PPy. Although DA-PPy has shown promise in many biological applications, its conductivity still requires further improvement, especially at higher DA/Py mole ratios. As a result, we developed new synthetic approaches to the preparation of DA-PPy nanostructures, which have both improved electrical conductivity and water dispersibility. Moreover, we explored the suitable application of each as-fabricated nanomaterials depending on the DA/Py reacting mole ratio. In particular, DA-PPy produced using a 0.032 DA/Py mole ratio demonstrated superior capacitance for supercapacitors, DA-PPy obtained from a 0.064 DA/Py mole ratio can be used as co-fillers in the epoxy network to prepare functional composites for electrically conductive adhesives (ECAs), DA-PPy synthesized from a 0.64 DA/Py mole ratio was found to have the impressive capability of absorbing electromagnetic microwaves for electro-magnetic interference (EMI) shielding applications. Due to the synergetic effect of DA modification, conducting polymer DA-PPy exhibit multifunctional and unique properties, which opens a brand new field of nanomaterial syntheses and applications.

Acknowledgements

This research project would not have been possible without the support of the following people: first and foremost I wish to express my gratitude to my supervisor, Prof. Boxin Zhao, who was abundantly helpful and offered invaluable assistance, support and guidance, without his knowledge and assistance this study would not have been successful. Deepest gratitude is also due to the members of my supervisory committee, Prof. XiansheFeng, Prof. Bo Cui, Prof. Mark Pritzker and Prof. Jin Zhang. Special thanks also to all my labmates for their time in helping with my thesis presentation and always being there to answer questions. I also wish to express my gratitude to my family and friends who helped me get through every day with their understanding and endless help.

Dedication

I dedicate this dissertation to my beloved families, especially....

to Dad Youbin Zhang and Mom Kun Tao, for opening my eyes to the world;

to grandparents Renqi Tao and Yongyin Ruan, for instilling the importance of hard work and higher education;

to the family members of Donghong Yao, Yun Tao, and Yuan Yao, for the motivation and encouragement to reach my dreams;

to the family members of Lun Tao, Huilan Wang, and Xinran Tao, for giving me the thirst for new knowledge and the potential to seek it;

to the family members of Zhenfan Zhang, Jing Tao, Lingyun Zhang and Allen Zhang, for the support and care throughout my studies in Canada;

I hope this achievement will complete the dream that you always had for me when I was a child. I am deeply thankful to my families for their love, support, caring, belief, sheer patience and sacrifices. Without them, this thesis would never have been written. I dedicate this thesis to the memory of my families, whose roles in my life were, and remain, immense.

At the end, I will express my great gratitude with my favorite lyrics "**You Raise Me Up**",

When I am down and, oh, my soul, so weary;
When troubles come and my heart burdened be;
Then I am still and wait here in the silence,
Until you come and sit awhile with me.
There is no life - no life without its hunger;
Each restless heart beats so imperfectly;
But when you come and I am filled with wonder,
Sometimes, I think I glimpse eternity.
You raise me up, so I can stand on mountains;
You raise me up to walk on stormy seas;
I am strong when I am on your shoulders;
You raise me up to more than I can be.

Table of Contents

List of Figures

List of Schemes

List of Tables

List of Abbreviations

AAO	Anodic Aluminum Oxide
AFM	Atomic Force Microscopy
APS	Ammonium Persulfate
CA	1,2-dihydroxybenzene or catechol
CNTs	Carbon Nanotubes
CVD	Chemical Vapor Deposition
DA	Dopamine
DA-PPy	Dopamine modified Polypyrrole
DBS	Dodecylbenzenesulfonate
DHI	5,6-dihydroxyindole
DMDES	Dimethyldiethoxysilane
DOPA	*L*-3,4-dihydroxyphenylalanine
DOX	Doxorubicin
ECAs	Electrically Conductive Adhesives
EMI	Electro-Magnetic Interference
EPR	Electron Paramagnetic Resonance
HPLC	High-Performance Liquid Chromatography
IR	Infrared
JKR	Johnson−Kendall−Roberts
MWCNTs	Multiwalled Carbon Nanotubes
NMR	Nuclear magnetic resonance
PA	Phenylethlamine
PDA	Polydopamine
PDMS	Polydimethylsiloxane
PE	Polyethylene
PEG	Poly(ethylene glycol)
PGA	Poly(L-glutamic acid)
PMA	Poly(methacrylic acid)
PPy	Polypyrrole
PVD	Physical Vapor Deposition
Py	Pyrrole
QDs	Quantum Dots
SEM	Scanning Electron Microscope
TEM	Transmission Electron Microscopy
ToF-SIMS	Time-of-flight Secondary Ion Mass Spectra
Tyrp2	Tyrosinase-related Protein 2
UMT	Universal Materials Tester
UV-Vis	Ultra-violet and visible
XPS	X-ray Photoelectron Spectroscopy

CHAPTER 1. INTRODUCTION

Inspired by the chemistry of the adhesive plaques of marine mussels, dopamine (DA), a biological neurotransmitter, has been found to have a remarkable capability to adhere and self-polymerize to form nanoscale polydopamine (PDA) films on supporting surfaces.[1] DA has a chemical structure of catecholamine. It can be regarded as a small molecule that mimics the adhesive component *L*-DOPA in marine mussels.[2] Based on the assumption that the coexistence of the amine and catechol groups is important for achieving underwater adhesion, DA has been proposed and demonstrated by Lee *et al*. as a multifunctional coating on various substrates, including both inorganic and organic materials.[3,4] Since then, interest has been shown in the exploration of PDA film for a range of applications, including conventional surface and material engineering and bio- and nanotechnology.[5,6] Nevertheless, the most fundamental aspect of a PDA thin film, its chemical structure, is still under debate at present.[1] Moreover, the mechanical and adhesion properties of the PDA films, which are almost equally essential as the function of the thin film itself, are still largely unexplored, even though its importance for applications has been realized.[7] A typical study on this aspect involves the contact angle measurement of the PDA film, which reveals its hydrophilic nature and associated surface energy to be 40 mJ/m^2.[8] The effects of coating temperature and DA concentration on hydrophobic polymers were also investigated, revealing that the PDA films became thicker with higher coating temperature and dopamine concentrations.[9]

The overall objective of this research is to use PDA to modify electrically conductive polymers to develop functional nanocomposites with desired properties. In order to achieve this

goal, four related topics have been identified and investigated:

- systematic investigations of the fundamental properties of the PDA film both in air and under water.
- application of DA for PPy functionalization.
- studies of the mechanism of the difference of DA on PPy adhesion and conductivity.
- improvement of DA-PPy synthesis to enhance conductivity and its potential application in advanced electronics.

At first, we performed a series of surface characterizations and mechanical tests to reveal the static and dynamic properties of PDA films coated on three typical well-defined substrates - glass, polydimethylsiloxane (PDMS) and epoxy. We found that PDA films are highly hydrated under wet conditions because of their porous membrane-like nanostructure and hydrophilic functional groups. Upon dehydration, the films form cracks when they are coated on soft substrates due to internal stresses and the large mismatch in elastic modulus. The adhesive pull-off force or the effective work of adhesion increased with the contact time, suggesting dynamic interactions at the interface. A significant decrease in friction forces in water was observed on all three material surfaces coated with PDA; thus, the film could serve as a water-based lubrication coating. We attributed the different behavior of PDA films in air and water to hydration effects.

The first part of the research findings provided insight into PDA film stability, mechanical and adhesive properties, which are critical for using PDA films as a general protocol to modify material surface chemistry. The effective transfer of this nano-material to practical engineering has also been attempted. One such application is the combination of PDA with polypyrrole (PPy), which has been extensively studied due to its economic preparation, long-term stability and good

biocompatiablity. In the second part, we incorporated DA into a typical pyrrole (Py) polymerization reaction; the resultant DA-PPy material exhibited improved dispersion characteristics, significantly enhanced electrical conductivity and a fibrillar morphology when compared to a PPy (no DA) control.[10] All of these new features make DA-PPy stand out as a promising candidate for many innovative applications.

While most of the earlier investigations were primarily focused on the performance of DA-PPy, much effort is necessary to explain their synthetic mechanism. The most important challenges would be to understand: (1) effect of DA/PDA on Py polymerization; (2) explanation of fiber structure of DA-modified PPy, (3) roles of DA in regulating PPy particle size and (4) the role of amine group in DA for PPy modification and enhancing adhesion. To address these questions, three bio-inspired catechol derivatives dopamine (DA), 1,2-dihydroxybenzene or catechol (CA), and *L*-3,4-dihydroxyphenylalanine (DOPA) were introduced and reacted with Py respectively in the third part of this research. It was found that PPy functionalized with these catechol derivatives (DA, CA, and DOPA) exhibited fibrous structure, smaller particle size, good water dispersibility and enhanced film adhesion. We also found that adding a small amount of catechols can improve PPy electrical conductivity. This rapid one-step in *situ* template-free method provided an alternative strategy for the facile production of PPy fibers. Among these three catechols, DA-PPy exhibits the smallest particle size and highest adhesion to glass substrate and electrical conductivity. In contrast, the control phenylethlamine (PA) modification had almost negligible influence on the PPy properties, which provides strong evidence that the catechol itself is responsible for the successful functionalization of PPy and overall performance improvement, instead of amine functional group or coexistence of both catechol and amine

moieties.[11]

Although DA-PPy has shown promise in many biological applications, its conductivity still requires further improvement, especially at higher DA/Py mole ratios. It has been found that the maximum conductivity of DA-modified PPy was 3.8 S/cm for the compressed pellets and 0.2 S/cm for the film, which are not adequate for high-performance electronics. Also, the maximum conductivity was only obtained at low DA/Py mole ratios, where the adhesion and particle size of PPy are relatively weak and large compared with the properties at higher DA concentration. As a result, in the last part of this research, we developed new synthetic approaches to prepare DA-PPy nanostructures, with higher electrical conductivity and water dispersibility. Moreover, we explored the suitable application of each as-fabricated nanomaterial depending on the DA/Py reacting mole ratio. In particular, DA-PPy produced using from a 0.032 DA/Py mole ratio demonstrates superior capacitance for supercapacitors; DA-PPy obtained from 0.064 DA/Py mole ratio can be implemented as co-fillers in an epoxy network of functional composites for electrically conductive adhesives (ECAs); DA-PPy synthesized from 0.64 DA/Py mole ratio reveals an impressive capability of absorbing electromagnetic microwaves for electro-magnetic interference (EMI) shielding applications. Due to the synergetic effects of DA modification, conducting polymer PPy exhibit multifunctional and unique properties, which opens a brand new field in nanomaterial syntheses and applications.

Overall, the fundamental properties of PDA, challenge of effective transfer to applications and open questions surrounding the mechanism of DA polymerization have attracted intense attention from many researchers. The results presented in this thesis have provided a useful foundation for further investigations into the PDA properties. This work and that which follows,

will also benefit applications that make use of PDA-functionalized conducting nanocomposites, which seem destined to play an important role in many new technologies in future. We believe our efforts and focus areas are distinct from those of other researchers and will provide complementary contributions to this field.

In the following Chapter 2, the principles of DA and Py polymerization and their polymer structures will be explained. Moreover, the most recent literature on the development of hybrid PDA functional nanomaterials will be discussed. Chapters 3 to 6 present the investigation results of our four research steps, which were identified and presented at the beginning of this chapter. The dissertation ends with Chapter 7, with the main concluding remarks based on the results obtained in this study, the main contributions of the thesis and also some recommendations for future work.

CHAPTER 2. LITERATURE BACKGROUND

2.1 Marine Mussel Adhesive

Biological systems have evolved well-adapted structures and materials at macro-, micro- and nano-scales through natural selection.[12] The observation and investigation of principles and functions found in these systems have inspired the development of a wide range of advanced materials.[13,14] The fabrication of polymer micro-pillars that replicate the dry adhesive of gecko toe pads and the construction of superhydrophobic surfaces that mimic the self-cleaning of lotus leaves are outstanding examples nature solving engineering problems.[15] In material science, researchers have also looked at nature to search for an universal and efficient coating strategy applicable to materials with any surface chemistry. More recently, biomimetic studies have opened a new route to the modification of various substrates inspired by the adhesive property of mussels.[2]

Water affects the mechanical, physical and chemical properties of an adhesive joint in several pathways: (1) boundary layer formation, (2) interfacial wicking and crazing, (3) hydrolysis and (4) moisture-induced plasticization or swelling.[16-18] All of these mechanisms may lead to the deterioration of adhesive performance and make water a surface contaminant.[19] However, mussels can attach to all types of wet surfaces both permanently and temporarily, inspiring the design of novel underwater adhesives.[20] Many of the current biomimetic applications were inspired by mussels: they can secrete glue proteins, which will rapidly harden to form a solid adhesive, bind strongly to all kinds of surfaces and resist the deterioration of water.[21] A range of different proteins (Mefp-1 to Mefp-5), located at the interface of plaque and

substratum has been isolated from the blue mussel Mytilusedulis (Figure 2.1a).[22] Studies of these adhesive proteins revealed the presence of a unique amino acid 3,4-dihydroxy-L-phenylalanine (DOPA), which is formed by post-translational oxidation of tyrosine and ranges from 3 mole% Mefp-2 to 30 mole% Mefp-5 (Figure 2.1b).[6,23]

To examine the functionality of DOPA in mussel adhesives, Messersmith and co-workers synthesized a series of DOPA-containing biodegradable block copolymers that can rapidly photo-polymerize into adhesive hydrogels.[24]After carefully studying the work of adhesion between the DOPA-containing hydrogels and a Ti surface, they found that the work of adhesion rose with increasing DOPA content in the hydrogels and the oxidation of the hydrogel significantly reduced the work of adhesion to Ti, suggesting that catechol is critical to this process.

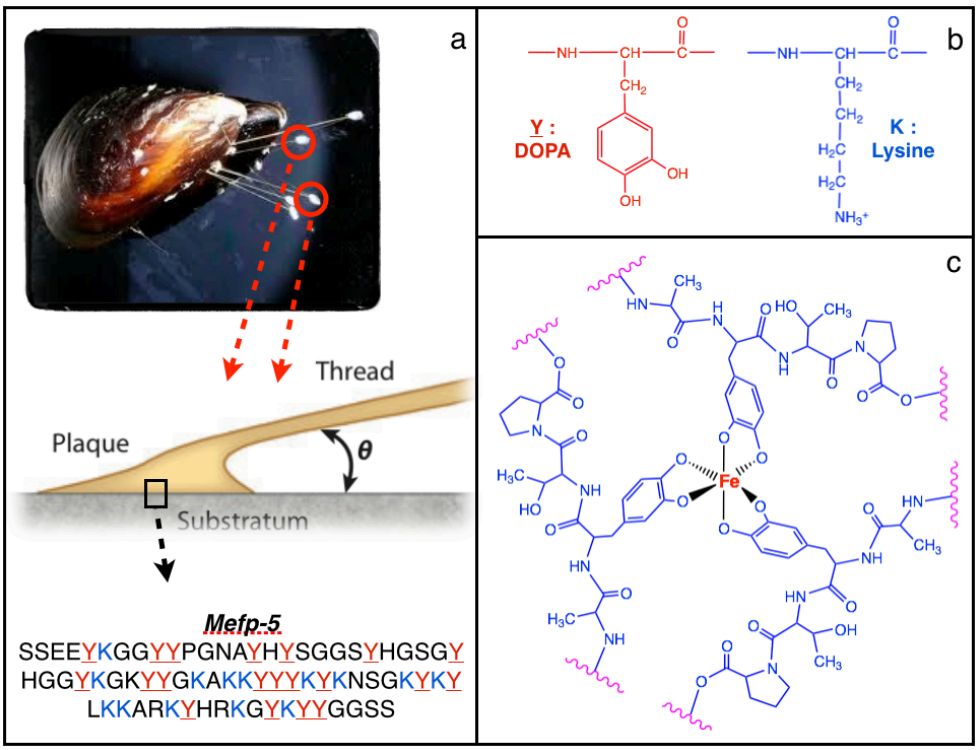

Figure 2.1. (a) Schematic illustrations of the interfacial location of Mefp-5 and the amino acid sequence of Mefp-5.[22] (b) Proposed three DOPA-protein coordinated Fe^{3+} center.[23] (c) Chemical structure of DOPA and lysine.[6] Reprinted with permission from ref 22. Copyright 2004 Wiley-VCH.

Similar investigations have also been conducted by Lee *et al*., who studied the adhesive strength between a single-molecule DOPA residue and different substrates by atomic force microscopy (AFM) (Figure 2.2).[25] A DOPA-modified AFM tip was brought into contact with a wet TiO_x surface; about 500 μN pull-off force was reversibly measured, revealing the possible non-covalent bond between catechol-DOPA and inorganic surfaces. Auto-oxidation of catechol-DOPA to quinone-DOPA decreased the pull-off force with inorganic surfaces, but formed irreversible, high strength covalent bonds with organic surfaces. Although the mussel adhesion mechanism has not been fully explained yet, it is likely to involve the reactive oxidation of catechol-DOPA to quinone-DOPA.

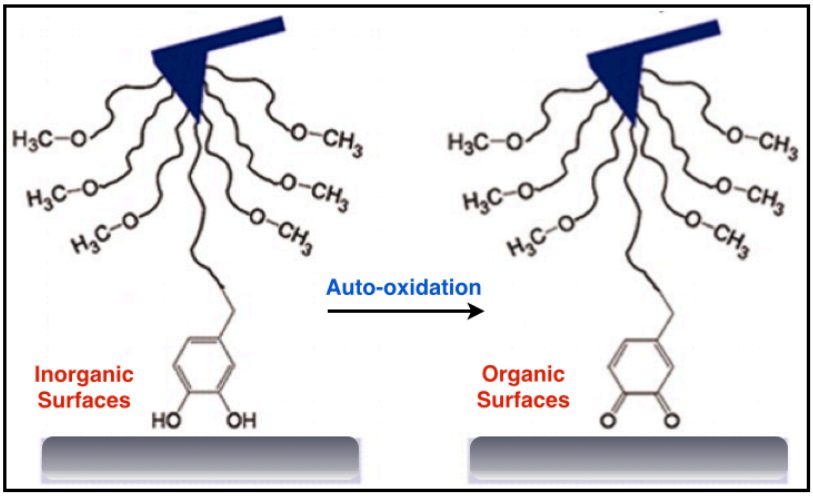

Figure 2.2. Schematic of catechol-DOPA-functionalized AFM tip interacted with inorganic surfaces and quinone-DOPA-functionalized AFM tip interacted with organic surfaces.[25] Reprinted with permission from ref 25. Copyright 2007 National Academy of Sciences.

Another interesting aspect of mussel adhesives is that their plaques are rich in transition metals, such as iron.[21] Thus, the potential role of iron in mussel adhesives has been considered. By investigating the metal-DOPA interactions in mussel adhesive plaques through electron paramagnetic resonance spectroscopy (EPR) and infrared spectroscopy (IR) techniques, Sever *et*

al. proposed a iron-DOPA complex structure, which involved Fe^{3+} bringing together three DOPA-protein chains to form $Fe(DOPA)_3$ (Figure 2.1c).[22] The coupling of the mussel proteins generates cross-links for further adhesive solidification and cohesive bonding. To test this hypothesis, Zeng *et al*. employed surface force apparatus to examine the bridging between two adjacent Mefp-1-coated mica surfaces in the absence and presence of two different Fe^{3+} concentrations (Figure 2.3).[26] Mefp-1 has shown strong adsorption to the mica surfaces, but the adhesive bridging in between two surfaces was almost negligible when no Fe^{3+} was present at the interface. After adding a small amount of Fe^{3+} (10 μM), significant cohesive bridging ($W_{ad} \approx 4.3$ mJ/m^2) between two non-contacting Mefp-1 films was detected. This bridging was fully reversible in water. With further increase in the amount of Fe^{3+} (100 μM) at the interface, the bridging adhesion diminished. Depending on the pH and the iron-to-DOPA ratio, each iron nucleus can either bind to one, two, or three DOPA ligands. Since protein cross-links can only occur at two or three DOPA-Fe^{3+} coordination, the monocatecholato-Fe^{3+} complexes formed at high Fe^{3+} concentrations are not capable of bridging. These research findings suggest that DOPA-metal interactions may also contribute to the strong underwater adhesion of mussels.

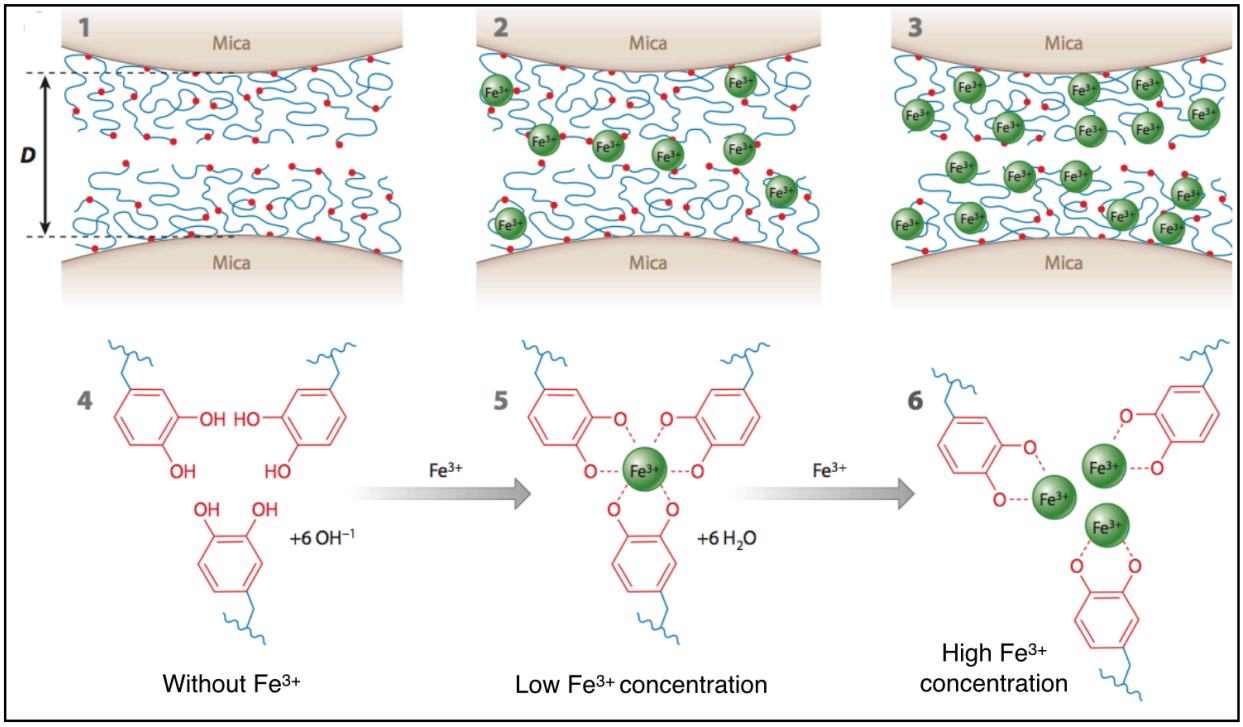

Figure 2.3. Schematic showing two Mefp-1 film coated mica surfaces: (1) without Fe^{3+}, (2) with 10 µM Fe^{3+}, and (3) with 100 µM Fe^{3+}. Also shown are the proposed chemical interactions between DOPA and Fe^{3+}: (4) no Fe^{3+}, (5) tris-DOPA-Fe^{3+} complexes, and (6) mono-DOPA-Fe^{3+} complexes.[26] Reprinted with permission from ref 26. Copyright 2010 National Academy of Sciences.

Mussel adhesive proteins have been found to be positively charged overall because their cationic amino acid residues lysine and arginine are approximately 18-23% more than the anionic counterparts.[27] In order to explore the potential influences of electrostatic charges on mussel adhesion, a set of copolymers combining both a DOPA motif and cationic charges has been developed by Wilker *et al*.[28] Styrene, dihydroxystyrene and *p*-vinyltolyltriethylammonium chloride were co-polymerized into a terpolymer (Figure 2.4), in which ammonium groups were introduced as cationic charge carriers. By measuring the lap shear adhesion of these co-polymers with varied cationic monomer mole ratios in the total composition, the highest degree of adhesion of 2.8 MPa in dry conditions and 0.4 MPa in wet conditions on aluminum substrates were

identified. The adhesion was then decreased with increasing content of the cationic monomer, probably due to electrostatic repulsion. It was concluded that positive electrostatic charge might provide additional surface interaction and bonding that further benefit the adhesion of mussel proteins.

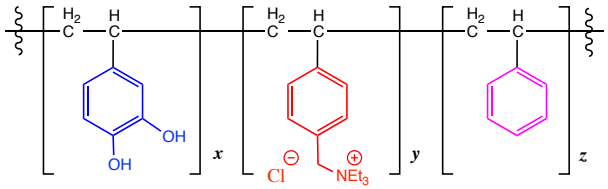

Figure 2.4. Chemical structure of poly[(3,4-dihydroxystyrene)-co- (p-vinyltolyltriethylammonium chloride)-co-styrene] copolymers.[28]

2.2 Mussel-Inspired DOPA-Containing Synthetic Adhesive

Due to the excellent adhesion performance of marine mussels displayed on virtually all surfaces and the multi-functional roles of DOPA in the adhesive proteins, significant biomimetic efforts have been made to synthesize underwater adhesives.[29,30] One simplified synthetic approach is to combine random linear or branched polymers with DOPA moieties. For example, biocompatible poly(ethylene glycol) (PEG) has been modified with DOPA. The structures of four such DOPA-modified PEGs are shown in Figure 2.5.[24]

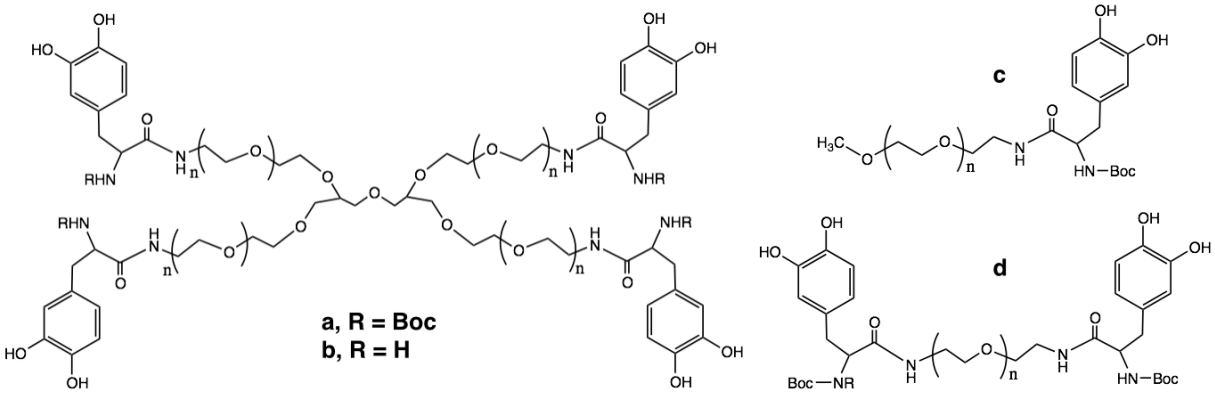

Figure 2.5. Chemical structures of DOPA-modified PEGs with four different ligands.[24]

Upon oxidizing with $NaIO_4$, HRP/H_2O_2, and MT/O_2, they polymerized into hydrogels, which exhibited enhanced mucoadhesivity and can be used for medical applications. Alternatively, DOPA moieties can be directly incorporated into the polymer backbone. One such example is poly[(3,4-dihydroxystyrene)-co-styrene)], which mimics the catechol side chain of DOPA. The synthetic strategy of this co-polymer is illustrated in Scheme 2.1 and could be utilized as a new approach to design DOPA-containing biomimetic adhesives.[31]

Scheme 2.1. Synthesis of poly[(3,4-dihydroxystyrene)-co-styrene)].[31]

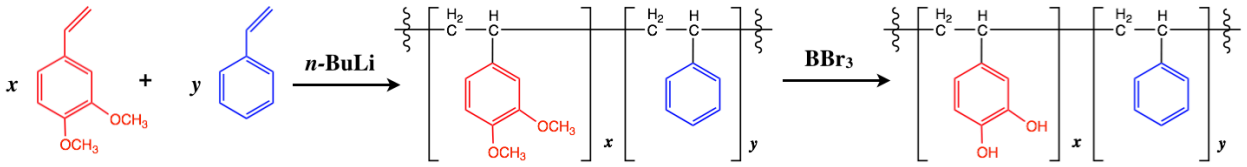

Scheme 2.2. Synthesis of adhesive co-polypeptides using N-carboxyanhydride monomers.[32]

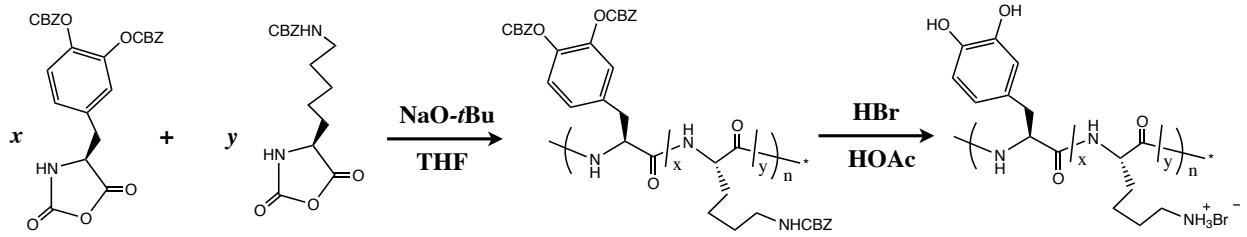

The synthesis of DOPA-containing polypeptides by copolymerization of *N*-carboxyanhydride monomers of lysine and DOPA is summarized in Scheme 2.2.[32] Tensile shear strength measurements were performed to evaluate the adhesion properties of *L*-lysine/DOPA binary copolymers. When suitably oxidized, such co-polymers exhibited moisture-resistant adhesive properties; the adhesive strength was proportional to the amount of DOPA in the co-polymer, but independent of the choice of oxidizing agents. The synthesis and

characterization of DOPA-containing copolymers not only inspired the design of adhesive materials for practical applications, but also yielded additional insights into the key features of DOPA in natural proteins.[33]

Another interesting application of DOPA is the combination of mussel-mimetic polymer with the gecko-inspired pillar structure. The remarkable adhesive ability of geckos is believed to rely on the sophisticated structure of their footpads. In order to achieve strong reversible wet/dry adhesion, Lee and coworkers developed a hybrid material consisting of an array of nanofabricated polydimethylsiloxane (PDMS) pillars coated with a 20 nm layer of poly(dopamine methacrylamide-co-methoxyethyl acrylate) film.[15] The adhesive forces between coated patterned surface and different substrates under dry/wet conditions were determined by AFM. It was found that after coating with the mussel-mimetic polymer, the adhesion of patterned PDMS pillar arrays increased nearly 15-fold in water. This behavior was also shown to be reversible over more than 1000 cycles in both dry and wet environments. This hybrid adhesive, which yielded strong reversible wet/dry adhesion, might open the door to the development of next generation bio-inspired adhesives.[34]

2.3 Dopamine Polymerization − Polydopamine

The most widely used PDA preparation strategy is the oxidation of a DA monomer solution under alkaline conditions (pH > 8.5). DA can be oxidized and spontaneously self-polymerize to form a deep brown film. The thickness of the PDA film can be precisely controlled by tuning the initial DA concentration, reaction time, temperature and the solubility of oxygen in solution.[35] In addition to atmospheric oxygen, other oxidants such as sodium periodate, potassium chlorate and

ammonium persulfate (APS) have been shown able to induce DA polymerization at high reaction rates in all acidic, neutral and alkaline aqueous media.[9,36] Moreover, PDA films deposited on polymer substrates were found to be thicker and smoother than that on glass at the same reaction conditions, suggesting that PDA film thickness might be related to the surface roughness and surface chemistry of the substrates.[7]Instead of adding different oxidants into the DA solution, DA polymerization can be triggered by UV irradiation, which generates singlet oxygen, superoxide radicals or hydroxyl radicals to oxidize DA at both acidic and basic conditions.[37] This method can be combined with photopatterning and has the advantage of fabricating PDA micropatterns on different materials. Alternatively, the biosynthesis of PDA involves an enzymatic oxidation of tyrosine or DOPA initiated by tyrosinase-related protein 2 (Tyrp2). This approach leads to the entrapment of active enzyme in the resulting PDA matrix, which is beneficial for potential biosensing applications.[38]

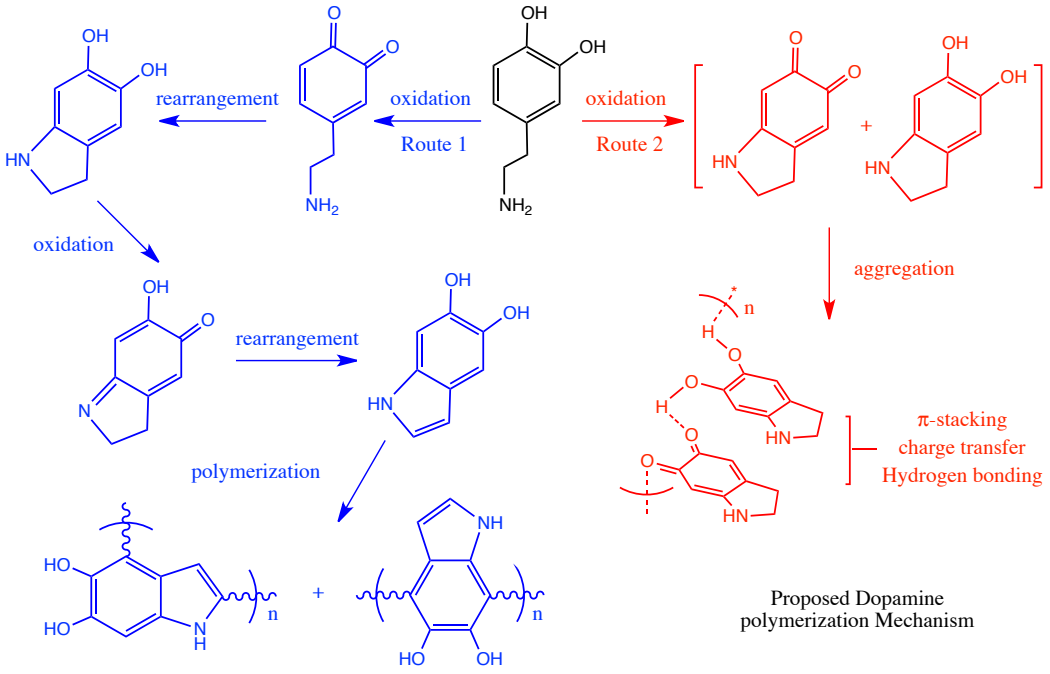

Figure 2.6. Dopamine polymerization mechanism: route 1, "eumelanin-like" oxidative polymerization cross-linked by covalent bonds;[1,6] route 2, oxidative monomers from cross-linked primarily via strong, noncovalent forces including charge transfer, π-stacking, and hydrogen bonding interactions.[40]

In recent years, the deposition of PDA thin films has emerged as a common surface functionalization method in many applications.[5] However, the PDA film assembly mechanism and the chemical structure are still not entirely understood due to its complicated redox process and the formation of many intermediates during DA polymerization.[39] Furthermore, the characterization of PDA structure by common analytical techniques is difficult because of its insolubility in water and most organic solvents.

Since PDA was first discovered in 2007, numerous different PDA structures have been proposed in the literature. Following Messersmith and coworkers' research findings, time-of-flight secondary ion mass spectra (ToF-SIMS) of the PDA films have shown the existence of a variety of dihyroxyindoles and derivatives, which are analogues and intermediates of melanin species.[1] As a result, the oxidative polymerization process of DA has been proposed to be similar to the formation of melanin. Under oxidizing conditions, catechol group protons in DA deprotonate to DA-quinone, which can be structurally rearranged into cyclic intermediates. Then the monomers are covalently linked through coupling reactions at the positions adjacent to the catechol functional groups or on the nitrogen heterocycle to form the PDA structures (Figure 2.6, route 2). Another proposal for PDA formation involves three characteristic steps: (1) oxidation of catechol to quinine, (2) cyclization of amine to a five-membered α-hydroxyketone and (3) supermolecular aggregation through charge transfer, π-stacking and hydrogen bonding interactions (Figure 2,6, route 2).[40] Solid-state ^{15}N nuclear magnetic resonance (NMR) confirmed the first two steps, which are also consistent with the previous model. However, solid-state ^{13}C NMR analysis indicated that the cyclized, nitrogenous species were saturated indoline structures. On the basis of their research findings, Bielawski *et al.* demonstrated that the monomers were

cross-linked primarily via strong noncovalent forces instead of the covalent bonds between the aryl rings.

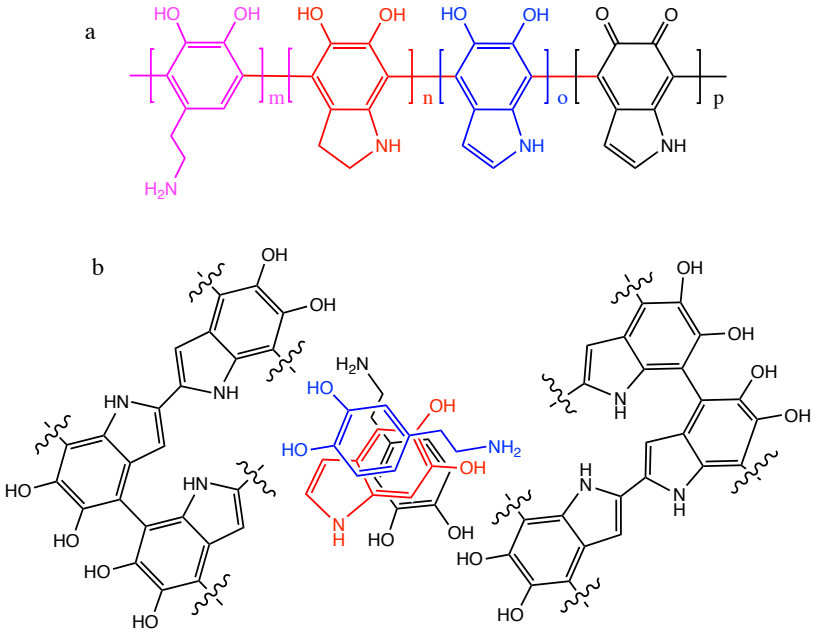

Figure 2.7. Two proposed PDA structures: a, covalently linked monomers through C−C bonds between benzene rings;[41] b, $(DA)_2$/DHI trimer entrapped within PDA complex.[42]

The debate over the previous two PDA structural models focuses on whether the monomers are cross-linked via covalent bonds or noncovalent forces. The “eumelanin-like” model (Figure 2.6, Route 1) was supported by Buehler *et al.*; they performed a series of computational calculations on PDA and observed a Young’s modulus of 4.1−4.4 GPa at a high degree of polymerization (70%), which is in agreement with the 4.3−10.5 GPa of natural eumelanin films and synthesized PDA films obtained by nano-indentation experiments. On the other hand, computational calculations on the "non-covalent aggregate" model (Figure 2.6, Route 2) yielded a much lower Young’s modulus than that obtained experimentally.[41] Thus, the second model might not accurately represent the overall PDA structure due to the large mismatch between the simulated Young’s modulus of pure aggregates and the experimental values of the PDA film. In

addition, Beck *et al.* also supported the alternative of covalent bonding of monomers based on the unambiguous results obtained by different analytical methods (Figure 2.7a).[42] They found that: (1) PDA oligomers occurred in a different state of unsaturation, (2) DA units exist and (3) open-chain dopamine units exist. Thus, they proposed an alternative PDA structure in which all monomers are covalently linked by C−C bonds between their benzene rings instead of the nitrogen heterocycles.

In parallel with the “eumelanin-like” model and the "non-covalent aggregate" model, Lee *et al.* believed that the formation of PDA involved the combination of both oxidative polymerization and non-covalent stacking. High-performance liquid chromatography (HPLC) coupled with mass spectrometry analysis confirmed that the previously proposed PDA oxidative polymerization through covalent bonds also occurred in this model.[43] Simultaneously, a significant amount of unpolymerized DA and its oxidative product 5,6-dihydroxyindole (DHI) were detected. In the final structure, they formed a stable complex $(DA)_2$/DHI, which was tightly entrapped within PDA complex, as depicted in Figure 2.7b. Further investigations revealed that the encapsulation of the $(DA)_2$/DHI trimer was quite stable and not easily released from the PDA system.

2.4 Polydopamine Thin Film

Many coating strategies can be used to deposit thin films with precisely controlled thickness and functionality. However, most of these methods have limitations with respect to material compositions, deposition conditions and/or process costs. For example, layer-by-layer deposition can only be performed on a charged surface,[44] monolayer self-assembly requires noble metal

substrates or surfaces of oxides,[45] Langmuir-Blodgett films are formed by repeating exposures of the solid substrate to liquid[46] and plasma deposition normally requires high temperatures and sometimes a vacuum.[47] In this regard, the emerging PDA coatings have been developed to modify almost all known materials surfaces under mild conditions. Significant efforts have been directed toward understanding the fundamental properties of this nanoscale polymer thin film for the effective transfer to functional devices and biocompatible coatings.[48,49]

2.4.1 Surface Properties

PDA thin films are most commonly prepared by immersing the substrates in a dilute aqueous Tris solution of DA hydrochloride at a marine pH environment.[7] The self-polymerization and deposition processes on various substrates under different reaction conditions have been investigated. It has been found thicker PDA films were deposited by increasing the initial concentration of DA, reaction time, temperature and the solubility of oxygen in solution.[35,50] Besides using atmosphere O_2, other oxidants such as sodium periodate, potassium chlorate and ammonium persulfate have shown remarkable ability to induce DA polymerization at higher reaction rate in all acidic, neutral and alkaline aqueous media.[35] Moreover, PDA films deposited on PDMS and epoxy substrates were found to be thicker and smoother than that on the glass at the same reaction conditions, which indicated that PDA film thickness might be related to the surface roughness and surface chemistry of the substrates.[7] The surfaces of the PDA films tend to be rough due to the formation of agglomerates in solution, which deposit onto the film surface to form a heterogeneous morphology. However, compared with PDA films deposited under ambient air, more uniform and smooth PDA coatings were obtained by polymerization under a pure O_2

atmosphere. An explanation for this behavior is that, the conjugated planar supermolecular structures are more regularly stacked under a pure O_2 atmosphere, which leads to much less polymer aggregation.[51]

The surface energy is considered to play an important role in the surface properties of polymer films, such as the wettability and adhesion. Yang *et al*. performed a series of contact angle measurements on PDA-coated PDMS surface to evaluate the surface energy of PDA films.[8] The static water contact angle was measured to be 65°, revealing the hydrophilic nature of this PDA coating. The water contact angle hysteresis was determined to be 60° by dynamic contact angle measurement, suggesting dynamic interactions occurred between water molecules and PDA film.[8] Other probe liquids were dispersed on the PDA surface. The resulting contact angles measured with these liquids are shown in Table 2.1 and were used to estimate the surface energy γ according to van Oss' method and Wu's method with water as one of the pairing parameters.

Table 2.1. Surface energy of PDA films determined from contact angle measurements.[8]

	γ_{LW}	γ_{AB}	γ^+	γ^-	γ (mJ/m^2)	θ (°)
Diidomethane	50.8	0.0	0	0	50.8	51.2 ± 2.6
DMSO	36	8.0	0.5	32	44	23.3 ± 1.9
Ethylene glycol	29	19.0	1.92	47	48	43.3 ± 1.2
Formamide	39	19.0	2.28	39.6	58	42.5 ± 2.6
Glycerol	34	30.0	3.92	57.4	64	67.2 ± 4.5
Hexadecane	27.5	0.0	0	0	27.5	16.4 ± 1.2
Water	21.8	51.0	25.5	25.5	72.8	64.8 ± 3.7
Polydopamine						
Van Oss	30 ± 3.9	10 ± 5.0	1.4 ± 1.4	17.7 ± 4.3	40 ± 8.9	
Wu	22.5 ± 8.9	22.2 ± 5.7				

Surface free energy (γ), apolar component (γ_{LW}) of γ, polar component (γ_{AB}) of γ, electron-acceptor (γ^+) and electron-donor (γ^-) parameters of γ_{AB} were obtained from ref 8. $\gamma_{AB} = 2(\gamma^+\gamma^-)^{1/2}$; $\gamma = \gamma_{LW} + \gamma_{AB}$. The contact angles (θ) were obtained on polydopamine coated PDMS substrates using different liquids and were interpreted according to the VanOss and Wu methods with water as one of the pairing parameters.

2.4.2 Biocompatibility

The catechol derivatives, including PDA, exist in a variety of living systems and participate in a broad range of biochemical processes. For example, catecholamines including epinephrine, noradrenaline and DA are biologically significant hormones and neurotransmitters that are responsible for conveying nerve impulses, regulating heart rate and controlling the oxygen supply to the brain in the human body. PDA is a major component of naturally occurring melanin and so shows excellent biocompatibility. To determine the possible toxicity of PDA, Ku *et al.* adhered mammalian cells such as fibroblasts, osteoblasts, neurons and endothelial cells to PDA surfaces and found that PDA did not hinder the viability or proliferation of mammalian cells, indicating its non-toxic nature.[52] In line with these results, a complicated PDA capsule structure assembled using a calcium carbonate template under mild conditions was reported by Zhang and coworkers.[53] They accommodated three different enzymes including glucosidase, α-amylase and β-amylase into a single PDA capsule. This system displayed enhanced enzymatic activity, which further reflected the negligible cytotoxicity of PDA.

2.4.3 Stability

The stability of PDA films deposited on silica in aqueous solutions at different pH has been investigated by Bernsmann *et al*.[54-56] They found that the thickness of the PDA film formed at pH = 1 and then measured in the dry state decreased by 14% after 54 h. The films also showed no measurable changes in thickness when formed at pH = 3 and 11 for more than 24 h. In contrast, the PDA films were quantitatively removed within 15 min of exposure to sodium hydroxide solutions at pH 13. This can be attributed to either the dissociation of the silicon oxide layer

covering the silicon slide or the fact that PDA is stable in acidic and neutral solutions but becomes soluble in strongly alkaline solutions.

2.5 Applications of Polydopamine

In recent years, PDA thin films have emerged as an important multifunctional bio-inspired coating material since the pioneering work reported by Messersmith and coworkers in 2007.[1] Compared with bulk materials, PDA thin films are almost 2-D and have a larger surface-to-volume ratio, which make them more sensitive to surface properties and interactions.[57] Because PDA films contain a high density of biological-relevant catechol functional groups, they have a remarkable ability to render materials biocompatible via immobilizing, regulating or sensing biomolecules.[58] Moreover, catechols can interact with both organic and inorganic substrates through covalent bonds, making PDA film a universal anchor for surface modifications.[59]

Beside the intrinsic di-catechol functional groups, the co-existing *o*-quinone groups can also be modified to form new surfaces with additional properties. Figure 2.8 summarizes the PDA modification protocols based on Schiff base formation and Michael type addition.[33] o-quinone functional groups are generally sensitive to both thiols and nitrogen derivatives under basic conditions to form a thiol adduct, amine adduct or o-quinonimine. The post-modification of PDA surfaces was first demonstrated by Lee *et al*.,[1] who reacted PDA films with thiolatedmethoxy-PEG, aminatedmethoxy-PEG and 50% thiolated hyaluronic acid to form different organic add-layers on top. This approach was then adopted for grafting molecules of interest on thiol or amine post-modified PDA surfaces, including the bioconjunction of

thermolysin enzyme, amphotericin B or poly(L-lysine).[60]

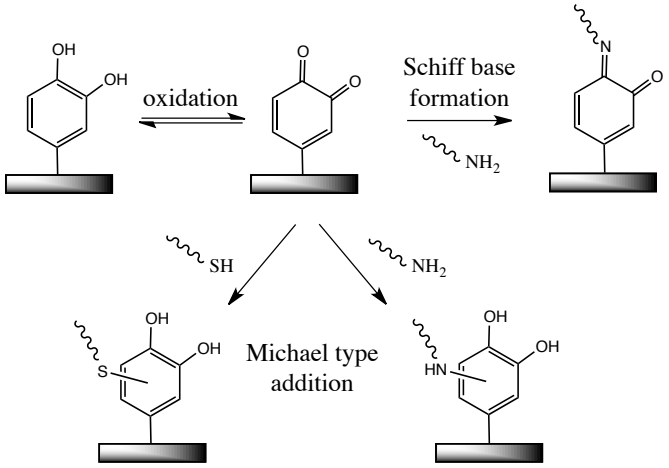

Figure 2.8. Possible reaction pathways of oxidized catechol though Schiff base reaction and Michael addition.[33]

With the help of PDA films, Lee *et al*. developed a general modification strategy for functionalizing diverse surfaces (Figure 2.9).[61,62] This strategy involved one-step immersion of substrates in a mixture of DA and desired molecules. The molecules were then dissolved with DA and immobilized onto substrate surfaces during DA polymerization. Depending on the chemical and biological properties of immobilized molecules, surfaces with different functions could be obtained for many applications, such as tissue regeneration, hematopoietic cell adhesion, anti-bacterial surface preparation, surface-initiated polymerization and silicification.[63]As a result of such broad ranges of functionalities, PDA films have proven to be a versatile platforms for the development of new functional materials and coatings with unique structures and fascinating properties of potential application to biomedical-, electronic- or energy-related industries. The state-of-the-art PDA film will be discussed in the following sections to give specific examples of the effect of PDA coatings on interfacial properties.

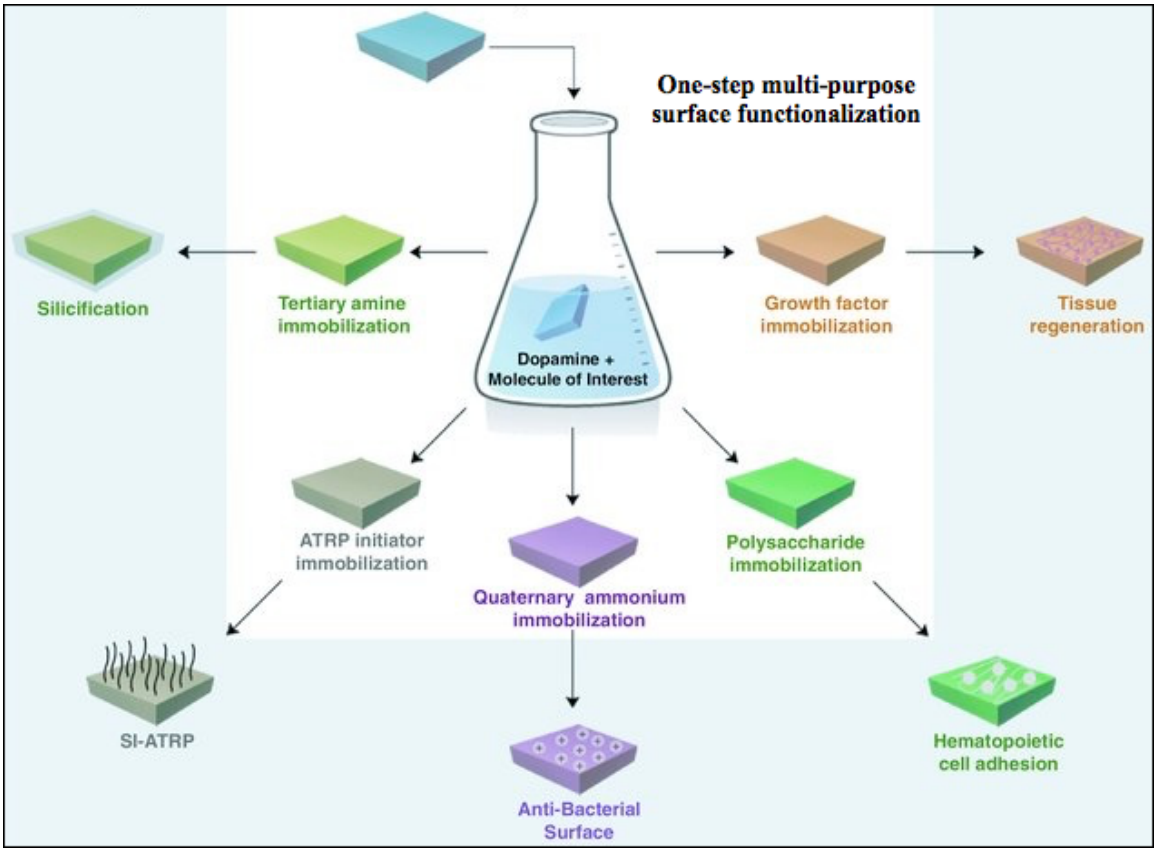

Figure 2.9. Schematics of the one-step modification of solid substrates.[61] Reprinted with permission from ref 61. Copyright 2012 Wiley-VCH.

2.5.1 Polydopamine Films for General Biological Applications

PDA films have been proved useful for grafting of biomolecules because the catechol/quinone groups may form covalent bonds with nucleophilic molecules.[60,64] One protein-binding example is trypsin, which can conjugate on a variety of PDA-coated surfaces and still remain enzymatically active.[4] Due to the negative charge at physiological pH, PDA is also able to facilitate biomineralization processes by reacting with metallic cations.[65] Indeed, inorganic hydroxyapatite crystals can be mineralized on versatile PDA-coated materials.[66] Moreover, the adhesion of different mammalian cells to a PDA-coated micropatterned PDMS substrate has been tested. It was found that the cells selectively adhered only to the

PDA-modified regions of the substrate and aligned with the PDA patterns.[67] The enhanced cell adhesion to PDA coating may be potentially useful for 3D tissue fabrication. Furthermore, the PDA coating has also been found useful in biosensing techniques. One such example is the attachment of a single live *E*. coli cell to the tip of a PDA-modified AFM cantilever. This novel single-cell probe preparation method is versatile and may have great potential for exploring cell-cell interactions. Instead of modifying deposition substrates, PDA can be directly coated on biomolecules. For instance, yeast cells was coated with a PDA layer and subsequently modified with an avidin ad-layer. The functionalized PDA coating was able to physically stabilize, protect and control living yeast cells. In addition, the encapsulated yeast cells can be effectively immobilized on any biotin-functionalized surface via avidin-biotin complexes formation.[68]

2.5.2 Polydopamine Films for Advanced Drug Delivery Systems

Pioneering works have successfully demonstrated that adherent PDA-based coating can be deposited on many substrates. Alternatively, the substrates may also serve as sacrificial templates, which can be removed after PDA film formation in order to yield stable hollow PDA capsules. These capsules, with the advantages of controllable film thickness and high biocompatibility, may offer a new polymer capsule fabrication method for drug/gene delivery.[69,70]

The first PDA capsule assembly strategy was reported by Caruso and coworkers, who coated silica spheres with a thin layer of PDA film by oxidative self-polymerization of DA in Tris buffer (10 mM, pH 8.5), followed by hydrofluoric acid/ammonium fluoride solution etching to remove silica particle cores and form robust capsules.[71] This approach was proven to work well on SiO_2 particles with different sizes and mesoporous structures. Biocompatibility tests have shown

almost no toxicity of the PDA capsules to living cells, which is important for drug delivery. This work first demonstrated the possibility of applying PDA to construct versatile nanocapsules, which opens the door to the development of more sophisticated PDA-based DDS. Biodegradability has always been considered as an important criterion for designing novel drug delivery vehicles.[72] As a result, Caruso *et al*. developed a range of biodegradable poly(*L*-glutamic acid) (PGA)-conjugated PDA capsules using the preparation process illustrated in Figure 2.10a.[72] At first, different amounts of DA monomer were conjugated with PGA via amide bond formation. These PGA-PDA polymers were then assembled and deposited onto silica particles at 10 mg/mL solution (pH = 9) for 12 h. Stable PGA-PDA capsules with tailored film thickness were obtained after the silica core was removed, as confirmed by AFM and TEM (Figure 2.10b and 2.10c). Capsules obtained from this method were exposed to protease solution to investigate their degradation behavior. Fluorescently labeled lysozyme was preloaded in the PDA capsules and degradation was monitored via the release of the enzyme. Lysozyme release reached equilibrium after 15 h, indicating the degradation of the PGA-PDA shells, which enabled the diffusion of the encapsulated cargo. This capsule fabrication method, which combined the advantages of a biodegradable material with the spontaneous self-polymerization of DA, made a significant contribution to the assembly of degradable capsules.

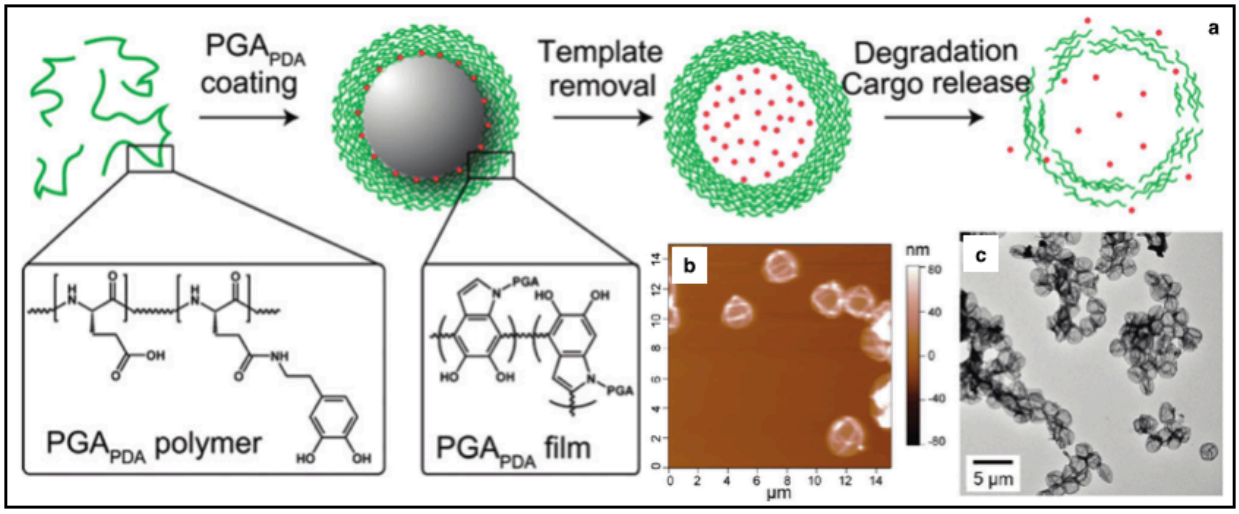

Figure 2.10. (a) Preparation protocol of PGA-PDA capsules; (b) AFM and (c) TEM images of PGA-PDA nanocapsules.[72] Reprinted with permission from ref 72. Copyright 2011 American Chemical Society.

Recently, a more complicated PDA capsule structure assembled using a calcium carbonate template under mild conditions was reported by Zhang and coworkers (Figure 2.11).[53] The capsule assembly process involved three steps: (1) glucosidase was encapsulated in the lumen of a capsule containing a calcium carbonate template; (2) β-amylase was entrapped with the PDA capsule membrane; and (3) α-amylase was covalently attached onto the outer surface of the PDA layer. The diameter and shell thickness of the capsules can be controlled by the choice of template size and DA concentration. The successful development of this novel cascade system, which accommodated three different enzymes in separable locations with a single PDA capsule, demonstrated the possibility of using a PDA capsule as a standard platform for drug delivery of multienzyme systems.

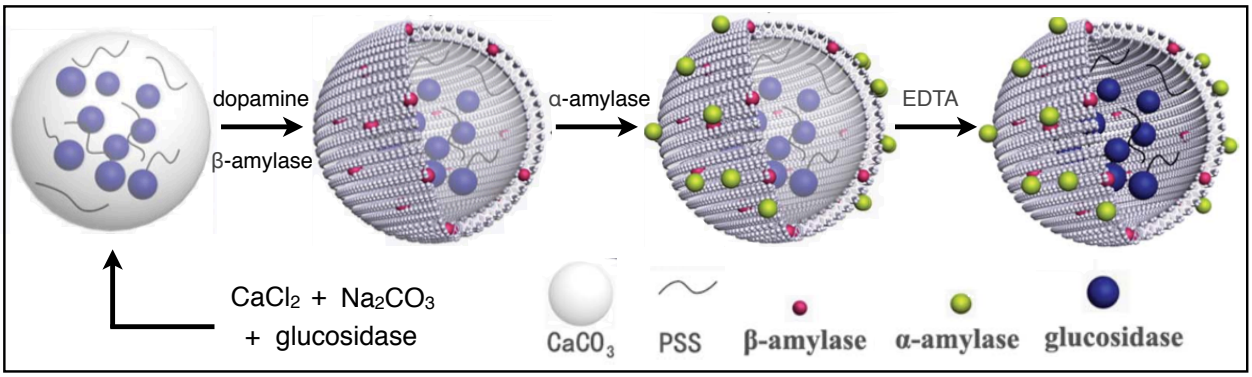

Figure 2.11. Schematic for the construction process of multienzyme PDA capsule system.[53] Reprinted with permission from ref 53. Copyright 2011 RSC.

Instead of using "hard" silica as template, the same group also reported the preparation of monodisperse PDA capsules by using "soft" emulsion droplet cores (Figure 2.12a).[73] In this work, monodisperse and stable emulsion templates were first prepared by base-catalyzed hydrolysis and partial condensation of dimethyldiethoxysilane (DMDES).After controlled deposition of PDA on the surfaces of the emulsion droplets, the PDA-coated emulsion droplets were isolated by centrifugation. Similar to the removable silica cores, the emulsion templates were dissolved by aqueous ethanol under mild conditions to form PDA capsules with precisely controlled diameter and shell thickness in the range of 400 nm to 2.4 mm and 10 to 140 nm, respectively (Figure 2.12b-d). Many functional components, such as magnetic Fe_3O_4nanoparticles, fluorescent quantum dots (QDs) and hydrophobic anti-cancer drugs (thiocoraline, TC) could be preloaded in the emulsion droplets and then subsequently entrapped in the PDA capsules. Along with the excellent biocompatibility of PDA, this simple and versatile method is potentially useful to assemble nanocarriers loaded with different drugs. In the following section, we will dedicate more space to discuss a particular drug delivery application of PDA nanocapsules prepared by this method.

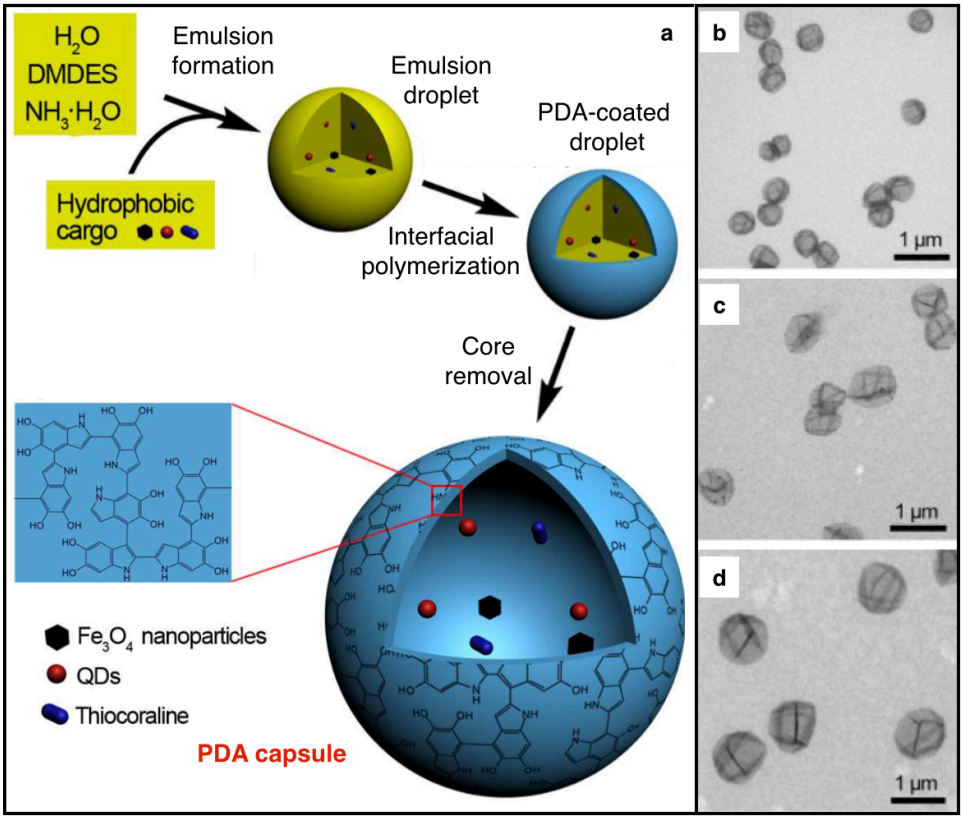

Figure 2.12. (a) Schematic representation of the encapsulation of hydrophobic species in PDA capsules, obtained by using DMDES emulsion templates; TEM images of PDA capsules prepared from emulsion templates at different DMDES emulsion condensation times: (b) 4 h, (c) 8 h, and (d) 24 h.[73] Reprinted with permission from ref 73. Copyright 2010 Wiley-VCH.

In order to achieve controlled and targeted drug release, PDA capsules should be functionalized with various functional moieties such as targeting ligands, pH-sensitive functional groups and enzymes with redox behavior, to respond to intracellular stimuli. Caruso and coworkers reported a facile approach to immobilize a pH-cleavable polymer-drug conjugate on PDA capsules for intracellular drug delivery.[74] In this work, pre-synthesized poly(methacrylic acid) (PMA_{SH}) with 13.5% thiol-modification and a maleimide hydrazine derivative of an anticancer drug doxorubicin (Dox) were conjugated. Then monodispersed PDA capsules prepared by the aforementioned method (Figure 2.12a) were incubated with the polymer-drug

conjugates (PMA_{SH}-Dox) at pH = 8. This resulted in the coupling of thiol and quinone functional groups to form PMA_{SH}-Dox immobilized PDA capsules (Scheme 2.3). The Dox loading capacity in each PDA capsule was determined to be 6.45×10^{-16} g by ultraviolet-visible (UV-Vis) spectrophotometry and flow cytometry.

Scheme 2.3. Immobilization and pH-depend release of Dox (labeled as red dots) from PDA capsules.[74] Reprinted with permission from ref 74. Copyright 2012 American Chemical Society.

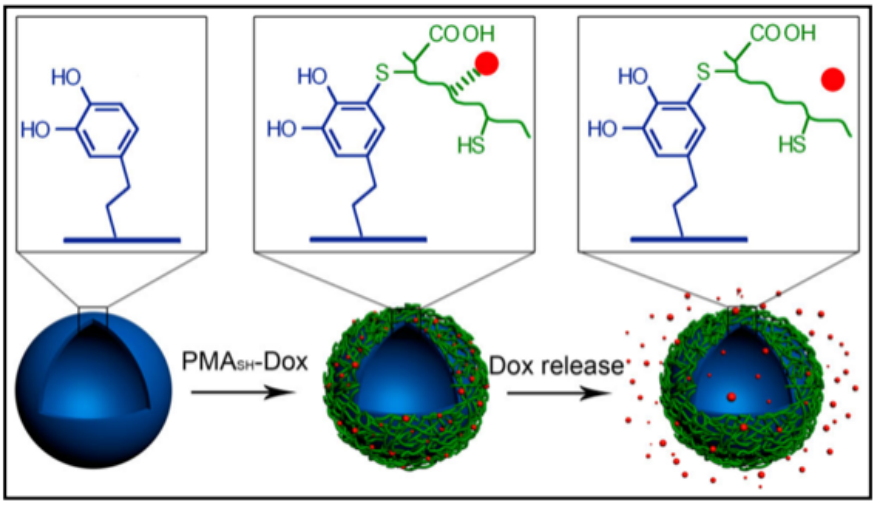

2.5.3 Polydopamine Films for Hydrophobic/Hydrophilic Coatings

Due to their hydrophilic and self-adhesion nature, PDA films can form as a generic coating to modify surfaces and make them hydrophilic. Lee and coworkers reported a straightforward solution-based modification method that transformed superhydrophobic surfaces into hydrophilic substrates (Figure 2.13a). Polyfluorosilane-coated anodic aluminum oxide membranes were coated with PDA thin films. The resulting water-adhesive but hydrophobic surfaces, which could retain water droplets at a high water/surface contact angle even when the surfaces were tilted to 180° (Figure 2.13b). This dip-coating surface modification approach was also applied to overcome the poor wetting capabilities of polyethylene (PE). After depositing a thin layer of

PDA, the functionalized hydrophilic PE can be used as separators to improve power performance in Li-ion batteries (Figure 2.13c).[75]

Alternatively, PDA films can also serve as mediator to bond to hydrophobic ad-layers. Xu and coworkers combined the adhesive ability of PDA with a lotus-leaf-inspired hierarchical structure to develop highly water repellent microparticles. PDA films were deposited on core particles and then used as templates to adhere silver nanoparticles. The resulting core/shell/satellite composites exhibited extremely water repellence after further treating with alkanethiol.[76]This strategy can be applied to diverse surfaces due to the nonselective adhesion of PDA coatings. As a result, bio-inspired PDA coating can produce either hydrophobic or hydrophilic functionalized surfaces.

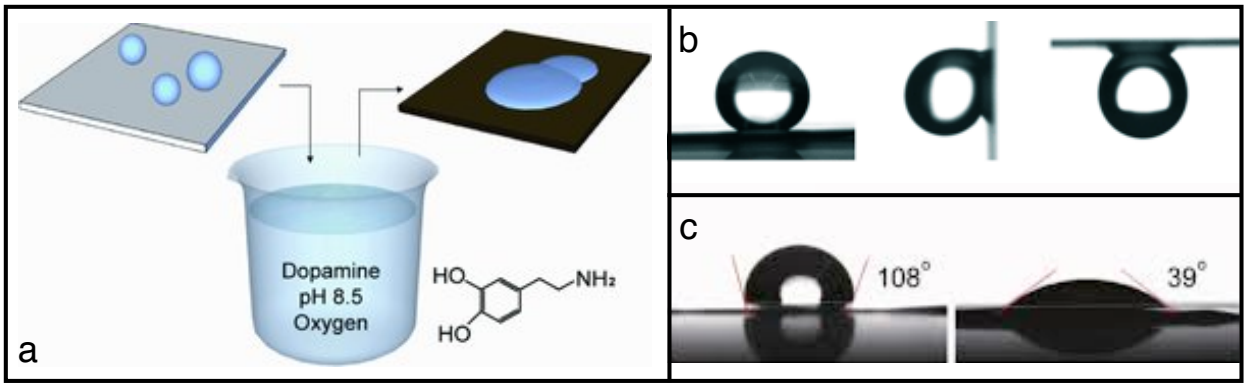

Figure 2.13. (a) Schematic illustration of the PDA surface treatment using a simple dip-coating. (b) Water droplet on the PDA-coated superhydrophobic surface remained attached at 90° and 180°. (c) Contact angle images of PE separators before (left) and after (right) the PDA coating.[75] Reprinted with permission from ref 75. Copyright 2011 Wiley-VCH.

2.5.4 Polydopamine Films for Nanocomposites Functionalization

Due to their high biocompatibility and superparamagnetic behavior, iron oxide nanoparticles have attracted much interest in many fields, such as terabit magnetic storage devices, catalysis, sensors and magnetic resonance imaging.[77] Since di-catechol functional groups can be effectively

chelated to the ferric ions, PDA film is considered a high affinity coating to modify iron oxide nanoparticles. For example, γ-Fe_2O_3 nanoparticles were deposited with a reactive PDA-based polymer, capable of binding His-tagged silicatein.[78] The surface-bound silicatein has been shown to actively catalyze polycondensation of silicon alkoxides in solution, forming a protective silica shell around the iron oxide nanoparticles. These results suggested the possibility of bridging biomolecules with inorganic nanomaterials by PDA surface functionalization.

Scheme 2.4. Synthesis procedure for water-dispersible PDA-modified CNTs.[81] Reprinted with permission from ref 81. Copyright 2013 American Chemical Society.

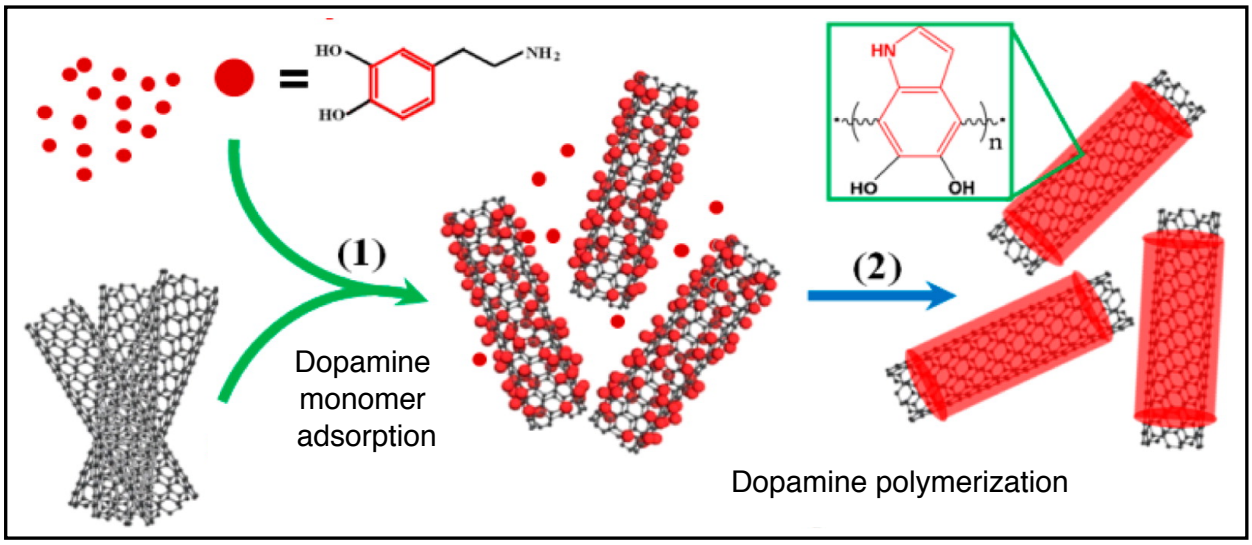

PDA has also found applications in the use of carbon nanotubes (CNTs), which normally require surface modification to ensure their wide applications.[79,80] Traditional CNT functionalization methods often involve harsh reaction conditions that may destroy their structures and subsequently compromise their high conductivity and excellent thermal stability. To this end, Yang *et al.* reported a facile multi-wall carbon nanotube (MWCNT) surface modification strategy under mild conditions (Scheme 2.4).[81] DA monomer was first adsorbed onto the MWCNTs via π-π stacking interactions. The oxidative polymerization of adhered

monomer was then triggered by adjusting the solution pH. As a result, a layer of PDA film was deposited on the surface of MWCNTs, forming a water-dispersible core/shell MWCNTs structure with the inherent properties of the pristine MWCNTs remaining intact.

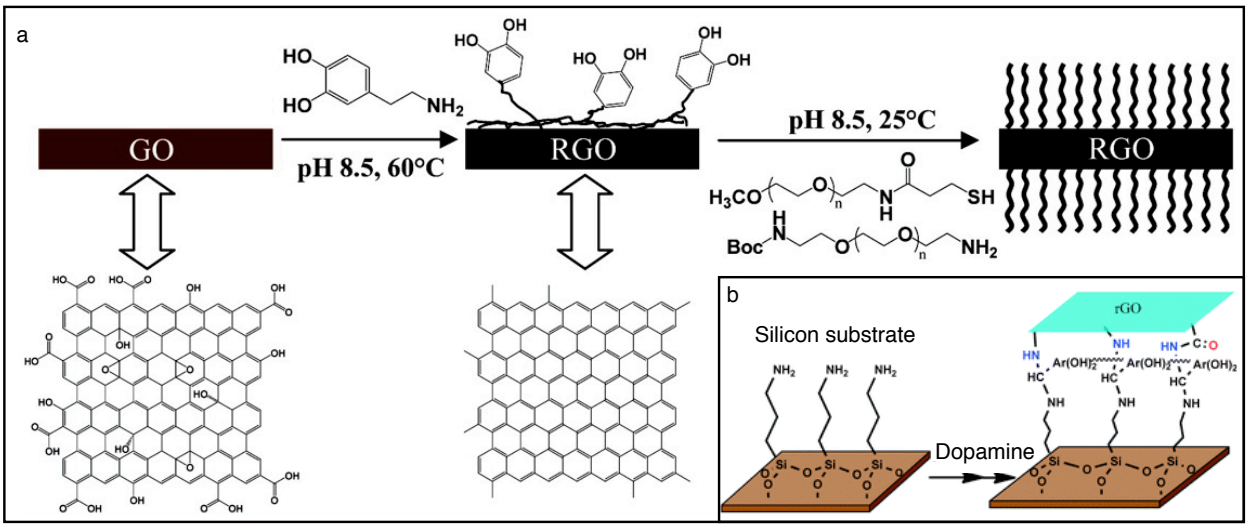

Figure 2.14. (a) Schematic illustration of the preparation of PDA-coated graphene and PEG-graphene. (b) Proposed schematic view for the assembly of graphene film on a silicon wafer through PDA coating.[85] Reprinted with permission from ref 85. Copyright 2012 American Chemical Society.

Graphene is another carbon-based nanomaterial that can be functionalized by PDA chemistry.[82,83] Fu *et al*. reported a facile method that can reduce graphene oxide and form an adhesive layer on its surface simultaneously via DA polymerization.[84] The modified surface was then grafted with PEG brushes, resulting in water-dispersible graphene (Figure 2.14a). Another DA-inspired reagent norepinephrine has also shown similar functionality. Graphene oxide can be reduced and coated with poly(norepinephrine) though pH-triggered oxidative polymerization. Further investigations revealed poly(norepinephrine)-coated graphene to be a versatile platform for secondary modifications, such as ring-opening polymerization of carprolactone or formation of gold nanoparticles on surfaces, that provide antibacterial properties.[85] The poor adhesion between graphene and substrates due to the weak interfacial bonding is a major drawback for

many applications. To solve this problem, Wang and coworkers introduced a PDA coating as an adhesive layer firmly bonded onto a wide range of substrates and acting as an active platform for graphene oxide reduction and deposition (Figure 2.14b).[86] Thus, the assembled graphene films were able to adhere onto various substrates and exhibit unique tribological properties, such as friction reduction and wear resistance.

2.6 Polypyrrole: A Conducting Polymer

In recent years, PDA has arisen as a promising research subject in various fields ranging from the fabrication of energetic coatings to the preparation of functional composite materials. We have applied PDA to the syntheses of functional conducting polymer nanocomposites. Conducting polymers are organic polymers that conduct electricity similar to metals, but at the same time retain the mechanical properties of conventional polymers.[87] In the last two decades, over 25 conducting polymers have been reported since polyacetylene was first found conductive after halogen doping in 1977.[88] Typical examples of this system include poly(*p*-phenylene), polypyrrole, polythiophene and polyaniline. One of the common features of these conjugated structures is the alternating carbon–carbon double bonds or *p*-system in their backbones.[89] Their electrical conductivity can change from insulating or semiconducting to highly conductive depending on the level of doping. The doping process is performed by chemical or electrochemical oxidation (*p*-doping) or reduction (*n*-doping) of a polymer, which subsequently acquire positive or negative charges in their polyconjugated matrix.[90] This process is also reversible; the initial polymer structure can be recovered after removal of the dopant. Conductive polymers have been attracted more and more attention since Heeger, MacDiarmid and Shirakawa

were awarded the Nobel Prize in Chemistry in 2000 “for the discovery and the development of electrically conductive polymers”.[91] Among these conductive polymers, polypyrrole (PPy) has been extensively investigated because of its unique electrical properties and its potential applications in a variety of technological areas, such as anti-corrosive coatings, batteries, supercapacitors and biosenors.[92-95]

2.6.1 Polypyrrole Synthesis and Conduction Mechanism

Two common methods of synthesis of PPy exist: electrochemical and chemical.[96] The former method produces a PPy film with high conductivity, but is limited by low yields, difficult-to-control film growth and heterogeneity. In order to produce PPy more practically, chemical synthesis has been attempted for the large-scale production. Both methods involve the oxidative polymerization of pyrrole monomer according to the proposed reaction mechanism illustrated in Scheme 2.5.[89,90,92]At first, the oxidation of Py molecules yields delocalized radical cations, which resonate between three different states. The most stable radical cation dimerises and expels two protons to form a bi-pyrrole dimer, which can react with a newly formed radical cation to continue chain growth. The final form of PPy is a long conjugated backbone with two resonance structures including aromatic and quinoid. These two states are neutral and cannot conduct electrons.[97]Upon further oxidation, the positive charges associated with the oxidized state are delocalized over several Py units and form a radical cation (polaron) or a dication (bipolaron). This produces negatively charged counterions in solution to maintain the charge balance. This process is referred to as doping, and leads to the absence of electrons in the PPy polymer chain and the formation of "holes" (*p*-type conduction).[98,99]

Scheme 2.5. Polypyrrole formation mechanism and its neutral aromatic and quinoid states, and chemical structures of oxidized polaron and bipolaron forms.[89,90,92]

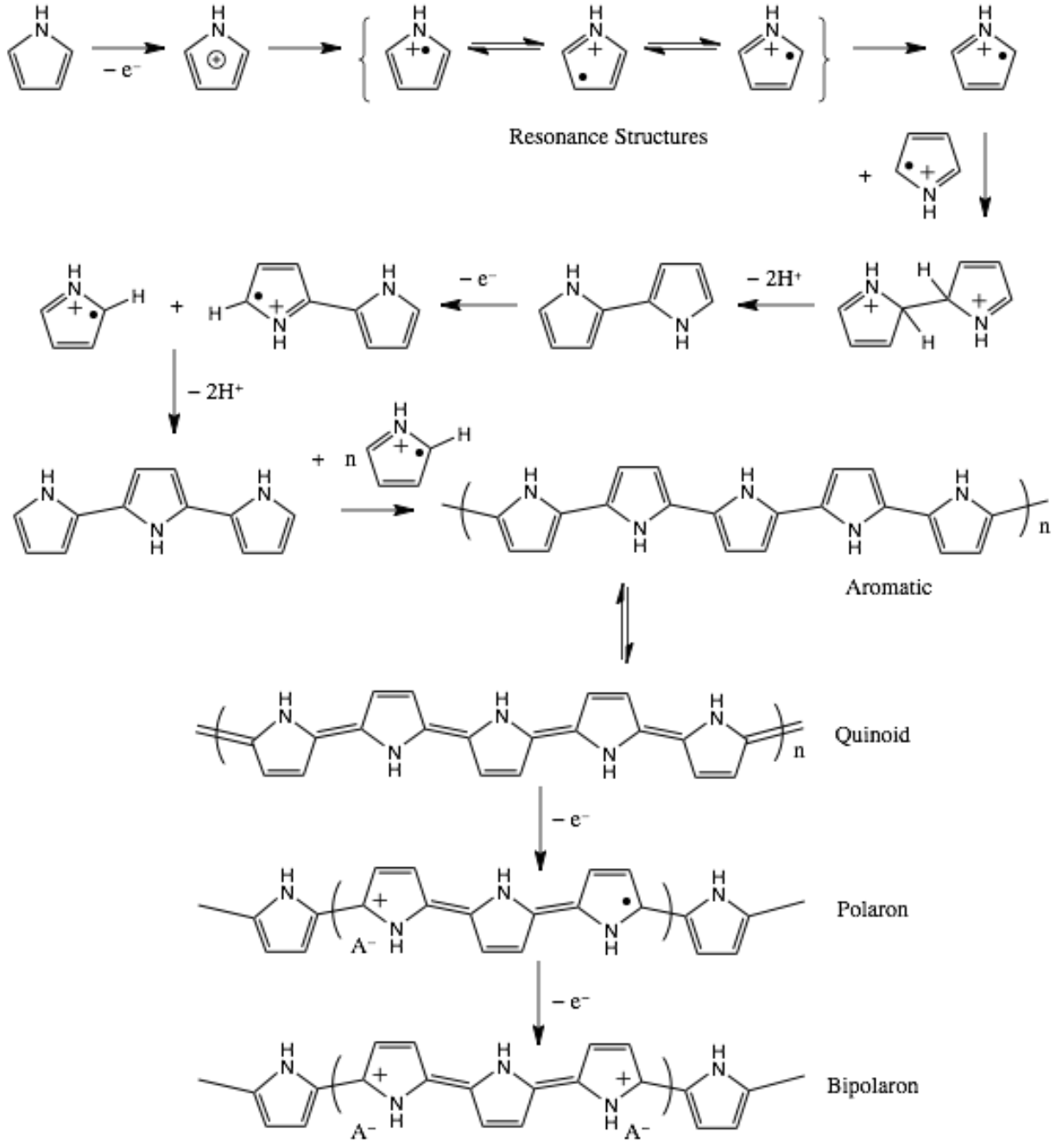

2.6.2 Properties of Polypyrrole

The electrical conductivity of PPy at room temperature varies from 10^{-4} to 10^{2} S/cm, depending on the preparation method. The stability in air of doped PPy is relatively high, but starts to degrade above 150 °C depending on the dopant anion. The PPy films obtained by electrodeposition are relatively brittle; their tensile strength and Young's modulus with different dopants vary from 8 to 100 MPa and 0.4 to 4 GPa respectively.[97] X-ray diffraction investigations indicate PPy is mostly amorphous and usually yields only a diffuse halo. Crystalline domains make up only 15% of the total volume. PPy obtained by chemical oxidation appears as a black precipitate, which is insoluble in water and most organic solvents due to its rigid structure and cross-linking. This makes it extremely difficult to process and functionalize.[100]

2.6.3 Modification of Polypyrrole

To broaden PPy applications, researchers have modified and elaborated its chemical syntheses in many different ways to achieve PPy with desired properties.[101,102] The fabrication of different PPy nanostructures has already been demonstrated since controlled its morphology and shape is a key criterion for integration into microelectronic devices. Several methods of template-directed synthesis have been developed. For example, Zhang *et al*. prepared wire-, ribbon-, and sphere-like PPy nanostructures by using different types of surfactants and lamellar inorganic/organic mesostructure templates formed during in-situ polymerization and automatically degraded after completion of polymerization.[103,104] Other templates including anodic aluminum oxide (AAO), V_2O_5 nanofibers and MnO_2 nanowires, which were adopted to prepare PPy nanotube structures must be removed by solvent etching or chemical reactions.[105]

Another important aspect of PPy modification is electrical conductivity improvement. As a conducting polymer, many of its applications require high electrical conductivity. Thus many attempts namely in-situ modification or post-modification have been made to improve PPy conductivity.[106] For instance, Lim *et al*. incorporated iron oxide nanocomposites as an additive into PPy to give the resulting nanocomposites both magnetic properties and high conductivity.[107] Schnoor *et al*. demonstrated a simple and versatile route to attach PPy to the surface of CNT and subsequently increase the conductivity of the nanocomposites.[108] Chen *et al*. applied chemical oxidation to synthesize graphene quantum dots (GQDs), which can be used to dope PPy and improve its conductivity for high-performance dye-sensitized solar cell applications.[109] Zhang *et al*. prepared PPy/Ni/GNs (nickel graphite nanosheets) composites by oxidative polymerization of Py monomer in the presence of Ni/GNs. The electrical conductivity of such composites reached as high as 5.0×10^2 S/cm, which is two orders of magnitude higher than that of undoped PPy.[110]

Solubility is another drawback that limits the wide application of PPy. In order to improve the PPy processability and dispersibility, Liebscher *et al*. copolymerized pyrrole and 3-(1-pyrrolyl)-propanoic acid to achieve smaller and more uniform particles, that were more soluble in organic solvents and water compared to PPy.[111] Kim *et al*. developed a soluble and conducting PPy doped with dodecylbenzenesulfonate (DBS) sodium salt and covalently linked poly(ethylene glycol) (PEG). The PPy-DBS-PEG composite synthesized by co-polymerization was soluble in m-cresol, in amounts proportional to the DBS molar percentage.[112] Hsu *et al*. prepared PPy/graphene composites through a simple procedure that involved in-situ chemical oxidative polymerization of Py in the presence of various amounts of poly(styrenesulfonate) Such composites processed in this manner exhibited high conductivity, water dispersibility and ethanol

solubility.[113] Although the aforementioned examples combined the merits of PPy with different materials, its poor mechanical and adhesion properties are still major obstacles for further usage. Also, most of the modifications reported in the literature involve harsh post-treatment conditions (low pH, toxic additives and non-environmentally friendly solvents), which drastically damage the biocompatibility of PPy and limit its bio-related applications.

CHAPTER 3. FUNDAMENTAL INVESTIGATIONS OF POLYDOPAMINE THIN FILMS IN DRY AND WET CONDITIONS*

3.1 Introduction

With the rapidly growing demand to miniaturize the devices in biomedical, electronic or energy related industries, thin film technologies have been developed and extensively used in the application of such advanced functional materials as semiconductors, biosensors, corrosion resistant coatings and medical polymers.[114,115] Compared with bulk materials, thin films are almost two-dimensional and have larger surface-to-volume ratios, which make them more sensitive to surface properties and interactions.[116] Many coating strategies exist to deposit thin films with precisely-controlled thickness and functionality: plasma deposition, layer-by-layer deposition, deposition of Langmuir-Blodgett films, monolayer self-assembly and emerging polydopamine (PDA) coating.[44,117,118] Among these techniques, PDA coatings has been proven to be "versatile" and "multifunctional". In order to effectively transfer the PDA coating into engineering applications, the stability, mechanical and adhesion properties of the coating films are almost equally important as the function of the thin film itself. In this article, we report an experimental study of the surface and material properties of PDA thin films deposited on different substrates both in air and in water.

Inspired by the chemistry of the adhesive plaques of marine mussels, dopamine, a biological neurotransmitter, has been found to have a remarkable ability to adhere and self-polymerize to

---

* This chapter has been published in *Biomacromolecules* **2013**, *14*, 349-405.

form a nanoscale PDA film on support surfaces.[2] Dopamine, with the chemical structure of catecholamine, can be regarded as a small molecule mimic of the adhesive component *L*-DOPA, of marine mussels.[6] Based on the assumption that the co-existence of the amine and catechol groups is important for achieving underwater adhesion, dopamine has been proposed and demonstrated by Lee *et al*. as a multifunctional coating for various substrates, including both inorganic and organic materials (Figure 2.1a).[1] Since then, we have seen an increasing interest in the exploration of PDA film in a range of applications, including conventional surface and material engineering and emerging bio- and nanotechnology. Nevertheless, the most fundamental aspect of PDA thin film, its structure, is still under debate at present. The well-accepted dopamine polymerization mechanism is shown in Figure 2.6 (route 1),[67] where catechol is oxidized to a quinone, followed by its structural rearrangement and polymerization; an alternative pathway for PDA formation involves supermolecular aggregation achieved through charge transfer, π-stacking and hydrogen bonding interactions (Figure 2.6, route 2).[40]

Since PDA films contain a high density of functional groups (amino and catechol) on their surfaces, they can be used to immobilize, regulate and sense biomolecules, *e.g.* cells, proteins and amino acids.[58,119] A large number of studies have been conducted on the surface modification with PDA on various substrates for bioengineering, including biomolecule grafting, cell adhesion, biomineralization and drug encapsulation.[66,71,120] These studies have provided strong evidence that the use of PDA films is promising way to modify material surface chemistry. In contrast, the mechanical and adhesion properties of the PDA film are still largely unexplored even though their importance has been realized.[56,121-125] A typical study on this aspect was the contact angle measurement of PDA films, which revealed their hydrophilic nature and the associated surface

energy to be 40 mJ/m^2.[54] The effect of coating temperature and dopamine concentration on hydrophobic polymers has also been investigated. It was shown that the PDA films became thicker with higher coating temperature and dopamine concentration.[8] Our previous research focused on studying the properties of the PDA coating with contact adhesion and adhesive bonding tests. However, these PDA thin film investigations so far have been concerned only with the film itself instead of the influence of the substrates. Furthermore, most of those studies focused on PDA in dry conditions. However, it is important to measure the mechanical and adhesion properties of PDA thin films in wet conditions since this is usually how they are used in bioengineering applications. From our studies and other recent reports in literature, we hypothesize that the material properties of hydrated PDA films are significantly different from those of dehydrated ones, affecting their mechanical stability and functionalities.

The objective of this study is to investigate the mechanical stability and durability of PDA films, which are essential to the successes of their applications. A series of experimental studies were carried out to characterize the PDA thin film coated on three typical well-defined substrates, glass, polydimethylsiloxane (PDMS) and epoxy to investigate the material behavior of PDA films under a mechanical stress/strain field and the effects of coating substrates. Micro-indentation measurements, combined with Johnson–Kendall–Roberts (JKR) contact mechanics theory were used to systematically study the tribological properties (i.e. adhesion, friction and wear) of the PDA thin films when they are dry and immersed in water. We found that the fundamental properties of PDA under water are not equal compared to those exhibited in dry conditions, revealing a significant hydration effect on the surface chemistry and qualities of the coatings.

3.2 Experimental

3.2.1 Materials

The PDMS (Sylgard 184 elastomer kit, Dow Corning Corp.) solution was prepared by mixing the elastomer base and crosslinker at a weight ratio of 10:1. The flat sheet of PDMS was made by casting 2 ml of PDMS solution onto a microscope slide and curing at 90 °C for 1.5 hours in ambient air. The epoxy (322, Dow Corning Corp.) solution used for making elastomers was prepared by mixing the elastomer base and crosslinker at a weight ratio of 100:13. The flat sheet of epoxy was made by casting 2 ml of epoxy solution onto a microscope slide and curing at 70 °C for 10 min and 130 °C for 1 hour in ambient air. The hemispherical tip of PDMS with a diameter of 3 mm was made by first molding the PDMS solution into a hemispherical shape using a custom-made Teflon mold and then coating the resulting tip with another layer of PDMS solution to make the tip surface smooth. The tip core was cured at 90 °C for 15 min and the tip coating along with the core was then cured at 90 °C for 1.5 hours. The radii of the tips were about 2.9 mm, varying slightly from batch to batch; the exact values were determined by analyzing the side view images taken during each indentation test.

The coating of PDA thin films on glass, PDMS, and epoxy substrates was performed inside a petri dish by immersing the substrates in a dilute aqueous solution of dopamine hydrochloride (Fisher BioReagents), buffered to pH 8.5 (2 mg of dopamine per milliliter of 10 mM tris). To minimize the deposition of PDA micro/nano aggregates formed during the coating process, all samples were placed upside down in the buffer solution. After 24 hours of coating, the samples were rinsed with ultrapure water and dried in air or stored in ultrapure water.

PDA nanoparticles were synthesized via the oxidation of dopamine solution (2 mg of

dopamine per milliliter of 10 mM tris) by atmospheric oxygen in an open vessel at room temperature for 24 hours. The black nanoparticles were collected from the solution by centrifugation (8000 rpm) for 15 minutes, then washed with ultrapure water for 3 times, and stored in ultrapure water.

3.2.2 Methods

The surface characteristics of the PDA thin film were examined by optical microscopy (Carl Zeiss Axio Observer. Z1m), scanning electron microscopy (SEM; Zeiss LEO 1550) and two types of atomic force microscopy (NanoWizard II AFM, JPK Instruments AG, Berlin; and Dimension 3100 AFM, Veeco Metrology Group). The adhesion and friction tests were performed on a custom-made micro-indentation apparatus, as illustrated in Figure 3.1. A hemispherical PDMS tip or probe was mounted on a load cell (Transducer Techniques TMO-2) that was attached to a compact nanopositioner (PI P-611. XZS) with a resolution of 0.2 nm and a 100 μm travel distance. The nanopositioner was fixed on a movable linear stage (Newport ESP-MFA-CC) with a range of 25 mm. The movement of the PDMS tip was controlled by the nanopositioner and a displacement controller (PI E-625. PZT). An inverted optical microscope (Carl Zeiss Axio Observer. Z1m) equipped with a CCD camera (Carl Zeiss Axio Cam 1Cm1) was used to monitor the area of the contact spot and its deformations. The load, displacement, contact area and time were recorded using a custom-written LabVIEW program.

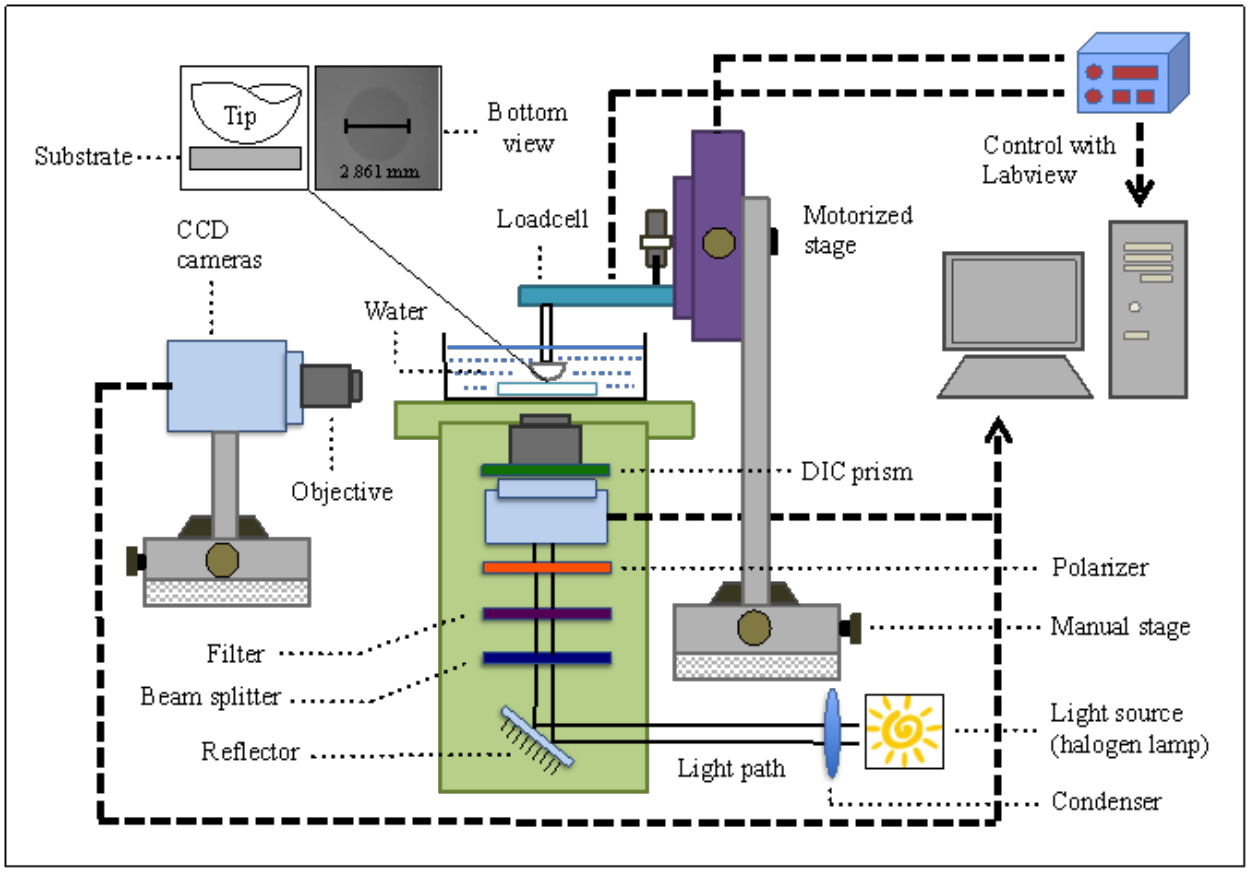

Figure 3.1. Schematic of the microindentation apparatus consisting of a hemispherical elastomer probe attached to a load cell and displacement controllers (a nanopositioner and motorized linear stage), a sample stage (with a water bath) attached on an inverted optical microscope, a standalone side-view camera, and a LabVIEW controlling program with a computer and monitor.

Micro-indentation measurements of the PDMS tip on glass, PDMS and epoxy substrates were done at room temperature. In each experiment, a tip was brought into contact with a flat substrate at 0.1 μm/sec until a preload force of 5 mN, then held in contact for 120 sec and finally refracted at the same speed. The bottom view of the contact spot between a probe and a substrate was recorded during the test. The associated force and contact radius were analyzed in the framework of JKR contact mechanics. For friction tests, a PDMS probe was brought into contact with a substrate until a normal force of 0.1g, 0.5g, 1g or 2g was reached. Then, three cyclic reciprocating lateral movements of the substrate were carried out with a sliding speed of 30 μm/s

while keeping the normal force constant using a force-controlling feedback system. During the underwater indentation and friction tests, a stronger light source, polarizer and image filter were utilized to obtain high quality images of the contact spots. Both tips and substrates were immersed in water for half an hour before testing.

For contact angle measurements, a syringe pump was used to inject and withdraw water or diiodomethane at a constant rate of 100 μL/min on PDA coated epoxy substrates. Advancing and receding angles were measured by expanding the volume of a 5 μL water or diiodomethane droplet and subsequently withdrawing the droplet. The images of the drop were recorded and analyzed by a custom-developed LabVIEW program. All measurements were performed in ambient air at the room temperature.

For gravimetric experiments, three types of PDA nanoparticles were prepared: (1) hydrated PDA prepared by blotting the "free water" from the wet fresh powder with a piece of filter paper; (2) partially-hydrated PDA prepared by evaporating the "surface water" from the first sample in a 95% humidity chamber for 2 days, and (3) dehydrated PDA prepared by air drying the wet fresh PDA powder at room temperature for 5 days. The weight of each sample was measured by an analytic balance with 4 decimal unit accuracy (i.e. 0.1 mg). Three repeats of each gravimetric experiment were performed.

3.3 Results and Discussion

3.3.1 Surface Characterizations of Polydopamine Thin Films

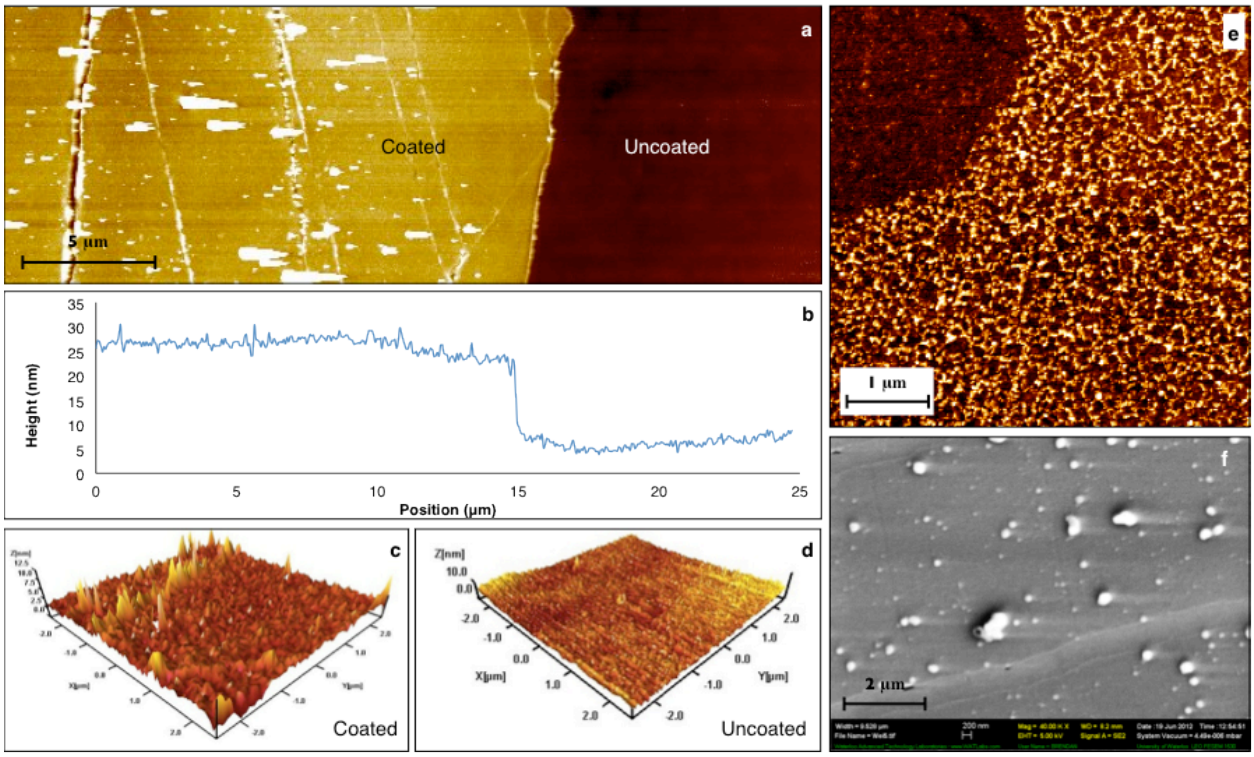

Figure 3.2. Surface characterizations of polydopamine thin films: (a) a typical AFM topography image of PDA-coated and uncoated PDMS substrate; (b) cross-section plot from the AFM image showing the thickness of the PDA film deposited on PDMS substrate; (c) 3-D AFM image of PDA coated PMDS; (d) 3-D AFM image of uncoated PDMS; (e) AFM topography image of PDA coated glass surfaces showing the nano-porous structures of PDA film; the dark area at the left top corner is partially-coated surface; (f) SEM image of PDA coated PDMS surface, showing the micro-sized PDA particles.

The surface qualities of PDA thin films coated on the glass, epoxy and PDMS substrates were characterized by optical, scanning electron and atomic force microscopy. The optical images of the PDA deposited on glass and epoxy surfaces in dry and wet conditions showed a smooth and homogeneous surface. In contrast, numerous micro-sized cracks were present in the PDA film deposited on PDMS surface after dehydration, while no cracks were found when the film was stored in water. The thickness and surface roughness of the PDA thin films were determined by AFM as shown in Figure 3.2a-d. The thickness of PDA thin films deposited on

glass, PDMS and epoxy substrate were found to be 12.4 ± 0.9 nm, 16.5 ± 1.1 nm, and 15.5 ± 0.5 nm, respectively. The root-mean-square (rms) surface roughness was measured for both uncoated substrate and PDA coated surface of the three substrates to be 7.4 ± 0.2 nm and 15.5 ± 0.4 nm for glass, 3.8 ± 0.8 nm and 9.0 ± 2.5 nm for PDMS, and 2.3 ± 0.4 nm and 8.4 ± 0.8 nm for epoxy. These data reveal that the PDA films on the two polymer substrates are thicker and smoother than that on the glass. Figure 3.2e is a high-resolution AFM image of a PDA thin film coated on glass, showing its non-continuous membrane-like porous structure at the nanoscale. This porous structure may have contributed to the relatively high measured roughness, compared to the film thickness. An SEM image of PDA on PDMS substrate is shown in Figure 3.2f, revealing some deposited PDA particles with size ranging from 50 nm to 80 nm. It is likely that the deposition of PDA nanoparticles on the PDA film was inevitable during the polymerization process. The PDA nanoparticles on the substrates may increase the heterogeneity and roughness of the surface, which may further influence the adhesion and friction properties of the film. In this work, we examined the nature of this self-polymerized PDA coating as its own, instead of the ideal (smooth and homogenous) PDA surface.

We further investigated the cracks on the PDA thin film coated on PDMS in dry conditions. Estimated from the AFM topographic images (a typical AFM image is shown in Figure 3.3a), the cracks were about 50 nm in width and 15 nm in depth. The cracking of the PDA films has also been reported on silicon oxide substrate and poly(*L*-lactide) fiber surface in dry conditions by other researchers.[56] In the following, we applied the channel cracking model to explain the cracking mechanism of PDA thin films on PDMS substrates in dry conditions. For a thin elastic film bonded to a thick elastic substrate (Figure 3.3b), the driving force for the growth of cracks is

defined as an energy release rate, as expressed in Equation 3.1:

$$G = Z\frac{\pi}{2}\frac{\sigma^2 h}{E^*} \quad (Equation\ 3.1)$$

where σ, h, and E^* represent the residual stress, film thickness, and plane-strain elastic modulus, respectively.[126] In the case of PDA film, the residual stress comes from the dehydration process during drying. The crack geometric factor Z depends on the elastic mismatch between the film and the substrate, and the precise geometry.[127,128] Beuth calculated Z as a function of the two Dundurs parameters α and β for most practical material combinations and planar geometry: the parameter α characterizes the elasticity mismatch between the film and the substrate as defined in Equation 3.2; its numerical value ranges from −1 (which corresponds to an elastic film on a rigid substrate) to 1 (which corresponds to a rigid film on an elastic substrate). The parameter β is determined by the shear modulus and the Poisson's ratios of both the film and substrate; its value is well approximated by $\alpha/4$.[129]

$$\alpha = \frac{E_f^* - E_s^*}{E_f^* + E_s^*} \quad (Equation\ 3.2)$$

Beuth rigorously calculated $Z(\alpha, \beta)$ values as a function of α (the effect of β on the results is minor and can be neglected) as shown in Figure 3.3c.[130] It is noted that Z does not change significantly when α is negative, but increase rapidly when $\alpha > 0$, especially in the range from 0.5 to 1. Based on his data, we simplified the relationship between Z and α and fit it into a power-law function (Equation 3.3) that is also plotted in Figure 3.3c. This power-law fitting curve overlaps with the Beuth's original plot.

$$Z = 1.2587(1 - \alpha)^{-0.631} \quad (Equation\ 3.3)$$

For comparison, Beuth's original Z_O values and the Z_S values obtained from our simplified

Equations are almost identical (insert table of the Figure 3.3c). In the following, we used Equations 3.1 to 3.3 and the previously determined elastic modulus and surface energy of PDA to obtain insights into the cracking phenomena of PDA films.

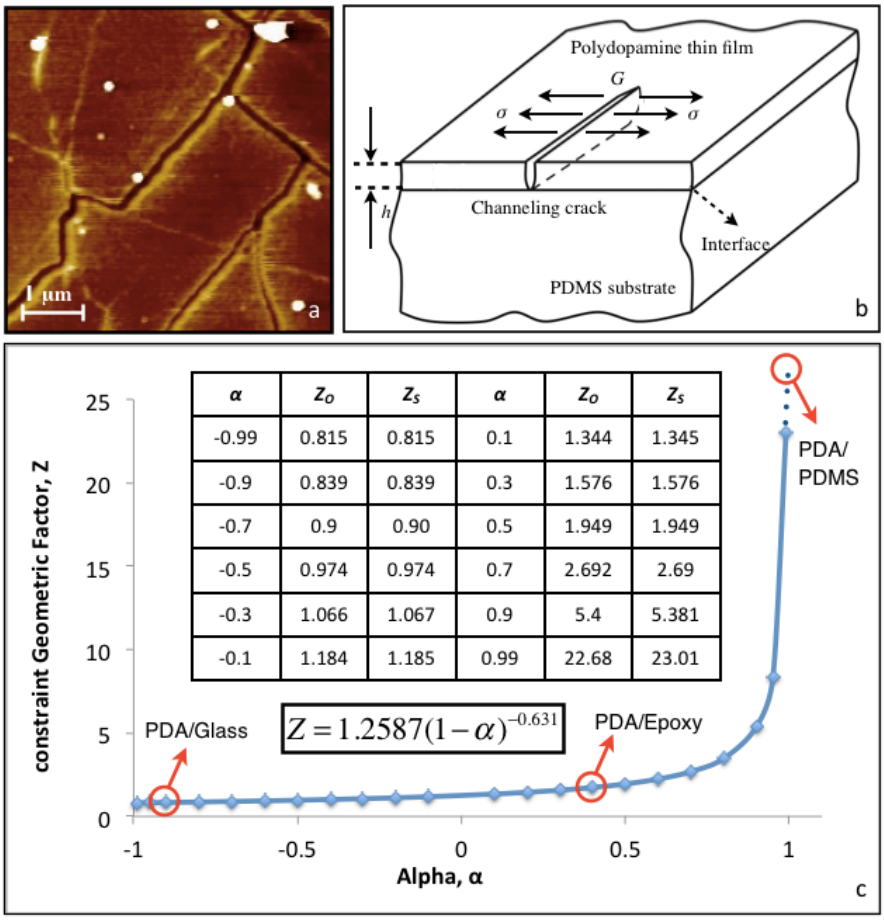

α	Z_O	Z_S	α	Z_O	Z_S
-0.99	0.815	0.815	0.1	1.344	1.345
-0.9	0.839	0.839	0.3	1.576	1.576
-0.7	0.9	0.90	0.5	1.949	1.949
-0.5	0.974	0.974	0.7	2.692	2.69
-0.3	1.066	1.067	0.9	5.4	5.381
-0.1	1.184	1.185	0.99	22.68	23.01

Figure 3.3. Cracking of dehydrated PDA films on PDMS surface: (a) AFM image of PDA thin film cracks on PDMS substrate; (b) illustration of a channel crack in PDA thin film on PDMS substrate; (c) values of function $Z(\alpha)$ with respect to the parameters α, and the comparison with Beuth's original data.

In our previous study, we determined $\alpha \approx -0.8$ for PDA coated glass and $\alpha \approx 0.999$ for PDA coated PDMS.[8] Similarly, for PDA coated epoxy ($E_S^* = 4.57$ GPa),[131] the elasticity mismatching parameter α is determined to be 0.4. The Z values were calculated using Equation 3.3 as shown in Figure 3.3c: $Z = 0.87$ for PDA-glass, $Z = 1.74$ for PDA-Epoxy, and $Z = 98.38$ for PDA-PDMS.

Assuming the residual stress left after drying is the same on the three different substrates, the fact that no cracks formed on PDA-glass and PDA-epoxy suggests that their Z values are not high enough to generate a channel crack. In contrast, the Z value for PDA-PDMS is high enough to drive a channel crack at the same stress. Tentatively, we further the analysis to estimate the residual stress σ during the drying of PDA film by assuming G to have its minimum value, i.e. the work of cohesion of PDA film, $G = W_C = 2\gamma$ (where $\gamma = 40$ mJ/m^2). In this way, the residual stress can be calculated from Equation 3.1 to be 176 MPa. Note that the real residual stress should be far above this value since G is often higher than the work of cohesion.

3.3.2 Adhesion and Contact Deformation of Polydopamine Thin Film Coatings

The work of adhesion is a key thermodynamic parameter for characterizing the interactions between two dissimilar surfaces. We employed two methods (thermodynamic calculation and micro-indentation measurements) to determine the work of adhesion of PDA films and probe the PDMS surface in air and in water. Our purpose was to elucidate the effect of water on the adhesive properties of PDA films. Preliminary tests showed the hydrophobic PDMS tips displayed a moderate adhesion to the substrates, allowing for the examination of the effect of the PDA films.

The Owens-Wendt method was applied to estimate the work of adhesion from the surface energy components of the contacting surfaces.[132] For two surfaces α and β contacting in air (A), assuming air behaves like vacuum, the work of adhesion (W) can be calculated by Equation 3.4:

$$W_{\alpha A\beta} = \gamma_\alpha + \gamma_\beta - \gamma_{\alpha\beta} = 2\left(\sqrt{\gamma_\alpha^d \gamma_\beta^d} + \sqrt{\gamma_\alpha^P \gamma_\beta^P}\right) \quad (Equation\ 3.4)$$

On the other hand, the work of adhesion (W) between the α and β in water (H) is determined as:

$$W_{\alpha H\beta} = \gamma_{\alpha H} + \gamma_{\beta H} - \gamma_{\alpha\beta}$$

$$= 2\left(\gamma_H^d + \gamma_H^P + \sqrt{\gamma_\alpha^d \gamma_\beta^d} + \sqrt{\gamma_\alpha^P \gamma_\beta^P} - \sqrt{\gamma_\alpha^d \gamma_H^d} - \sqrt{\gamma_\alpha^p \gamma_H^p} - \sqrt{\gamma_\beta^d \gamma_H^d} - \sqrt{\gamma_\beta^p \gamma_H^p}\right) \text{(Equation 3.5)}$$

The surface energy data from the literature are given in Table 3.1; the calculated works of adhesion between polymer PDMS and different substrates with/without a PDA coating both in air and in water are summarized in Table 3.2.[6,54,133,134] For uncoated substrates, water increased the work of adhesion for PDMS and epoxy and decreased it for glass. On the other hand, the works of adhesion for the three PDA-coated substrates in both air and in water are identical because the PDA films were assumed to mask the chemical nature of the substrates. These thermodynamic values are used in the following analysis to compare with the experimentally determined results.

Table 3.1. Dispersion (or non-polar) and polar components of different solid/liquid surface energy at room temperature.

γ (mJ/m^2)	γ (mJ/m^2)	γ_d (mJ/m^2)	γ_p (mJ/m^2)
Water	72.2	21.2	51
PDMS-184	18.0	18.0	0
Epoxy	46.2	41.2	5
Glass	69.79	24.79	45
Polydopamine	40	30	10

Table 3.2. The works of adhesion between a PDMS tip and different substrates in air and in water room temperature.

Work of Adhesion (mJ/m^2)	Thermodynamic Work of adhesion		Measured Work of adhesion		Effective Work of adhesion	
	In Air	In H_2O	In Air	In H_2O	In Air	In H_2O
PDMS	36.00	102.36	35.5 ± 1.9	19.5 ± 2.8	67.3 ± 5.1	113.5 ± 4.7
PDA-PDMS	46.46	56.14	36.1 ± 1.1	2.38 ± 0.9	92.6 ± 21.1	46.4 ± 11.7
Glass	42.24	5.92	41.3 ± 1.8	3.6 ± 0.8	119.1 ± 20.2	68.5 ± 17.9
PDA-Glass	46.46	56.14	37.5 ± 2.2	4.8 ± 1.8	104.2 ± 7.3	95.7 ± 6.1
Epoxy	54.46	68.57	40.9 ± 2.1	14.8 ± 0.9	116.9 ± 16.4	164.8 ± 13.1
PDA-Epoxy	46.46	56.14	39.8 ± 2.5	2.1 ± 0.1	112.1 ± 18.1	79.4 ± 11.2

The adhesion contact behaviors of PDA films were investigated by micro-indentation (Figure 3.1) during the compressive loading and the unloading processes. We employed this technique to examine the dynamic adhesive properties of the PDA coating on glass, PDMS and epoxy substrates both in air and in water. Figure 3.4 shows the plots of the compressive force vs. displacement during the loading, contact/holding and unloading processes on the PDA-coated epoxy surfaces at different contact times (a) in air and (b) under water. For all the experiments carried out in dry conditions, the surface force induced a "jump-in" mechanical instability when the surfaces are close enough. While in water, this phenomenon was not observed since the surface forces are much smaller than those in dry conditions. The shape of the "loading" curve did not change while the shape of the "unloading curve" changed significantly with contact time, where the pull-off force increased with time.

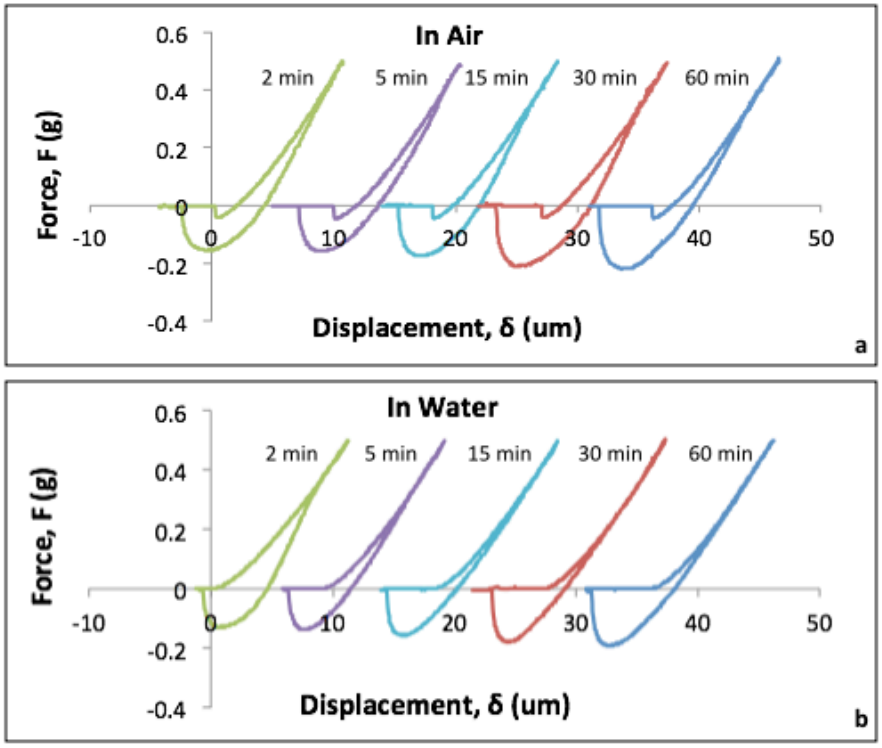

Figure 3.4. Typical plots of the compressive force vs. displacement during the loading, contact/holding and unloading processes of the micro-indentation measurements on the PDA-coated epoxy surfaces at varied contact time (a) in air and (b) in water.

We analyzed these data in the framework of JKR contact mechanics.[135] When a hemispherical probe with radius R and elastic modulus E_1 is brought into contact with a flat surface with elastic modulus E_2, the work of adhesion (W) and the combined elastic modulus (K) are related to the applied load (F) and the radius of the contact area (a) by Equation 3.6:

$$a^3 = \frac{R}{K}\left[F + 3\pi RW + \sqrt{6\pi RWF + (3\pi RW)^2}\right] \quad (Equation\ 3.6)$$

Figure 3.5 plots the typical cubic contact radius vs. force curve for the contact adhesion between two surfaces (PDMS tip on PDA-epoxy substrates both in air and in water). During the JKR experiments, a and R values were obtained by analyzing contact deformation in the bottom view and tip image in the side view, respectively, F was recorded by the LabVIEW program, and W and K were determined by fitting the JKR model to the loading curve using. The values of W obtained this way are summarized in Table 3.2. In dry conditions, the values determined from the micro-indentation experiments are in the same order of magnitude as the ones determined by the Owens-Wendt method. Although the three substrates have varied surface energy and work of adhesion with the PDMS probe, the adhesion properties of their coated surfaces are almost identical, indicating that the nanoscale PDA film masked the surface chemistry of the substrates. In contrast, the measured works of adhesion by indentation test were significantly different from the calculated thermodynamic work of adhesion in wet conditions other than the one on a bare glass surface. The measured works of adhesion on the three PDA-coated surfaces were similar; but they were lower by more than one order of magnitude than those in dry conditions, reflecting the detrimental effects of water on adhesion. It should be noted that although cracks were found on dry PDA-PDMS, no film delamination occurred during the micro-indentation process. Also, since the area of the cracks was approximated to be only about 0.1% of the contact area, the

cracks have a negligible effect on the interactions between the tip and the PDA coating.

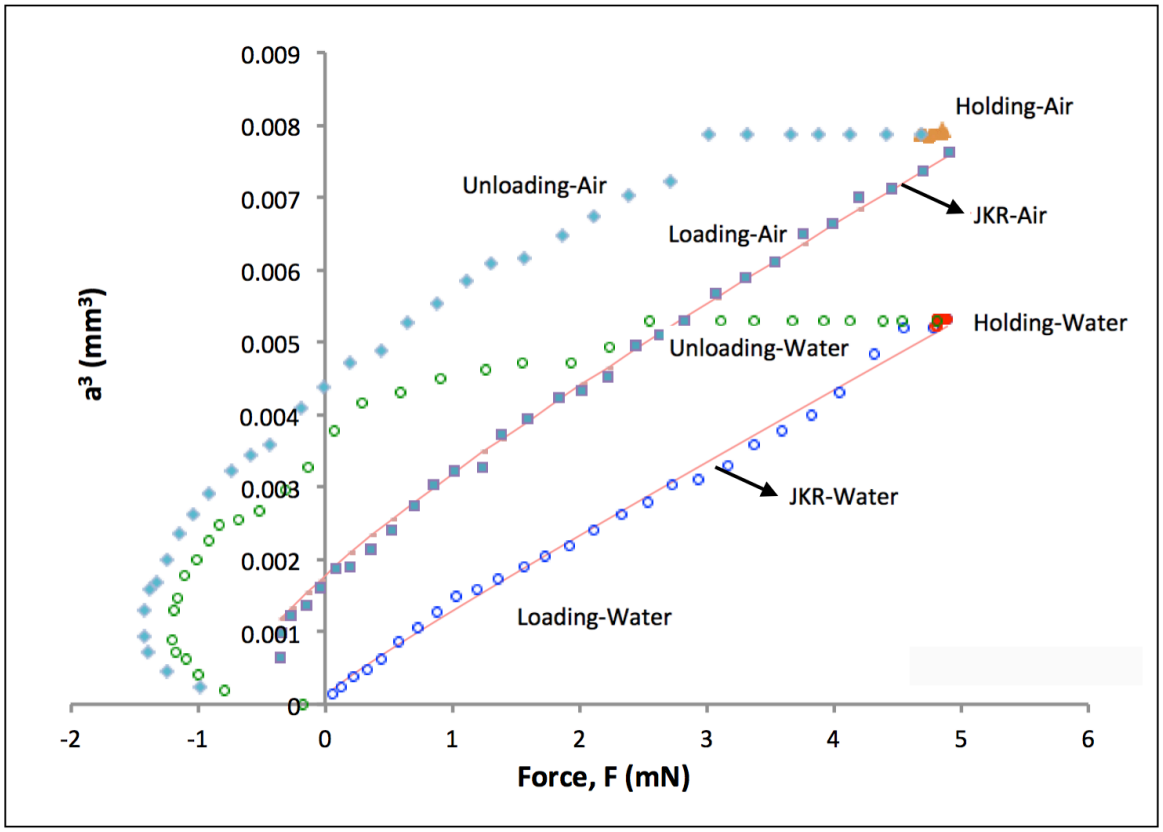

Figure 3.5. Plot of the cubic contact radius vs. the compressive force during the loading, contact/holding and unloading processes of the micro-indentation measurements on the PDA-coated epoxy surfaces in air and water. The solid lines are the JKR fitting curves to the loading process.

As shown in Figure 3.4, the loading curves and the unloading curves were not reversible, i.e., a significant amount of loading-unloading hysteresis. This hysteresis indicates time- and/or load-dependent interactions occurred between the PDA films and the PDMS probe surfaces, which consumed extra energy other than the thermodynamic free energy as predicted by the JKR theory. It is useful to characterize the effective adhesion energy using the adhesive tensile force or pull-off force at the separation. This characterization might provide insights into the dynamic adhesion interactions of the PDA films. To perform further analysis, we extracted the pull-off

force from Figure 3.4 and converted it into the effective work of adhesion (W_{eff}) using Equation 3.7:[18]

$$F_{Pull-off} = \frac{3}{2}\pi R W_{eff} \ (Equation\ 3.7)$$

The effective works of adhesion with 120 s contact/holding time are listed in Table 3.2, which are much larger than the works of adhesion measured from the loading curve. Figure 3.6 plots the effective work of adhesion as a function of the contact time. The effective work of adhesion calculated from unloading is significantly higher than that measured during loading process and increases nearly linearly with contact time both in air and in water. This trend is reasonable considering the hysteresis effect and energy dissipation during the JKR loading-unloading cycle. Also, the changes in the effective work of adhesion with respect to the PDA coating are similar to those of the thermodynamic and measured work of adhesion.

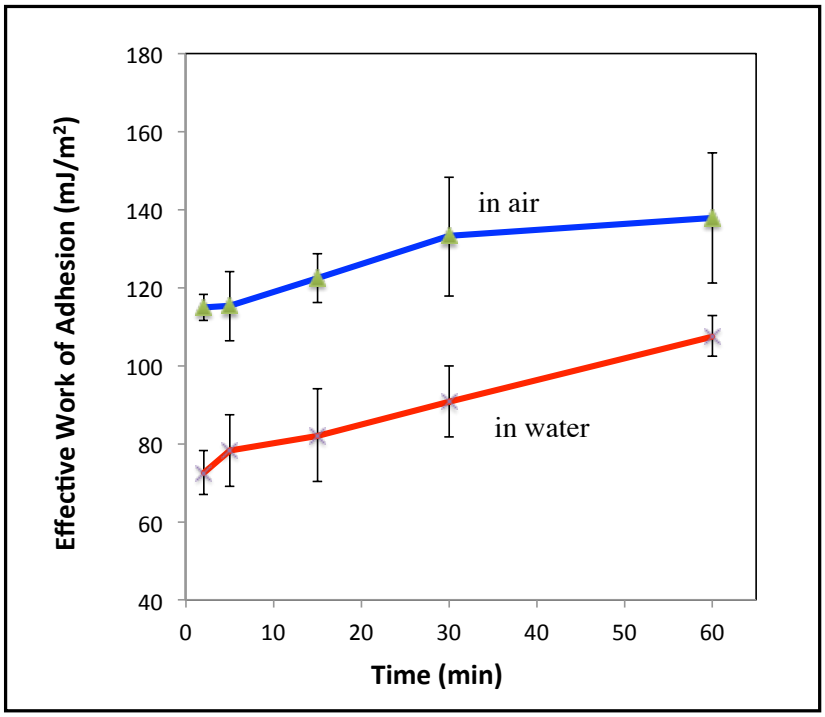

Figure 3.6. The effective work of adhesion $W_{eff} = 2F_{Pull-off}/3\pi R$ as a function of the contact time for the micro-indentation tests on PDA-coated epoxy surfaces in air and in water.

3.3.3 Friction Behavior of Polydopamine Thin Films Coated on Different Substrates

Along with the adhesion properties, friction properties of a thin film are major concerns in the applications of thin films where both the normal loading force and the lateral shearing force are involved. The lateral force may damage the coating or even delaminate the film from its substrate. To the best of the authors' knowledge, no systematic study of the friction properties of PDA thin films has been reported. The lateral motion and force sensing components of the micro-indentation apparatus allowed us to investigate friction properties of the PDA films coated on the three substrates at different preloads. Figure 3.7 shows the friction traces in term of the lateral forces as a function of displacement of the PDMS tip on the PDA-PDMS (Figure 3.7a) and PDA-epoxy (Figure 3.7b) substrates at 0.5 g indentation force in water. The average frictional force decreased with the number of cycles on PDA-PDMS substrate. This suggests that the sliding motion damages the PDA film coated on the PDMS substrate. We did not see the decrease in the friction force for PDA coated on the epoxy and the glass substrates.

Figure 3.7c shows the contact spots obtained from the tests. The contact spot changed during the sliding process irrespective OF the type of substrates: in air, the initially circular contact spot was deformed into a gibbous moon shape became smaller. The sliding caused the PDA film coated on PDMS to crack and delaminate in the region ahead of the contact spot. No invisible cracks or signs of delamination appeared on the films coated on glass and epoxy surfaces. In general, the degree of damage was more pronounced in air than in water on PDMS surfaces.

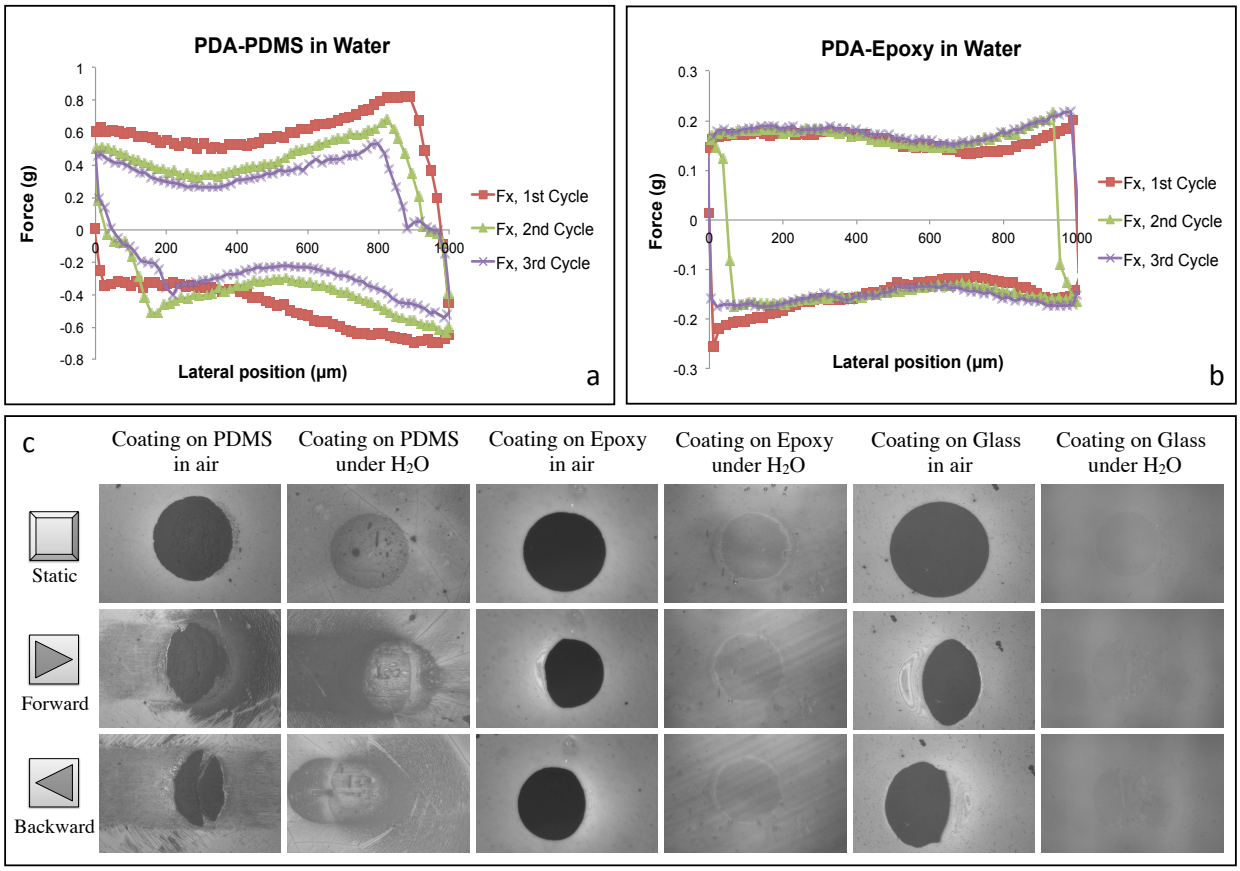

Figure 3.7. The plots of friction force vs. lateral displacement during three cycles of reciprocating friction tests of (a) PDA-coated PDMS surfaces in water (b) PDA coated epoxy in water; (c) optical images of PDA-coated surfaces in dry and wet conditions during reciprocating friction tests including the initial contact (top panels), forward sliding (middle panels), and the subsequent backward sliding (bottom panels).

Figure 3.8 shows the relationship between the load and the friction forces under different circumstances. The friction force F_f was calculated by averaging the values of lateral forces during sliding. It is generally proportional to the load with a finite intercept at zero preload. We applied the classical Amontons' Law (Equation 3.8) to these dataset, and the friction coefficient (μ_A) between a PDMS tip and PDA coated/uncoated three substrates in dry and wet conditions at different loading forces were calculated and summarized in Table 3.3.[136,137]

$$\mathrm{F_f} = \mu_\mathrm{A}\mathrm{F_N} \ (Equation\ 3.8)$$

The Amontons-type coefficient of friction μ_A at the low preload 0.1 g is significantly larger than

those at high preloads, indicating the influence of molecular adhesion on friction. A careful examination reveals that PDA coating significantly reduced μ_A in water for all circumstances but increased μ_A for most situations in air other than the glass surface with 1 g preload. In addition to the Amontons' Law, the Bowden & Tabor theory (Equation 3.9), which added the adhesion component "σ_A" to Equation 3.8, was found to fit the friction behavior of smooth surfaces where the molecular adhesion effect is pronounced.[138,139]

$$F_f = \mu_B F_N + \sigma_A \ (Equation\ 3.9)$$

It should be noted that the coefficient μ_A in Equation 3.8 is not the same as μ_B in Equation 3.9. μ_A can be determined by Amontons' Law on each force point in Figure 3.8 and may vary at different loads, while μ_B is identified as the slope of each line and independent of preload. It appears that Equation 3.9 is more applicable to the friction behaviour of the PDA films, suggesting the nanoscale porous structures of PDA films have not significantly limited the effect of molecular adhesion.

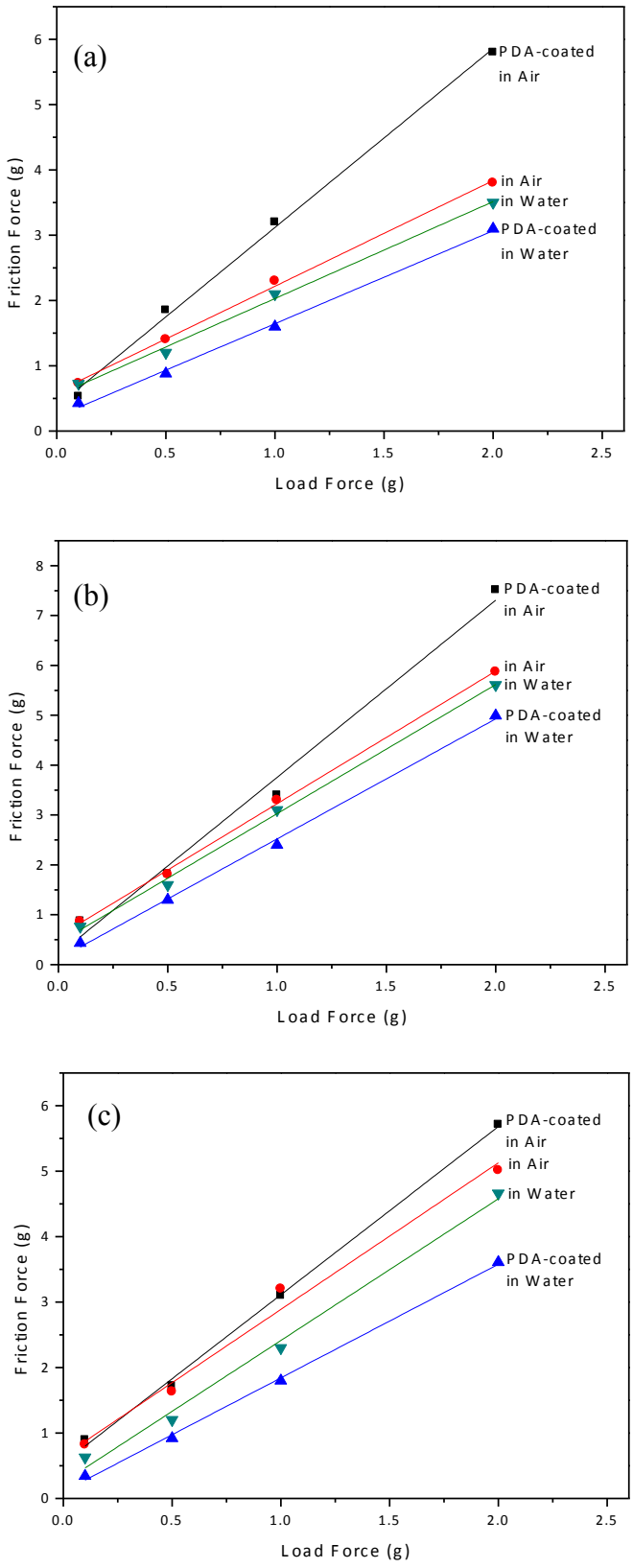

Figure 3.8. Plots of loading forces vs. friction forces on bare and PDA-coated (a) PDMS, (b) epoxy and (c) glass in air and in water.

Table 3.3. The friction coefficient (μ_A) between a PDMS tip and three different substrates (bare and PDA-coated) in air and in water at four different indentation forces.

Friction coefficient (μ_A)	0.1 g		0.5 g		1 g		2 g	
	Air	H_2O	Air	H_2O	Air	H_2O	Air	H_2O
PDMS	5.31	7.26	2.80	2.40	2.30	2.10	1.90	1.75
PDA-PDMS	7.30	4.28	3.70	1.96	3.20	1.60	2.90	1.55
Glass	8.20	6.29	3.26	2.40	3.20	2.30	2.56	2.33
PDA-Glass	8.93	3.44	3.44	1.84	3.10	1.80	2.86	1.81
Epoxy	8.65	7.66	3.62	3.20	3.30	3.10	2.94	2.81
PDA-Epoxy	8.71	4.33	3.64	2.60	3.40	2.40	3.76	2.55

Table 3.4. The adhesion component (σ_A) and friction coefficient (μ_B) between a PDMS tip and three different substrates (bare and PDA-coated) in air and in water.

	σ_A (In Air)	σ_A (In Water)	μ_B (In Air)	μ_B (In Water)
PDMS	0.6	0.55	1.62	1.48
PDA-PDMS	0.38	0.22	2.74	1.42
Glass	0.65	0.25	2.24	2.16
PDA-Glass	0.54	0.11	2.57	1.73
Epoxy	0.57	0.44	2.66	2.59
PDA-Epoxy	0.2	0.11	3.55	2.41

In the framework of Bowden & Tabor theory (Equation 3.9), a detailed examination of the friction behaviours of PDA films was performed and the fiction coefficient (μ_B), adhesion component (σ_A) listed in Table 3.4. For PDA-coated glass and epoxy substrates, water changed both the fiction coefficient (μ_B) and the adhesion component (σ_A); on uncoated surfaces, water influenced σ_A more significantly than μ_B for all three substrates. Compared with dry conditions, σ_A was found to be smaller in water, which indicates that water may deteriorate the adhesion. Moreover, the PDA coating increased μ_B in air, but decreased them in water for both glass and epoxy substrates. These trends are also consistent with the effect that PDA coating brought to μ_A (friction coefficient from Amontons' Law) at different indentation forces. It is also interesting to

note that although Equation 3.9 was not applicable to PDA-coated PDMS, the frictional data plotted in Figure 3.8a fell into a similar trend as the other two substrates. Overall, the lower friction forces and friction coefficients after coating PDA on all three substrates in water suggest that the PDA thin films might function as lubricant in aqueous environment. It is interesting to note that the self-polymerized dopamine is not a good adhesive in water although the dopamine is a "sticky" biomolecule containing the typical functional groups of mussel adhesive proteins.

3.3.4 Hydration of Polydopamine Thin Films

The lubrication function of PDA coatings in water indicates that the PDA films might be highly hydrated. A direct comparison of the behaviour of PDA films in a dry condition and in water supports this indication. First, no crack is observed in PDA films in water while numerous micro-sized cracks occur on the PDA-coated PDMS because of the residual stress due to dehydration. Second, the work of adhesion measured by micro-indentation in the dry condition is similar to the corresponding thermodynamic work of adhesion. In contrast, the measured work of adhesion by indentation test in wet conditions is one order of magnitude lower than the calculated thermodynamic work of adhesion (Table 3.2). A possible explanation for this is that the water molecules may have penetrated or diffused into the PDA film so as to alter its surface chemistry which was not taken into account in the thermodynamic calculation.

The recent water contact angle studies of PDA film coated on PDMS conducted by Yang *et al*. revealed the possible formation of a hydration layer on the PDA film. Herein, we performed water contact angle experiments on PDA-epoxy to further verify the hydration effect of PDA films. Figures 3.9a and 3.9b present the typical optical water drop images of growing and

receding processes during the measurement. The advancing contact angle is 46° and the receding contact angle is about 5°. Thus, the contact angle hysteresis, $\theta_a - \theta_r$ was determined to be about 40°. After the water drop was completely withdrawn, a thin water layer remained on the PDA surface (Figure 3.9c and 3.9d). For comparison, it is noted that the contact angle hysteresis on a PDA-coated PDMS substrate was found to be 60°. Both studies showed a large hysteresis, small receding contact angle, significant pinning effect of the contact line; all of these phenomena are consistent with hydration or other water-PDA interactions. However, it is likely that surface roughness due to the PDA nanoparticles may contribute to the large contact angle hysteresis on PDA-coated PDMS and epoxy substrates. To address this concern, we performed contact angle measurement of diiodomethane on PDA-epoxy surface; diiodomethane is a non-polar organic liquid and is not able to hydrate the PDA surface. The hysteresis of its contact angle on the PDA surface is measured to be only 7° (Figure 3.9e and 3.9f); no diiodomethane trace was left on the PDA-epoxy surface after withdrawing the liquid (Figure 3.9g and 3.9h). Thus, while the roughness may affect the contact angle hysteresis, but in the light of the significantly higher water contact angle hysteresis of 40°, we may conclude that the effect of roughness is minor and the hydration of the PDA thin films is the dominant factor for water contact angle hysteresis.

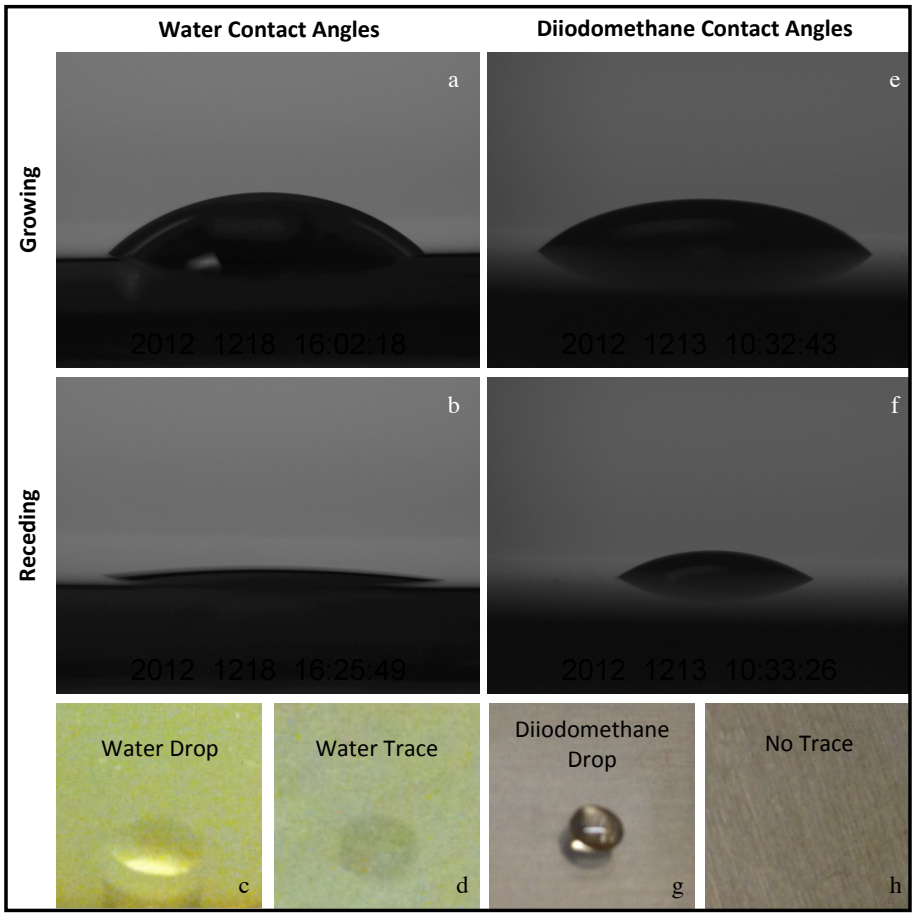

Figure 3.9. (a) Typical optical images of water contact angle at growing state; (b) typical optical images of water contact angle at receding state; (c) typical optical images of diiodomethane contact angle at growing state; (d) typical optical images of diiodomethane contact angle at receding state; (e) water drop on PDA coating; (f) water trace on PDA coating. (g) diiodomethane drop on PDA coating; (h) no trace on PDA coating.

From this study and recent literature, it appears that three types of hydration effects occur, as illustrated in Figure 3.10. First, at the surface, PDA contains many hydroxyl groups, which would attract water molecules to the surface and form hydrogen bonds with water molecules. Second, some water molecules may be trapped in the PDA film during the polymerization. Third, the water molecules can penetrate or diffuse into the porous membrane-like structure of PDA films and hydrate the free functional groups inside the films. All these actions may significantly reduce the rigidity of the PDA films and make it more durable under a mechanical stress field.

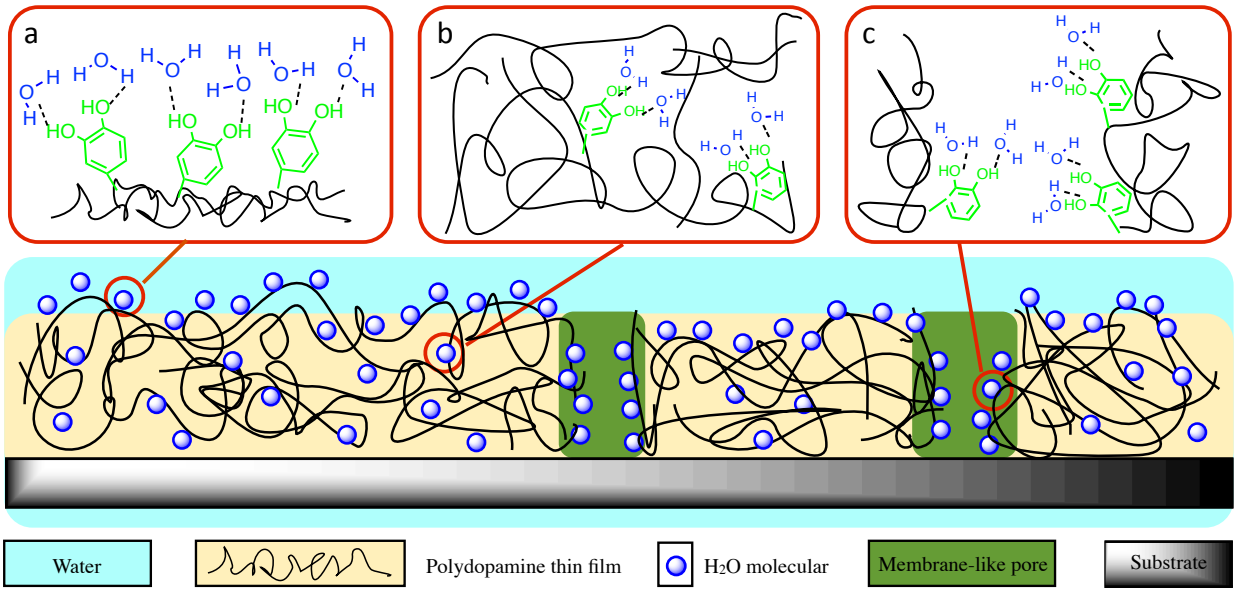

Figure 3.10. Illustrations of the hydration of polydopamine thin films: (a) surface hydration; (b) bulk hydration; (c) diffusion of water into the nano-pores of polydopamine films.

It is noted that the second and third hydration mechanism occur inside the PDA film and almost impossible to distinguish experimentally. Thus, to a first approximation, we may conclude that two types of water associated with hydrated PDA exist: free water and trapped or bonded water. It would be informative to determine the relative amount of these two types of water to further elucidate the hydration effects. For this, we assumed the PDA film and nanoparticles have the same hydration behavior since they formed simultaneously during the self-polymerization of dopamine. Classical gravimetric measurements were performed with collected PDA nanoparticles. The following three samples were prepared their weights measured: (1) hydrated, (2) partially-hydrated and (3) dehydrated PDA nanoparticles. The mass difference between the first and second sample was attributed to the "surface water", which was determined to be 248% ± 40% of the partially hydrated PDA nanoparticle weight. The mass difference between the second and third sample was attributed to the "bonded or trapped water", which was determined

to be 86 ± 5%. To fully elucidate the hydration effects and their technical implications, a high precision microbalance may be required to perform the gravimetric measurement directly on the PDA nanoscale films. We need also to know the chemical structure of PDA, which is still not clear at the moment. However, we may get indirect information from its analogue eumelanin. Eumelanin is a biological complex responsible for the pigmentation of skin, hair and eyes in human, with mechanical, electrical and optical properties that are strongly dependent on its hydration state. Based on the high similarities of these two compounds, it is reasonable to expect that the hydration of PDA films will have significant effects on their mechanical and chemical properties of the PDA thin films.

3.4 Conclusion

We investigated the surface and material properties of PDA films in terms of their morphology and adhesion, friction, wear and cracking properties in both dry and wet conditions. The surface properties were examined by optical, atomic force and scanning electron microscopy, showing a porous membrane-like structure of the PDA films. Micron-sized cracks were found on the PDA deposited on PDMS dry surface, which is imposed by the mismatch of elastic modulus between the rigid film and its soft substrate. Micro-indentation techniques in combination with thermodynamic calculations and JKR contact mechanics analyses were employed to study the tribological behaviors – adhesion in normal direction and friction in lateral direction – PDA films in both dry and aqueous conditions. The measured work of adhesion during loading in air between the PDMS tip and PDA-coated substrates is close to that of the calculated thermodynamic work of adhesion; work of adhesive measured on films immersed in water were

much lower than that the calculated thermodynamic work of adhesion. The adhesive pull-off force or the effective work of adhesion increased with the contact time, suggesting dynamic interactions at the interface. Friction properties of the PDA coating were characterized by both the friction forces and coefficients of friction. A significant decrease of friction forces in water were observed on all three material surfaces coated with PDA, indicating the PDA might serve as a water-based lubrication coating. These research findings revealed a strong hydration effect of the PDA coating in wet conditions, which may be responsible for the observed different adhesion and friction properties in air and in water.

Finally, it might be useful to summarize the technical implications of these research findings on PDA films for their effective transfer into practical engineering application. First of all, the hydrated PDA films are more durable than dry films. Dehydration should be avoided since it may make the PDA film crack and then lose its integrity when coated on a soft substrate. If a dehydrated film is to be used, it would be more appropriate to integrate the PDA coating with rigid substrates such as epoxy or glass. Second, the effective work of adhesion between PDA films and the contacting probe is lower in water than in air; both increase with time, indicating dynamic interfacial interactions. These dynamic phenomena and the effect of medium should be considered when using PDA films as an ad-layer to bond dissimilar materials. It is also interesting to notice the PDA coating reduced the friction coefficient of all three materials under water.

Combined with the hydrophilic and biocompatible nature of the PDA, the PDA coating may potentially function as a water-based lubricant for tissue engineering, e.g., to reduce the contact stresses and protect the biomaterials from wear and damage. We believe this approach may open

new paths for designing electrical devices with particular shape and miniaturized size due to its straightforward coating protocol, biocompatibility and controllable coating thickness.

CHAPTER 4. DOPAMINE FUNCTIONALIZATION POLYPYRROLE FOR IMPROVED ADHESION AND CONDUCTIVITY*

4.1 Introduction

With the rapidly growing demand for advanced electronic devices, interconnection technologies have been extensively used to provide fine conductive pathways between circuit elements in electronic manufacturing and packaging industries.[140,141] In the past decades, tin/lead solders have dominated the interconnect technologies.[142] However, they also are a major environment and human health concern due to the high toxicity of lead.[143,144] Therefore, great efforts have been made to develop novel interconnection materials that can potentially replace the tin/lead solders.[145,146] More recently, electrically conductive adhesives (ECAs) have attracted considerable attention as promising alternatives to provide robust and environmental-friendly bonding solutions in interconnection technologies. Compared to traditional soldering technology, ECAs offer many advantages such as lower processing temperature, simpler processing steps and finer-pitch interconnection. The application of ECAs can also enable new technology developments such as wearable electronics and biological sensor devices.[147-149]

The conventional ECAs typically consist of a polymer matrix that provides mechanical adhesion and good electrical conductivity.[150] The polymer resins are either thermosets or thermoplastics, containing conductive fillers normally consisting of metals such as gold, silver, copper and nickel in various shapes and sizes.[151] Currently, commercial ECAs mainly consist of

---

*Parts of this chapter has been published in *Macromolecular Rapid Communications* **2014**, *35*, 350-354.

epoxy resin and silver micro-flakes. However, due to the lack of connection among silver flakes in the polymer network, their electrical conductivity is too low to completely replace the traditional solders. Moreover, limited current-carrying capability, unstable contact resistance and poor impact and mechanical strength are also major obstacles, which have hindered the wide applications of ECAs as electronic interconnection materials.[152,153] Although the incorporation of silver-based materials (nanoparticles, nanobelts and nanowires) has a synergetic effect on the performance of ECAs, their high cost and complicated synthetic procedures are main drawbacks for wide industrial usage. In this work, we consider the alternation of dopamine-functionalized polypyrrole (DA-PPy) nanofibers their dispersion in solvents and application as a co-filler in epoxy-silver micro flake systems as a hybrid nanocomposite adhesive.

Polypyrrole (PPy) is a unique conducting polymer, which has been extensively investigated because of its relatively low cost, long-term stability and good biocompatibility.[101,154] However, PPy forms as a precipitate that is insoluble in water and in most organic solvents, making further functionalization and processing difficult.[155] Moreover, PPy has poor mechanical and adhesion properties, which are major obstacles for industrial usage. For example, Pyo *et al*. reported the self-delamination of PPy films deposited on actuators.[156]Faverolle*et al*. found that the adhesion between PPy coatings and bare glasses was practically non-existent.[155] Although researchers have been modifying PPy to address this adhesion problem, most of the modifications so far involved harsh post-treatment conditions (*e.g.* low pH, toxic additives and non-environmental friendly solvents). These harsh treatments reduce the biocompatibility of PPy and limit its potential applications. Thus, it is desired to develop a benign approach to modify PPy with good dispersibility and additional chemical and physical properties wider applications.[157]

More recently, inspired by marine mussel adhesive chemistry, researchers have investigated the use of dopamine (DA), a small biomolecule with a structure similar to that of the essential adhesive component of mussel protein, to self-polymerize to form nanoscale polydopamine (PDA) films on almost all support surfaces under alkaline conditions.[1,2,7] Since then, PDA has been intensively studied as a functional coating and adhesion improvement of numerous bio- and nano-related materials, as recently reviewed by Lee *et al*. and Dreyer *et al*.[4,158] In this regard, herein we report the synergetic combination of DA with PPy, to produce additional functional groups that improve the adhesion properties of PPy without limiting its biocompatibility. We found that the combination makes PPy more hydrophilic, so that it can be dispersed in water more uniformly, and unexpectedly, more electrically conductive by almost 2 orders of magnitude. To the best knowledge of the authors, this is the first time DA has been used to functionalize PPy. The new features of DA-PPy make the material stand out as a promising candidate for practical applications in ECA composites. In this work, DA-PPy nanofibers were implemented as co-fillers into the epoxy network; we found that the introduction of a small amount of DA-PPy nanofibers (1 wt%) resulted in a large improvement in conductivity of about 10 times relative to that achieved using conventional ECAs with the same silver flake weight fraction (56 wt%). Furthermore, such a conductivity enhancement can be achieved at a relatively low curing temperature of 150 °C without sintering.

4.2 Experimental

4.2.1 Materials

Pyrrol, ammonium persulfate (APS) and dopamine hydrochloride were purchased from

Sigma-Aldrich and used without further purification. DA-PPy powder was prepared by the following procedure (Figure 4.1). In a typical experiment, 0.05 g pyrrole monomer and 0.05 g dopamine hydrochloride were dissolved in 25 ml tris solution (pH = 8.5, 10 mM) and cooled down to 8 °C on a cooling plate. APS/Tris solution (0.5 g, 5 ml) was added to the DA/Py solution dropwise under vigorous stirring for 18 hrs at a reaction temperature maintained at 8 °C. Finally, the filtered precipitates were collected by centrifuging the resulting solution and sequentially washing with deionized water for 5 times. The washed precipitates were then freeze-dried for 24 hrs to produce powder.

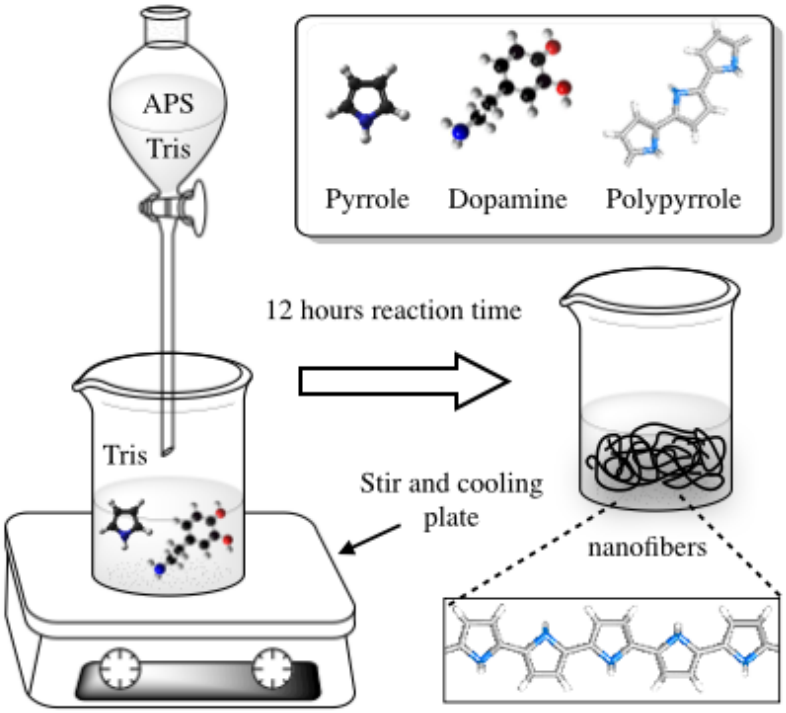

Figure 4.1. In *situ* polymerization setup for the synthesis of DA-PPy nanofibers (the pyrrole solution was in the flask; the oxidant solution was in the dripping funnel).

For the nanocomposite preparation, silver micro-flakes (10 μm, resistivity 1.59 μΩ/cm, density 10.49 g/cm^3) were purchased from Sigma-Aldrich as the main conductive filler in epoxy resin (DER 322; Dow Chemical). Triethylenetetramine (TETA) containing crosslinking agent

(DEH 24; Dow Chemical) was used to cure the epoxy. In a typical experiment, a small amount of acetone (6 wt% of the epoxy) was added to dilute the epoxy and then 5 mg of synthesized DA-PPy nanofibers along with 200 mg of silver flakes were added directly into the epoxy. The composite was agitated for 45 min using a vortex mixer followed by 45 min of sonication. After mixing, the curing agent TETA was added to the composite and the final mixture was poured into amoldof7×7×0.5mm^3 (L×W×D) made by adhesive tape on a pre-cleaned microscope glass slide. To make a smooth surface with controlled thickness, a clean copper plate was placed on top of the mold to squeeze out extra material. The sample was pre-cured for 30 min at 60 °C and then cured at 150 °C for 2 hrs. After curing, the copper plate and adhesive tape were peeled off. The above procedures were also applied to prepare other pastes at different DA-PPy weight ratios.

4.2.2 Methods

The electrical resistivity of the DA-PPy composite and film were measured by a four-point probe setup consisting of a fixture (Cascade Microtech Inc.) and a source meter (Keithley 2440 5A Source Meter, Keithley Instruments Inc.), as illustrated in Figure 4.2. The resistivity can be calculated by the following equation

$$\rho = \frac{\pi t}{ln\, 2} R\ (\Omega \cdot cm)\ (Equation\ 4.1)$$

Where *t* represents the pellet thickness and *R* is the measured resistance.

Washed and dried DA-PPy powder was examined using high resolution transmission electron microscopy (HRTEM, JEOL 2010F FEG) and scanning electron microscopy (SEM, Zeiss LEO 1550) experiments. For the dynamic light scattering (DLS, Malvern Zetasize nano-series Nano ZS90) and Zeta potential tests, freeze-dried powder was re-dispersed in water

before measuring. Fourier Transform Infrared Spectroscopy (FT-IR) measurements were performed on the compressed DA-PPy pellets using a NICOLET AVATAR 360 unit in absorption mode.

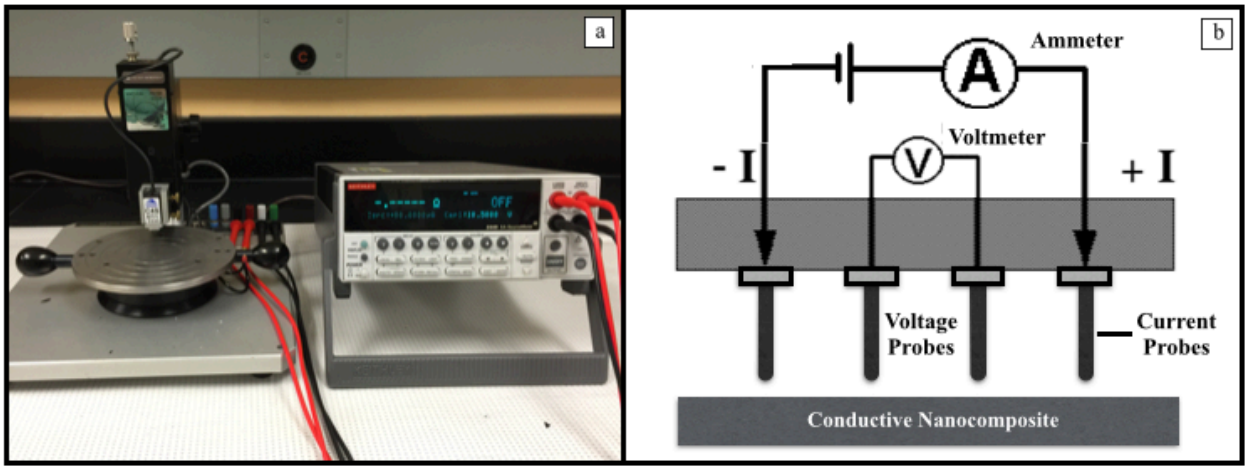

Figure 4.2. (a) Electrical conductivity measurement setup consisting of a four-point probe and source meter; (b) schematic illustration showing the circuit to measure the bulk resistivity of nanocomposites.

For the peel test, 1 ml of DA-PPy solution was directly cast into film on a 2 cm x 4 cm glass slide and dried at 80 °C for 5 hrs The samples were tested within 30 min after taking out from the oven to avoid moisture accumulation on the film. 180° peeling tests were performed using an Instron-like material tester (Texture Technologies Corp.). In a typical experiment, the glass substrate was fixed to a stainless steel panel with double-sided tape. The backing of the tape was attached to the DA-PPy film with about 200 N force to remove any trapped air bubbles. The top of the tape was gently folded back by 180°, and the tape was peeled from the bottom toward top of the film at a speed of 5 or 15 mm/s. The displacement, peeling force and time were recorded by a commercial UMT program for further analyses.

4.3 Results and Discussion

4.3.1 Morphological Characteristics of DA-PPy

The DA-PPy powder structures were characterized by scanning electron microscopy (SEM) (Figure 4.3). Figure 4.3a shows that pure PPy microstructure is globular shape with a diameter of about 300 nm. It is interesting to note that the DA-modified PPy has a fibrous morphology (Figure 4.3b). Although the mechanism of polymerization of DA and the structures of the resulting PDA are still under debate at present, it is clear that the polymerization of DA plays a vital role in the formation of the DA-PPy nanostructure. As the DA/Py mole ratio increases, the fibers become more twisted and tangled and their aggregations become more compact (Figure 4.3c). It is likely that the fibers are coated with PDA though strong hydrogen bonding and π-π interactions between the catechol functional groups of dopamine that are responsible for the better packing. The TEM image (Figure 4.3d) shows the morphology of a single core/shell DA-PPy fiber at 0.64 DA/Py mole ratio. The diameter and length of this nano-fiber are about 50 nm and 1 μm, in agreement with the dimensions estimated from SEM.

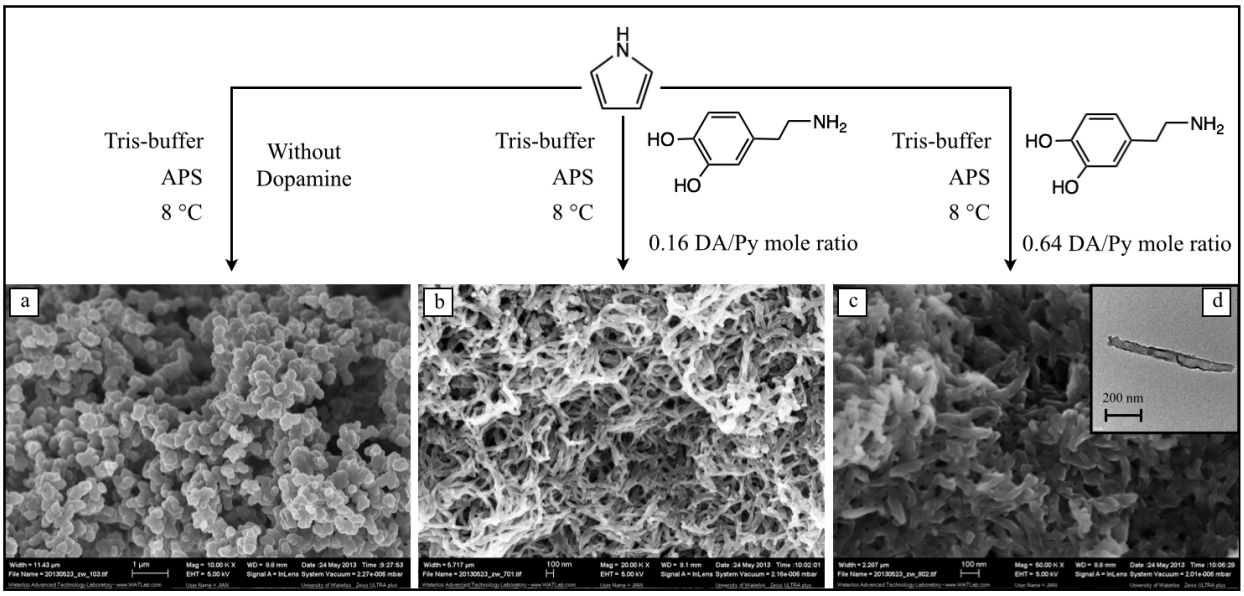

Figure 4.3. SEM images of (a) PPy with globular shape; (b) fibrous DA-PPy morphology obtained at 0.16 DA/Py mole ratio; (c) more compact fibrous DA-PPy morphology obtained at 0.64 DA/Py mole ratio and (d) TEM topography image of a single DA-PPy fiber obtained at 0.64 DA/Py mole ratio.

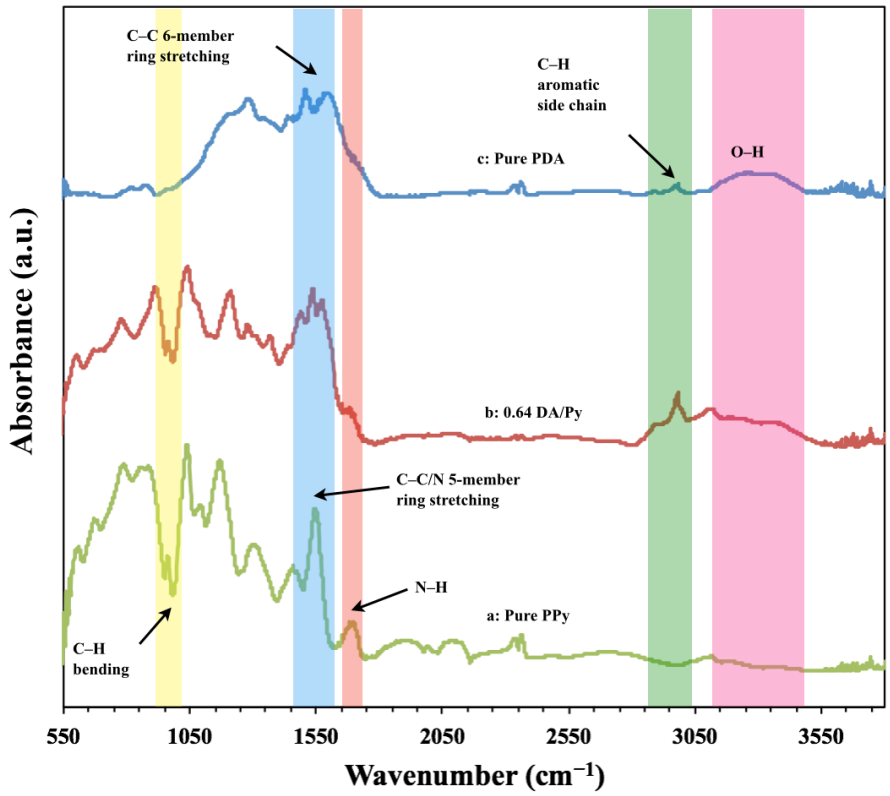

Figure 4.4. FT-IR spectra of: (a) pure PPy, (b) 0.64 DA/Py mole ratio DA-PPy and (c) pure PDA with their characteristic peak assignments.

The FT-IR spectra of pure PPy, DA-PPy obtained at 0.64 DA/Py mole ratio and pure PDA are presented in Figure 4.4. In the pure PPy spectrum (Figure 4.4a), the typical absorbance associated with asymmetric and symmetric ring stretching and C−N stretching are found at 1550 cm^{-1} and 1428 cm^{-1}. The peaks at 987 cm^{-1} and 1023 cm^{-1} region correspond to the C−H in-plane bending vibration.[159] The band of N−H stretching in the Py ring is located close to 1670 cm^{-1}.[160] The characteristic signal of pure PDA (Figure 4.4c) appears at 1495 cm^{-1} and 2946 cm^{-1}, which are due to the C=C stretching in the aromatic ring and C−H stretching of the aromatic side chain, respectively.[40] The broad band in the range of 3040 − 3400 cm^{-1} can be assigned to the peak of hydroxyl functional group.[161] By comparing the three spectra, it can be concluded that DA-PPy (Figure 4.4b) exhibits the characteristics of both pure PPy and PDA, supporting the observation that PDA has been successfully incorporated into the PPy network.

To check the dispersion of DA-PPy particles, 0.005 g washed powder was added into 3 ml of deionized water and mixed in an ultrasonic bath for 5 min. It was found that pure PPy is de-stabilized and precipitates immediately after mixing, while DA-modified PPy tends to remain dispersed uniformly. Figure 4.5a shows a digital image of the dispersion of the DA-PPy powders in deionized water after 6 hrs. It can be seen that a higher DA/Py mole ratio leads to better dispersion, while phase separation occurs at lower DA/Py mole ratio. Dynamic light scattering (DLS) experiments were performed to examine the change of particle size with respect to the DA/Py mole ratio. Note that DA-PPy dispersions at low mole ratio of 0 to 0.064 cannot be measured by DLS due to the aggregation of particles. Figure 4.5b showed that the particle size of DA-PPy decreased from 430 nm to 110 nm as the DA/Py mole ratio increased from 0.16 to 0.64. The result suggests that PPy becomes more hydrophilic with DA modification.

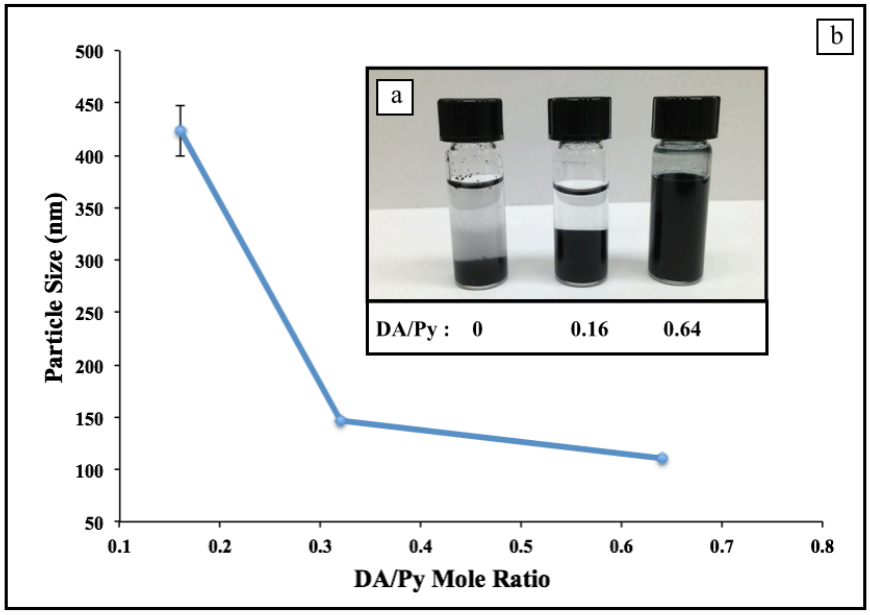

Figure 4.5. (a) Typical plot of practical size verses DA/Py mole ratio of DLS experiment; and (b) digital photo of vials with 3 ml water-dispersed DA-PPy solution after 6 hrs.

4.3.2 Adhesion Properties of DA-Modified PPy

A lack of good adhesion is one of the main problems of PPy films, which significantly limits their applications. To overcome this problem, we combined mussel-adhesive inspired DA with Py. The adhesion of PDA-modified PPy to a glass substrate was characterized by 180° peeling tests with the tape/PPy/glass system. In a typical experiment, 1 ml of a PDA-PPy reacted solution was directly cast into a film by drying the solution on a 2 cm × 4 cm glass slide at 80 °C for 5 hrs. The samples were tested within 30 min after drying to avoid moisture accumulating in the film. To test the bonding strength of the film on the glass, the DA-PPy film was taped by pressing a piece of Scotch tape with a pressure of 20 KPa. The pressure helps remove air bubbles trapped and establish good contact between the tape and the film. The bottom of the tape was gently folded back at 180°and the tape was peeled from the bottom upwards at a speed of 15 mm/s. The

delamination occurred either at the tape/PPy interface or PPy/glass interface. In our system, the peak force, which is defined as the force required to initiate peeling, is utilized to compare the adhesion between glasses and DA-PPy films.

Figure 4.6 presents a plot of the peak force versus DA/Py mole ratio at a constant peeling rate of 15 mm/s. The figure also shows the corresponding tape surfaces after peeling. We observed a clear trend whereby F_p increases with the DA percentage. At 0 and 0.032 mole ratios, interfacial failure mostly occurred at the film/glass interface where most of the film stuck to the tape after peeling. At 0.064 to 0.16 mole ratios, the failure occurred at both tape/film and film/glass interfaces. At 0.32 and 0.64 mole ratios, the failure occurred only at the tape/film interface since the tape after peeling appeared to be clean. It is important to note that pure PPy film can easily delimitate from glass, while the bond between PDA-PPy film formed at 0.64 DA/Py mole ratio and glass becomes so strong that the bond remained intact even at a peeling force of 350 N/m; this significant adhesion improvement can be attributed to the di-catechol functional groups in PDA, which are known for adhesion. Enhanced adhesion and particle dispersion of DA-PPy would make the material more useful for a number of engineering applications.

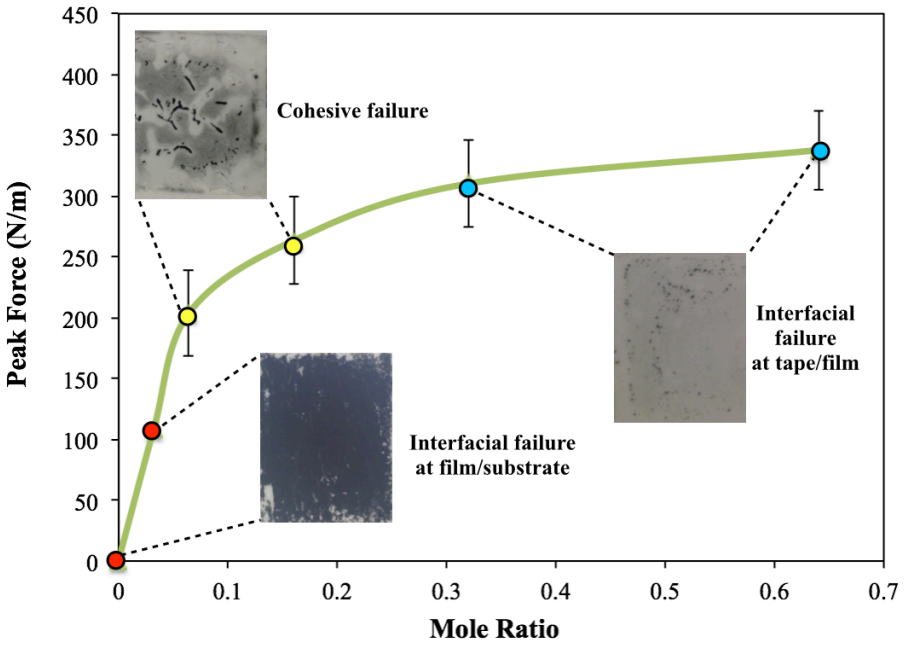

Figure 4.6. Typical plots of peak force verses DA/Py mole ratio at a constant peeling speed rate 15 mm/s, and the digital photo of corresponding tape surfaces after peeling were shown.

4.3.3 Electrical Properties of DA-Modified PPy

The electrical conductivities of PDA-PPy powder in the form of a compressed pellet and solution-casted films at various DA/Py mole ratios were characterized using a standard four-point probe setup to give the results shown in Figure 4.7. It was found that the mole ratio of DA/Py affected conductivity. A maximum conductivity of 3.8 S/cm for the compressed pellets and 0.2 S/cm for the film were measured at a 0.032 mole ratio, which are about two orders of magnitude higher than that of the pure PPy. We attribute the improvement in the PPy conductivity to the fact that PDA is negatively charged with a Zeta potential of −34.7 mV in water, and therefore may counterbalance the positive charge of PPy and act as a "dopant" to further improve the conductivity. The conductivities of PPy drop to 1.5 x 10^{-3} S/cm for the compressed pellets and 1.1 x 10^{-3} S/cm for the film at 0.32 DA/Py mole ratio, and reach almost non-conductive levels at

a ratio of 0.64. It is important to note that PDA by itself has been shown by to be non-conductive by four-point probe measurements of its compressed pellet and therefore, the phenomenon might be explained by the fact that there are more DA at higher DA/Py mole ratio, leading to thicker depositions of PDA on PPy and insulation. The conductivity of PPy compressed pellets has been found to be slightly higher than that of the films. This can be explained that by the fact that the film was directly casted from the product solution without purification to remove unreacted Py, PPy with short chains, and salt, all of which are detrimental to conductivity.

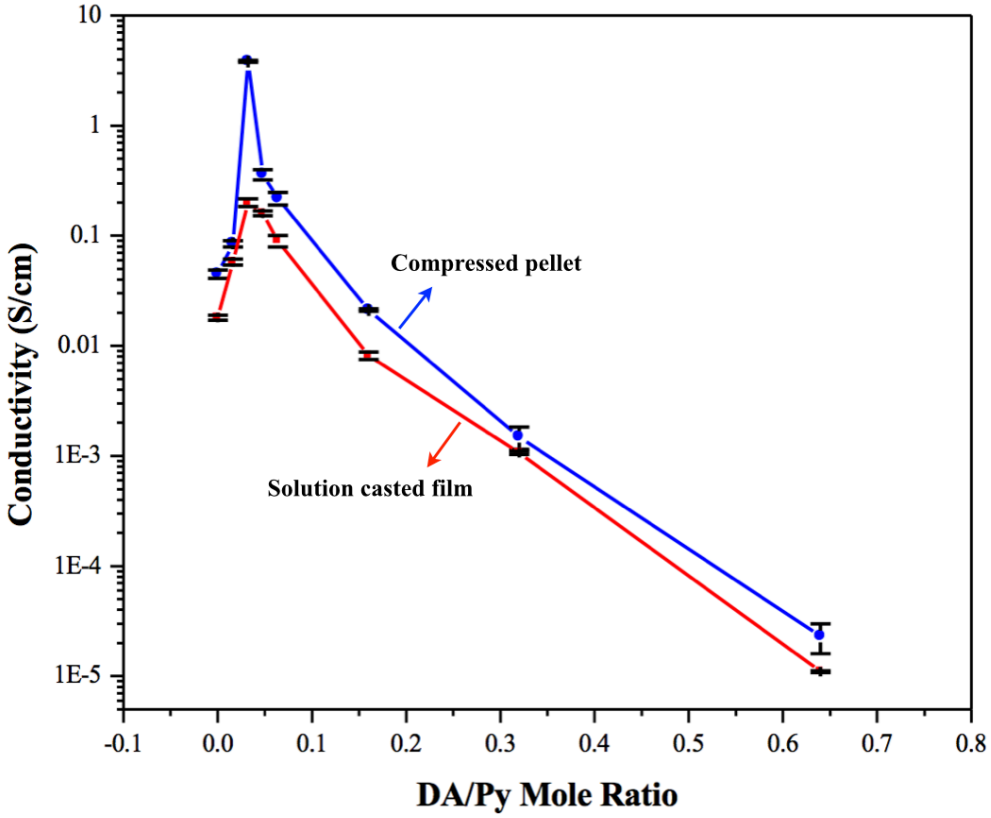

Figure 4.7. Electrical conductivity of the DA-PPy compressed pellets and film at various DA/Py mole ratio.

It is also worthwhile to mention that DA-PPy with higher conductivity can be obtained by combining PPy with other highly conductive materials, such as silver nanoparticles, graphene,

and iron oxides; the applications of these materials in biotechnology are limited due to poor processability, high cost and harsh reaction conditions. To achieve better biocompatibility, conductive PPy/cellulose-derivatives composites with a conductivity ranging from 10^{-4} to 100 S/cm have been prepared and investigated intensively by others. In comparison to the PPy/cellulose composition, our DA-modified PPy materials have similar conductivities but are much easier to prepare and process.

4.3.4 Electrical Properties of the Hybrid Electrically Conductive Adhesives

The improved dispersibility and electrical conductivity of DA-PPy nanofibers make them ideal as a co-filler inside the conventional formulation of ECAs. In order to investigate how DA-PPy nanofibers influence the overall electrical conductivity of the polymer composites, we used conventional ECAs containing only silver flakes at various weight fractions as a control. Figure 4.8 presents the electrical conductivity of conventional ECA versus the silver weight fraction. When the silver flake filler loading level exceeds the percolation threshold (40 wt%), the composites become conductive. the addition of any more silver flakes into epoxy does not significantly improve the electrical conductivity. For all hybrid ECA samples with DA-PPy nanofiber co-fillers, the absolute amount of silver flakes was kept constant, whereas the amount of DA-PPy was increased.

Table 4.1. Electrically conductive adhesive samples and the weight fraction of the silver flakes and DA-PPy cofillers.

Samples	Composition	Silver flakes wt%	DA-PPy wt%
Sample-1	Epoxy + 200 mg silver flakes + 5 mg DA-PPy	58.8	1.5
Sample-2	Epoxy + 200 mg silver flakes + 10 mg DA-PPy	57.9	3
Sample-3	Epoxy + 200 mg silver flakes + 15 mg DA-PPy	57.1	4.3
Sample-4	Epoxy + 200 mg silver flakes + 20 mg DA-PPy	56.3	5.6

Table 4.1 presents the quantities of silver flakes and DA-PPy nanofibers in the composite samples. The addition of DA-PPy nanofibers decreased the silver flake weight fraction from 58.2% to 56.4%, which is small enough not to affect the overall conductivity of the composites. The electrical conductivities of the hybrid ECAs with a fixed mass of silver flakes at various DA-PPy weight concentrations are plotted in Figure 4.8. It can be found that adding a small amount of DA-PPy nanofibers (1.5 wt%) remarkably improved the electrical conductivity to 1077 S/cm, which is 10 times higher than that of the conventional ECA containing 60 wt% silver flakes. The maximum conductivity of 2400 S/cm was achieved at 3 wt% DA-PPy nanofiber concentration. When more DA-PPy was added into the system, the electrical conductivity began to decrease, but still remained one order of magnitude higher than that of the conventional ECA with the same amount of silver. The electrical conductivity decrease at higher DA-PPy concentration can be attributed to the increase in number of contact points (contact resistance) resulting from the presence of more nanofibers, which may counter-balance the electrical conductive pathways that DA-PPy nanofibers added to the ECA.

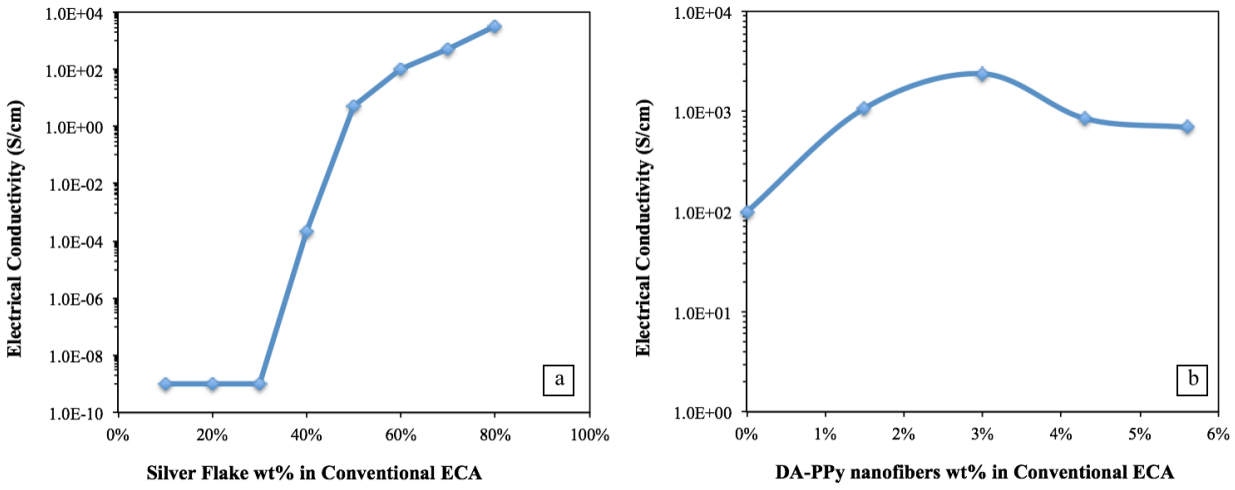

Figure 4.8. Electrical conductivity as a function of filler fraction for both the conventional adhesives filled only with micron silver flakes and the hybrid composites.

Implementation of hybrid filler systems composed of two or more components is one of the most commonly used strategies to develop novel ECAs with desired properties. For example, Jiang *et al*. incorporated surface functionalized silver nanoparticles into the silver flakes/epoxy ECA and low-temperature sintering of silver nanoparticles to decrease the number of contact points in the polymer matrix in order to improve the electrical conductivity of the ECA. Amoli *et al*. prepared a hybrid ECA that consisted of high aspect-ratio silver nanobelts and silver flakes. This hybrid system displayed a superior electrical conductivity comparable to that of a eutectic solder but with only a small amount of silver fillers. Zhang *et al*. combined silver nanowires with silver flakes in the epoxy blend and reported a significant improvement in electrical conductivity of the fabricated ECA. Compared to these studies, we used a conducting polymer instead of silver-based materials as a co-filler to reduce the total amount of silver as well as the final cost. Moreover, the nanocomposite conductivity at 3 wt% DA- PPy nanofiber and 57.9 wt% silver flakes was measured to be 2400 S/cm, which is comparable to that of conventional ECA with 80 wt% silver flake fillers. To obtain insights into the interaction DA-PPy nanofibers of with other conductive fillers within the conductive composite, SEM images of a conventional ECA and a hybrid ECA containing 3% DA-PPy nanofibers were examined. Figure 4.9a shows that silver flakes in the conventional ECA are separated by epoxy, indicating a non-continuous electrical network. In contrast, in the hybrid ECA, DA-PPy nanofibers were distributed evenly throughout the epoxy network without noticeable aggregation as illustrated in Figure 4.9b, c and d. Due to the homogenous dispersion of the nanofibers in the nanocomposite, the separated silver flakes were effectively connected, which led to the overall electrical conductivity improvement.

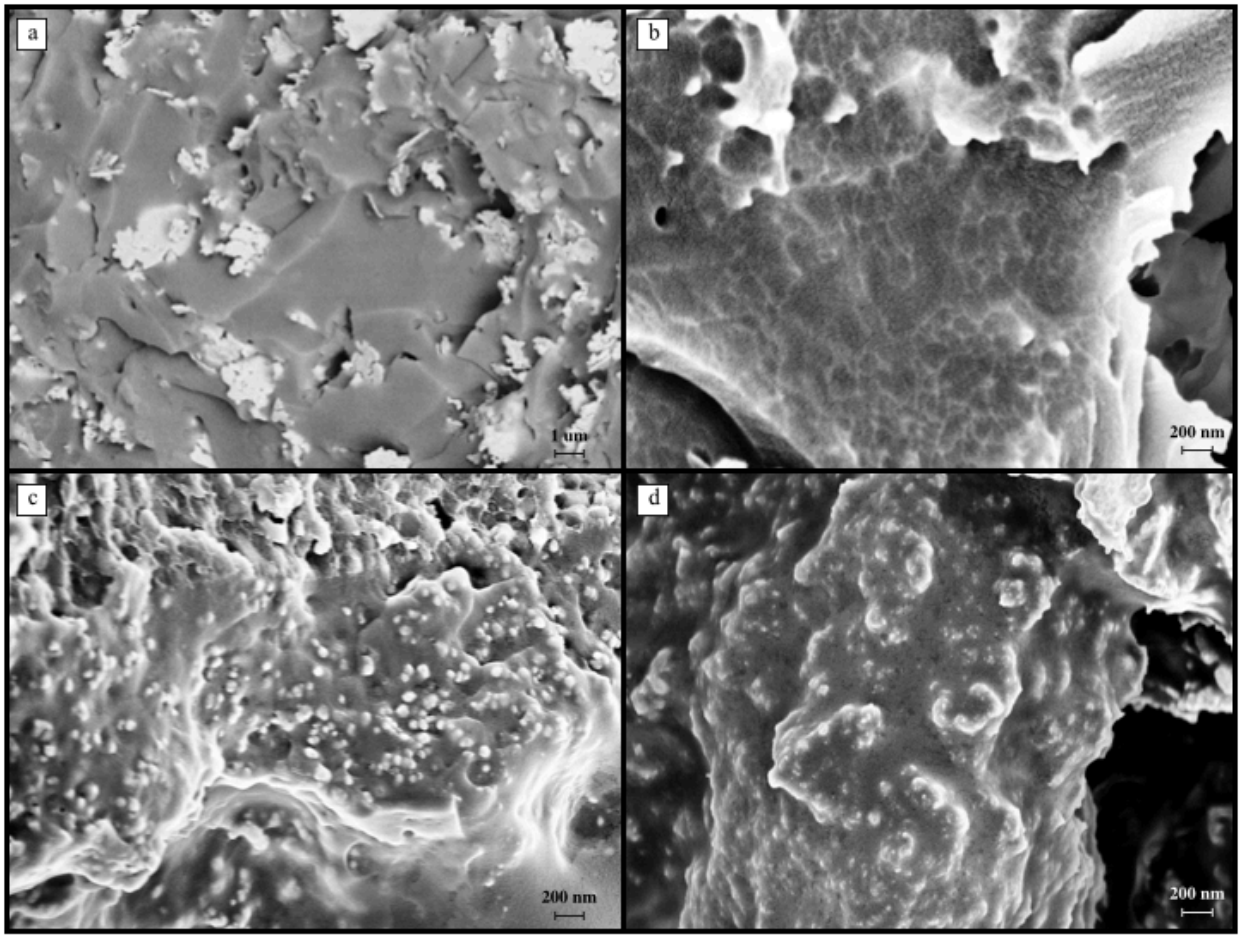

Figure 4.9. SEM images of (a) conventional ECA with only silver flake filler and (b, c and d) hybrid ECA containing 3% DA-PPy nanofibers.

4.4 Conclusion

PPy was functionalized with a "sticky" biomolecule DA. We found that the incorporation of PDA can: (1) change morphology of PPy structure from globular to fibrous; (2) increase adhesion of PPy proportionally to the DA/Py mole ratio; (3) alter electrical properties by raising the conductivity of PPy to a maximum value before decreasing with increasing PDA concentration and (4) decreasing particle size. All of these new features, combined with the biocompatible nature of these two molecules, significantly improved the processability of PPy and broadened their potential applications. Moreover, the modified DA-PPy nanofibers were successfully

incorporated into the system of conventional ECAs consisting of silver flakes and epoxy to make hybrid ECAs. Due to the bridging effect of DA-PPy nanofibers among the silver flakes in the epoxy network, hybrid ECAs displayed much higher electrical conductivity compared to the conventional ECAs. In particular, the introduction of 3 wt% nanofibers into a conventional ECA with 57.9 wt% silver flakes resulted in an electrical conductivity enhancement to 2400 S/cm, comparable to the electrical conductivity of an ECA filled with 80 wt% silver flakes. This functional inorganic/organic hybrid ECA significantly reduced the usage of silver-based nanofillers and may open the possibility of developing the next generation of innovative bio-nano electronic devices.

CHAPTER 5. MECHNISAM STUDY: HOW DOPAMINE AFFECTS POLYPYRROLE ADHESION AND CONDUCTIVITY*

5.1 Introduction

The catechol derivatives, which contain a distinct structure of a benzene ring with two neighboring hydroxyl groups, are found ubiquitously in nature. They exist in a variety of living systems and participate in a broad range of biochemical processes.[30] For example, catecholamines including epinephrine, noradrenaline and dopamine (DA) are biologically significant hormones and neurotransmitters that are responsible for conveying nerve impulses, regulating the heart rate and controlling the brain oxygen supply in the human body.[162] Marine mussels secrete *L*-3,4-dihydroxyphenylalanine (DOPA) containing adhesive proteins to adhere on different surfaces under wet conditions.[6] Catechol-based materials are commonly prepared by self-assembly of catechol functional groups induced by alkaline pH, enzymatic oxidation or electropolymerization. More recently, Ruiz-Molina developed a novel strategy that catechol-based materials can be obtained by the polymerization of functionalized catechols with ammonia, significantly broadening the potential applications of such materials.[163] Catechol moieties are remarkably reactive and can undergo many types of chemical reactions including those summarized in Figure 5.1.[34] The presence of the hydroxyl groups at the *ortho*-position makes this moiety ideal for chelating many di- or tri- valent metal ions to form stable complexes.[21] Also, they can strongly interact with various organic materials through covalent

---

* This chapter has been published in *Advanced Functional Materials* **2015**, *25*, 1588-1597.

bonding, π-π stacking and hydrogen bonding.[25] Moreover, upon oxidation, catechols can be oxidized into semiquinone radicals and o-benzoquinones, which are sensitive to both thiols and nitrogen derivatives such as proteins and amino acid, to form thiol adduct, amine adduct or o-quinonimine via Schiff base formation and Michael type addition under basic conditions.[34] Due to such versatility, catechol-based materials have been subjected to intense investigations, leading to the design and development of a large number of applications in biomedical engineering, nanotechnology and material science.[33]

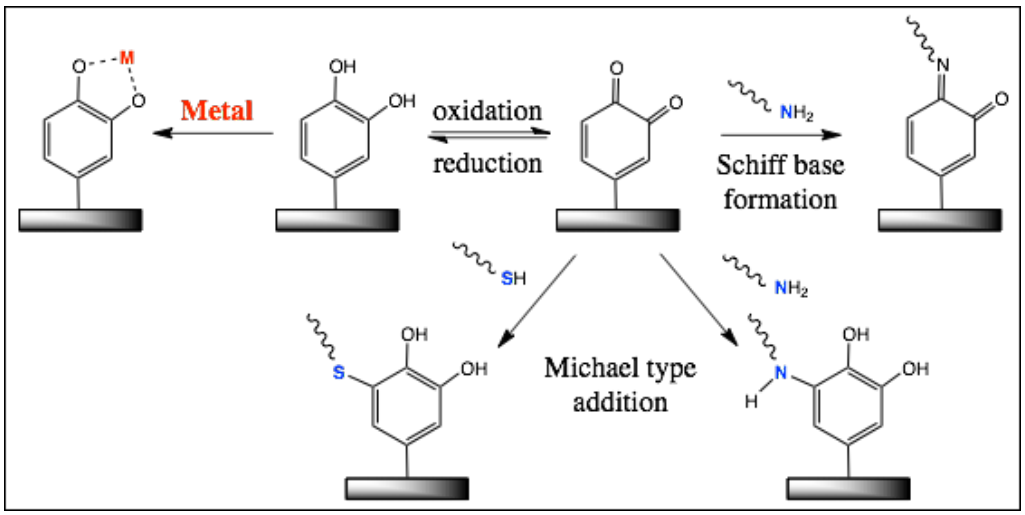

Figure 5.1. Possible chemical reactive pathways of catechol functional group.

Excellent adhesion is one of the most astonishing properties offered by catechol compounds.[164] Great efforts have been devoted to exploiting catechol to enhance interfacial adhesion of synthetic materials.[165] The general strategy of formulating adherent materials is that catechol moieties can either be directly incorporated into the polymer backbone or grafted onto macromolecules as side and end-chain groups. Lee *et al*. prepared a series of linear and branched poly(ethylene glycol) hydrogels modified with one to four catechol end groups, which exhibited enhanced mucoadhesivity that can be used for medical applications.[24] Westwood *et al*. distributed

catechol groups into polystyrene backbone to form a class of block co-polymers with improved adhesive strength.[31] On the other hand, catechols can act as cross-linkers in the framework of 2D or 3D architectures either by self-polymerization or coordination to metal irons. In particular, catechol-functionalized cellulose nanofibers displayed much stronger adhesive forces to inorganic surfaces in the presence of Fe^{3+} ions, which can be attributed to the bridging force provided by the formation of a $Fe(catechol)_3$ complex.[166]

In addition to being used as a universal platform for developing adherent complexes, catechol moieties have also emerged as multifunctional coating materials for the surface modification of various substrates.[5] DA can be oxidized and self-polymerize to form a nanoscale polydopamine (PDA) film on virtually all surfaces at basic conditions.[1] Notwithstanding that the DA polymerization mechanism is still not clear, PDA has arisen as a promising research subject in various fields ranging from the fabrication of energetic coatings to the preparation of functional composite materials.[158] We have applied PDA to the syntheses of functional nanocomposites. We reported some preliminary results of using dopamine to modify electrically conductive polypyrrole (PPy), which resulted in the improved dispersion in water and film adhesion.

PPy displays many striking properties, such as facile synthesis, long-term stability, high conductivity, and good biocompatiablity.[167-169] However, this unique conducting polymer has major downsides: PPy forms large particles that precipitate in water and in most organic solvents, and has poor mechanical and adhesion properties, making it difficult to process and functionalize for practical engineering.[155,156] In the previous studies, we employed in-situ polymerization of pyrrole (Py) with DA, and discovered that the morphology of PPy changed from globular to

fibrous after being functionalized by DA; the adhesion between PPy film and glass substrates was enhanced. In this work, we report a detailed and systematic investigation using three types of bio-inspired catechol derivatives (simple catechol (CA) and DOPA in addition to the dopamine) and 2-phenylethylamine (PA) in the synthesis of polypyrrole (PPy). These studies have provided strong evidence that catechol modification can be applied as a general protocol to functionalize conducting polymers to overcome the problem of poor water dispersibility and low interfacial adhesion. As a result of improved adhesion and dispersion, we demonstrated that modified PPy can be uniformly dispersed into polyvinyl alcohol (PVA) polymer matrix and casted into thin films, that can maintain mechanical integrity at much higher load and stress levels compared with DA-PPy films cast in water. With the capability of resisting mechanical strains and stresses, combined with high conductivity, as-fabricated DA-PPy/PAV coating could find broad applications in electronic device manufacturing.

5.2 Experimental

5.2.1 Materials

Pyrrole (Py, 98%), ammonium persulfate (APS), dopamine hydrochloride (DA), 1,2-dihydroxybenzene (CA), *L*-3,4-dihydroxyphenylalanine (DOPA), 2-phenylethylamine hydrochloride (PA) and polyvinyl alcohol (PVA) were purchased from Sigma-Aldrich and used as received. Modified DA-PPy was prepared by the following procedure. In a typical experiment, 0.12 ml or 0.116 gram pyrrole monomer and certain amount of dopamine hydrochloride (0.01 g, 0.02 g, 0.05 g, 0.1 g and 0.2 g) were dissolved in 25 ml Tris solution (pH = 8.5, 10 mM) and cooled down to 8 °C on a cooling plate. APS/Tris solution (0.5 g/5 ml) was added to the DA/Py

solution dropwise while stirring vigorously for 18 hrs at a reaction temperature maintained at 8 °C. The precipitates were filtered and collected by centrifuging the resulting solution and sequentially washing with deionized water for 5 times. The washed precipitates were then freeze-dried for 24 hrs to produce powder materials. The above procedure was also applied to prepare CA-PPy, DOPA-PPy and PA-PPy nanofibers at different mole ratios.

5.2.2 Film Fabrication

Modified PPy films were prepared by solution casting. In a typical experiment, 1 ml of DA-PPy solution was directly cast into film on a 2 cm x 4 cm glass slide and dried at 80 °C for 5 hrs. The samples were tested within 30 min after taking out from the oven to avoid moisture accumulation on the film. For fabricating DA-PPy/PVA films, 20 wt% DA-PPy dry powders were dispersed in 1 wt% PVA and 2 wt% PVA aqueous solutions, respectively; then 1 ml as-prepared solution was directly cast into film on a 2 cm x 4 cm glass slide and dried at 80 °C for 5 hrs. The film thicknesses of DA-PPy, DA-PPy prepared with 1% PVA and DA-PPy with 2% PVA solutions were measured to be 30 ± 2 μm by an optical profiler (MFP-D WLI 3D surface profilometer, Rtec Instruments Inc, USA).

5.2.3 Methods

After drying, the DA-PPy powders were examined using for high-resolution transmission electron microscopy (HRTEM, JEOL 2010F FEG) and scanning electron microscopy (SEM, Zeiss LEO 1550). In the dynamic light scattering (DLS, Malvern Zetasize nano series Nano ZS90) and UV-Vis spectroscopy (Agilent 8453A) experiments, freeze-dried powder was re-dispersed in

water and measured as quickly as possible to avoid particle aggregation. On average, each spectrum was completely recorded within three minutes. X-ray photoelectron spectroscopy (XPS, monochromatic Al Ka X-ray source, Thermo Scientific Alpha) was used to analyze the surface atomic composition of the modified PPy samples. The electrical resistivity of PPy composites and films was measured by a four-point probe setup consisting of a probe fixture (Cascade microtech Inc.) and a source meter (Keithley 2440 5A Source Meter, Keithley Instruments Inc.). The resistivity was calculated by using a standard method in literature:[170]

$$\rho = F\frac{\pi t}{\ln 2}\times\frac{V}{I}(\Omega\cdot\mathrm{cm}) \quad (Equation\ 5.1)$$

where t, I, V and F represent the pellet/film thickness, applied current, read-out voltage and dimensionless correction factor, respectively. The value of F depends on the ratio of t/s, where s is the probe spacing (s = 0.1 mm). From the four-point probe theory, F equals 1 as t/s approaches 0. In our system, since t/s = 0.1 for pellet and t/s = 0.015 for film, we approximate F = 1.

Peeling tests were performed on the Universal Materials Tester (UMR-1, CERT) shown in Figure 5.2a. A schematic illustration of the 180° peeling is presented in Figure 5.2b. In a typical experiment, a glass substrate was fixed to a stainless steel panel with double-sided tape. The backing of Scotch tape was placed onto the PPy film with about 200 g pressing force to remove the air bubbles between the tap and the film. The top of the tape was gently folded back at 180°; the tapes were then peeled from the bottom toward the top of the film at a speed of 5 or 15 mm/s. The displacement, peeling forces and time were recorded by a commercial UMT program for further analyses.

Scratch tests were performed on the same Universal Materials Tester (UMR-1, CERT) shown in Figure 5.2c. A schematic illustration of the scratch tests is presented in Figure 5.2d. The

scratch indenter was an ASTM standard 1 mm diameter stainless steel ball, which was mounted to a 10kg load cell. In a typical experiment, the indenter was brought into contact with a substrate at a speed rate of 5 μm/s until a normal force of 1g was reached. Then, the indenter was moved 20 mm horizontally along the film surface at a sliding speed of 0.1 mm/s while increasing the normal force linearly at a rate of 25 g/s to a maximum of 5 kg. The scratch track was then examined under a digital microscope (AD4113ZT, Dino-Lite) and analyzed by ASTM standard methods (D7027-test mode A).

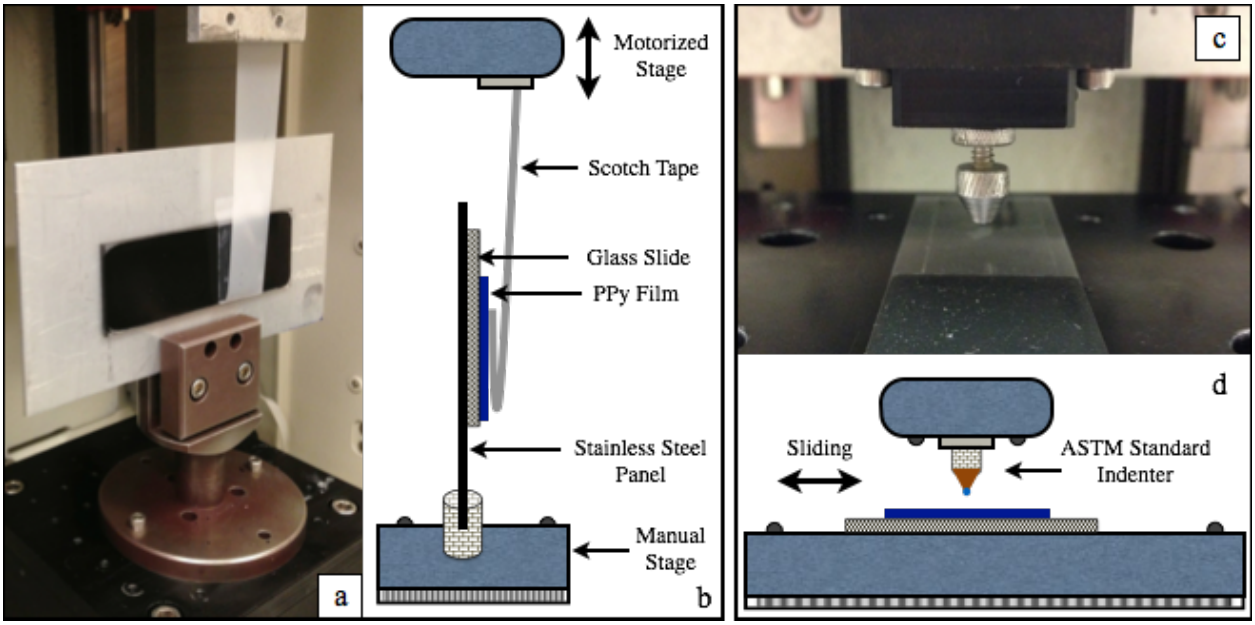

Figure 5.2. (a) Digital photo of a typical peeling test set-up; (b) A schematic illustration of the 180° peeling test; (c) digital photo of a typical scratch test set up; and (d) a schematic illustration of the scratch test.

5.3 Results and Discussion

5.3.1 Morphological and Structural Characteristics of Functionalized PPy

To investigate the effect of different functional groups (di-catechol and amine) on the morphologies of the resulting PPy nanostructures, pyrrole was polymerized in the presence of each of the following species: DA, CA, DOPA and PA. All the experiments were carried out

under the same reaction conditions so as to compare the modified PPy powder structures. SEM images of these structures are shown in Figure 5.3. As evident in Figures 5.3a, 5.3b and 5.3c, PPy modified by DA, CA and DOPA exhibits fibrous morphology, while the nanostructures of PA-modified PPy is globular with features having a diameter of about 250 nm (Figure 5.3d) and is almost identical to that of pure PPy. The PPy fibers obtained by reacting with catechol derivatives are twisted, tangled into compact aggregates due to the strong hydrogen bonding and π–π interactions. Further analysis of individual fibers by TEM as (Figure 5.3e, f, g), it shows that they have a diameter ranging from 40 nm to 70 nm and a length up to 1 μm. The TEM image in Figure 5.4a shows a single DA-PPy fiber morphology obtained at a 0.64 DA/Py mole ratio. Higher resolution images reveal a core/shell structure of the fiber (Figure 5.4b) and the coating shell (Figure 5.4c). These images suggest possible phase segregation between PPy and catechol. The fabrication of fibrillar PPy has already been demonstrated in previous studies since controlling the morphology and shape is a key criterion when integrating PPy into microelectronic devices. For example, Martin *et al*. prepared PPy tubes using an anodic aluminum oxide (AAO) template;[171] Manohar*et al*. reported the syntheses of PPy nanotubes with narrow pore size (10 nm) using a V_2O_5 nanofiber template;[104] Wu *et al*. employed MnO_2 nanowires as a reactive template to yield PPy fiber.[172] However, these approaches are allsomewhat complicated since they require removal of sacrificial templates. Our approach is rapid, one-step, in-situ and template-free; it provides an alternative strategy for the facile production of PPy nanofibers.

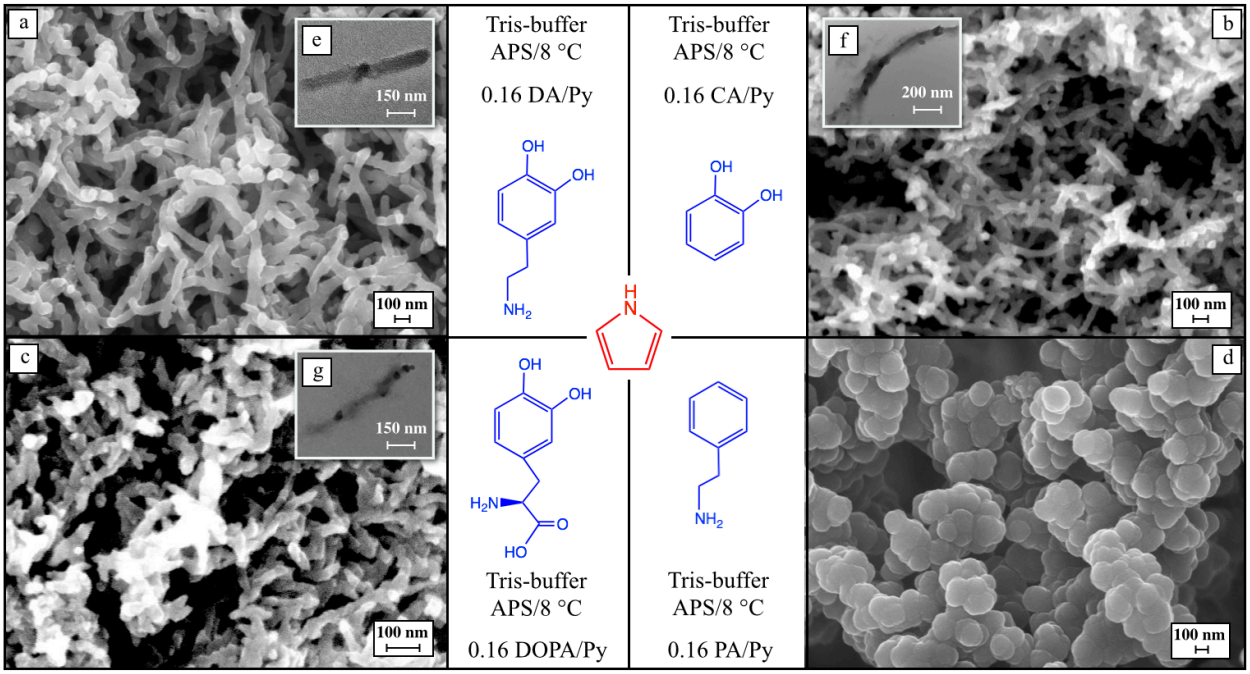

Figure 5.3. SEM images of (a) fibrous DA-PPy morphology; (b) fibrous CA-PPy morphology; (c) fibrous DOPA-PPy morphology and (d) PA-PPy with globular shape. TEM topography images of a single fiber resulted from (e) 0.16 DA/Py reacting mole ratio; (f) 0.16 CA/Py reacting mole ratio; and (g) 0.16 DOPA/Py reacting mole ratio.

Since no template guides the Py growth, we attributed the formation of catechol-PPy fibrous structures to the following phenomena and facts as observed in our experiments and reported in the literature. First, as revealed in Figure 5.3, the fibrillar morphology of catechol-PPy can only be obtained by in situ polymerization of Py in the presence of catechol derivatives. Thus, those catechol-PPy fibers likely contain catechol derivatives. Second, during the polymerization process, di-catechol functional groups can be oxidized to o-quinonimine, which can chemically react with the Py ring to minimize the formation of interchain links and side chains in the PPy network.

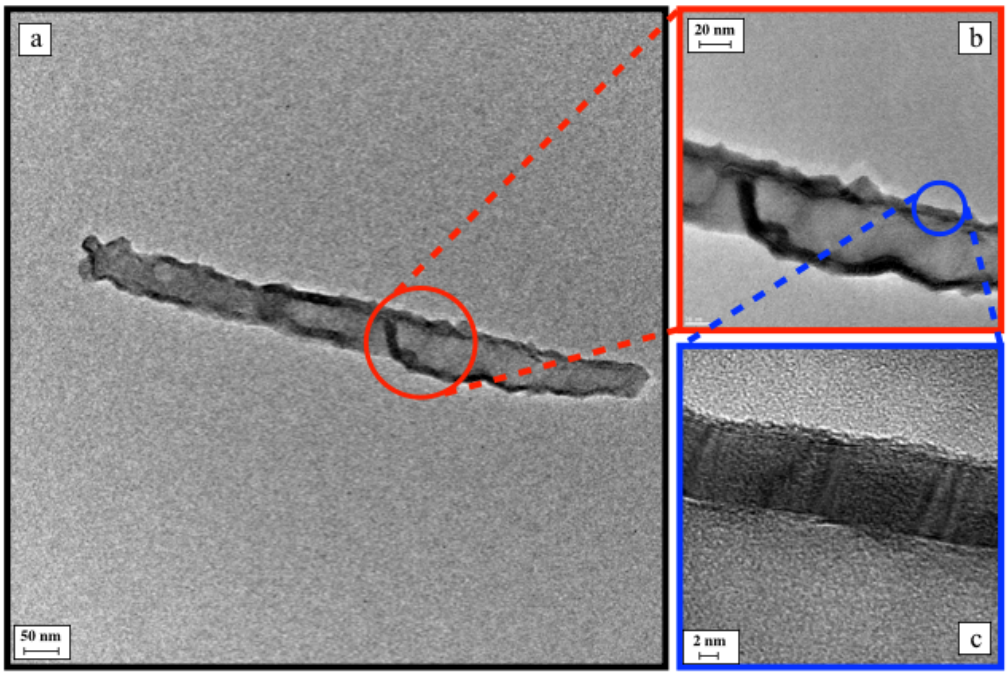

Figure 5.4. (a) TEM topography image of a single DA-PPy fiber resulted from 0.64 DA/Py reacting mole ratio; (b) the core/shell structure of the DA-PPy fiber; (c) a detailed image of the PDA coating.

Figure 5.5a illustrates the chemical structures of possible interchain links (connecting the nearest PPy backbones) and side chains (connecting to one PPy backbone) through 2,3/3,3 coupling of the Py.[173] Although most of the PPy chains are straight and Py rings are linked at the 2,5 positions, Pfluger and co-workers found that 33% the Py rings were structurally disordered (cross-linked or chain-terminating) based on X-ray photoelectron spectroscopy (XPS) studies.[88]Thus, by reacting with o-quinonimine functional group, *β*-sites of the Py can be blocked to ensure a complete *α*-*α* linear chain, leading to an ordered fibrous structure. Due to the universal driving force by surface energy minimization, the long hydrophobic polymer chains tend to entangle and twist in water. In the case of pristine PPy, this phenomenon may be more pronounced because of the strong hydrogen bonding and π-π interactions between each Py unit (Figure 5.5b). Therefore, pristine PPy exhibits granular morphology. However, after incorporating catechol derivatives, PPy polymer chains became shorter, more hydrophilic and

more sterically hindered. All of these changes may effectively prevent the agglomeration and entanglement of PPy chains and lead to the fibrous morphology of catechol-PPy.

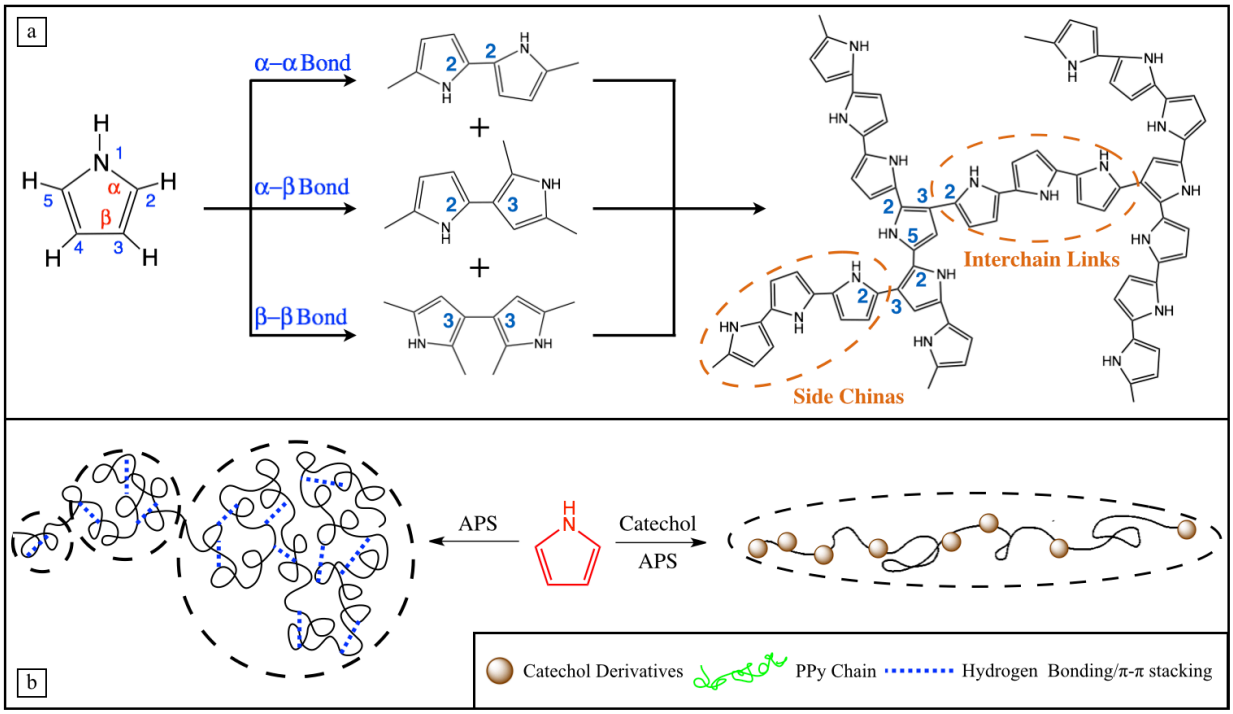

Figure 5.5. (a) Chemical structures of interchain links and side chains, and their formation mechanism, (b) a schematic illustration PPy globular and fibrous morphology formation.

DLS analyses were performed to investigate the effect of the catechol/Py mole ratio on the hydrodynamic diameter of the corresponding dispersion. Note that catechol-PPy synthesized with low catechol/Py mole ratios from 0 to 0.064, PA-PPy and pristine PPy could not be measured by the DLS due to the rapid aggregation of the particles. Figure 5.6a shows that the hydrodynamic diameter of DA–PPy, CA-PPy and DOPA-PPy decreases from 430 to 110 nm, 420 to 220 nm and 380 to 250 nm, respectively, when the catechol/Py reaction mole ratio increases from 0.16 to 0.64. The smaller hydrodynamic diameter at higher catechol/Py mole ratio may contribute to the better dispersion of functionalized PPy. To examine the dispersion of modified PPy, the pristine PPy, DA-PPy, CA-PPy, DOPA-PPy and PA-PPy composites were separately mixed in water. After

ultrasonication for 5 min, the samples were allowed to rest at room temperature. Figure 5.6b presents digital photos of each dispersion in deionized water after 5 h. Both the pure PPy and PA-PPy mixtures became unstable and precipitated immediately. By contrast, the catechol derivative-modified PPy formed excellent water dispersions due to the presence of the hydrophilic catechol groups. Moreover, for these composites, a higher catechol/Py mole ratio also led to better dispersions. The improved water dispersibility of the catechol-modified PPy composite is beneficial for its applications in practical engineering.

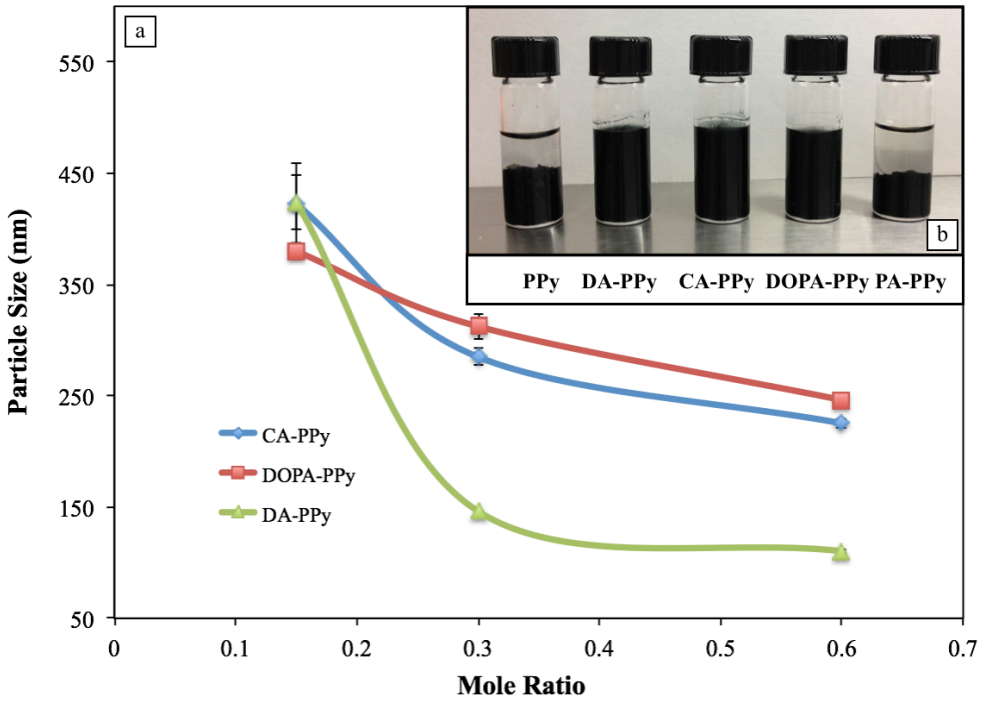

Figure 5.6. (a) Effect of catechol/Py mole ratio on hydrodynamic radius determined by DLS and (b) digital photo of vials with 3 mL water-dispersed pure and modified PPy suspension after 5 h.

To further analyze the PPy system, we performed X-ray photoelectron spectroscopy measurements on pure PPy and (DA, CA, DOPA and PA)-PPy composites at different compositions to obtain their surface compositions. The oxygen content of DA-PPy increased from 22.3% to 28.4%, CA-PPy increased from 19.9% to 23.6% and DOPA-PPy increased from

19.1% to 21.9% when the catechol/Py reaction mole ratio increased from 0.032 to 0.64. Due to the fact that no oxygen species is contained in pristine PPy, the oxygen content increase is presumably due to the fact that catechols were successfully grafted onto the PPy surface, likely through both covalent and noncovalent forces (charge transfer, π-stacking and hydrogen bonding interactions). Furthermore, compared with pure PPy, the N/C atomic ratio increased for all three catechol derivatives modified PPy at 0.64 catechol/Py reaction mole ratio, which is consistent with the theoretical values that catechols have higher N/C ratio than PPy. The above results further confirmed the presence of catechols on the modified PPy surface. For PA-modified PPy at both low and high PA concentration, no significant changes on the surface composition are observed compared with pure PPy, indicating PA had a negligible influence on PPy structure. It is noted that the pure PPy surface showed the presence of oxygen (530 eV, O 1s) and sulfur (170 eV, S 2p), which might be introduced from the oxidizing agent ammonium persulfate.

5.3.2 Adhesion Properties of Functionalized PPy

Our previous research findings indicated that the adhesion strength between DA-PPy film and a glass substrate was significantly improved by combining mussel-adhesive inspired molecule DA into the PPy nanofibers. In this work, we investigated the adhesion properties of DA-, CA-, DOPA- and PA-modified PPy films, respectively, and determine which functional component is critical for achieving strong adhesion.

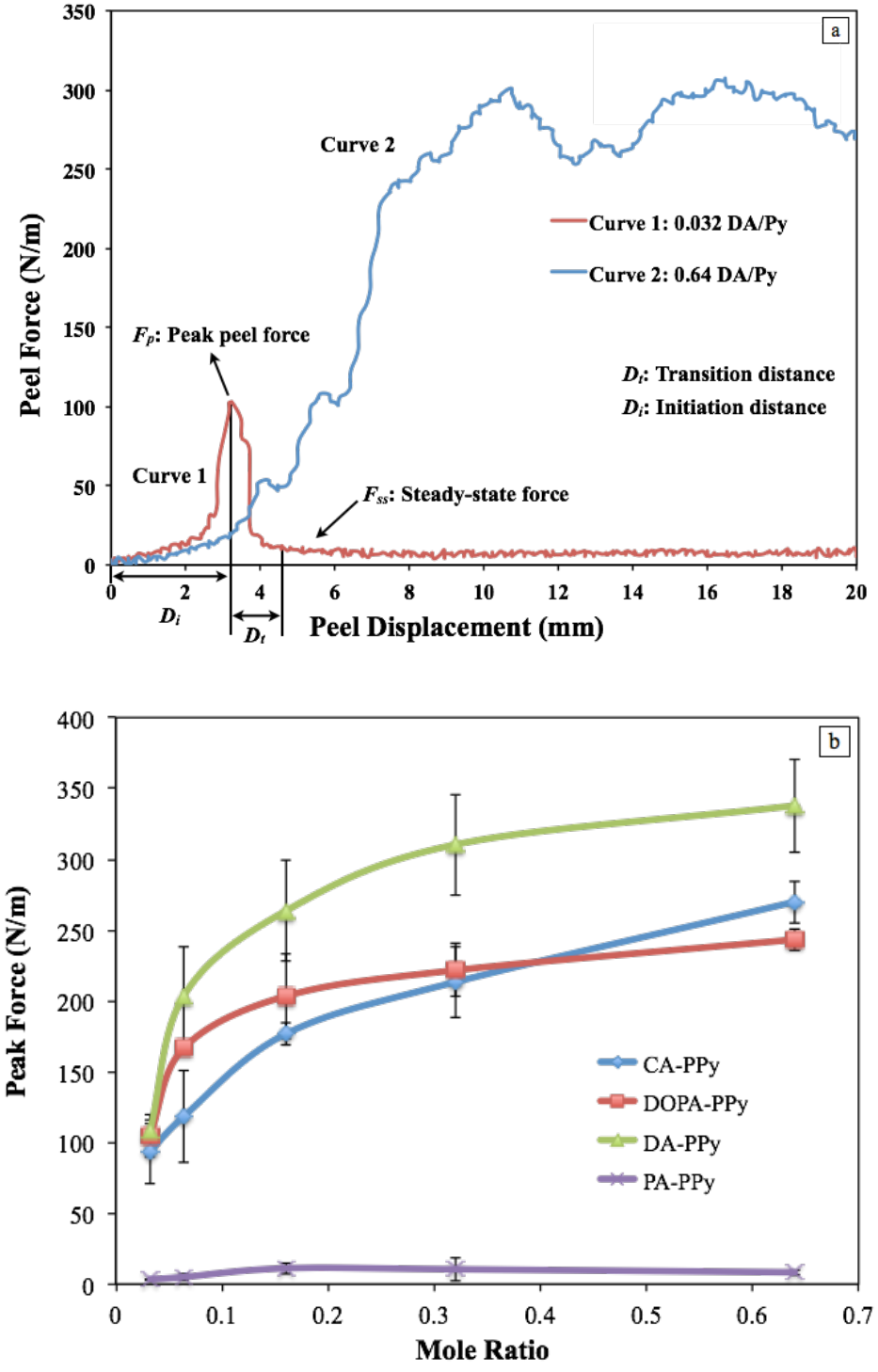

Figure 5.7. (a) Peeling curves of PPy films obtained at 0.032 and 0.64 DA/Py mole ratio at 15 mm/s peeling speed and the illustration of four peeling parameters: peak peel force (F_p), steady-state force (F_{ss}), initiation distance (D_i), and transition distance (D_t). (b) Plots of the peak force versus (DA, CA, DOPA and PA) /Py mole ratio at a constant peeling speed rate of 15 mm/s.

The adhesion properties of modified PPy were characterized by 180° peeling test, which is applied to examine the bonding strength between the modified PPy film and glass substrate. We have examined the tape/PPy/glass system, where the failure may occur either at the tape/PPy interface or PPy/glass interface. Two examples are presented in Figure 5.7a, which are the typical force-displacement curves obtained by peeling PPy nanofiber films at 0.032 and 0.64 DA/Py mole ratio from a glass substrate at 15 mm/s speed. Curve 1 shows the case of an interfacial failure between the glass slide and PPy film, i.e. the delamination of PPy film from glass; curve 2 shows the case of a failure at tape/PPy film interface at a higher DA/Py mole ratio. Four peeling parameters depicted in Figure 5.7a, can be extracted from curve 1: peak peel force (F_p), steady-state force (F_{ss}), initiation distance (D_i) and transition distance (D_t). In our system, the peak force (F_p) (i.e. the force required to initiate failure) has been utilized to compare the adhesion between glass and modified PPy films.

Figure 5.7b plots the peak force versus catechol/Py mole ratio of four modified PPy films at a constant peeling rate of 15 mm/s. For catechol-functionalized PPy films, F_p increases with the catechol mole percentage. Moreover, the interfacial failure shifted from film/glass to tape/film interfaces with increased catechol/Py mole ratio, indicating the rise in bonding strength between catechol-PPy and glass. It is also important to note that adding only a small amount of catechol derivatives can dramatically improve the adhesion by about three orders of magnitude. On the other hand, PA modification had almost a negligible influence on the adhesion. Furthermore, the PA-PPy film delaminated from the glass at all PA/Py mole ratios. It is concluded that catechol functional group itself is responsible for the adhesion improvement of PPy film instead of the amine functional group or coexistence of both catechol and amine

moieties. Such a finding is consistent with that reported in the literature. Deming and co-workers performed tensile shear strength measurements on a catechol-containing polypeptide to evaluate its adhesion property. They also found that the adhesive strength of this co-polymer was proportional to the amount of catechol moieties in the polymer backbone, but independent of the choice of oxidizing agents.[32] Smaller particle size is another factor that may contribute to the strong catechol-PPy adhesion. Smaller sized particles provide larger surface area for interactions such as hydrogen bonding and van der Waals forces at the film/glass interface. Moreover, it was noticed that solution with a smaller particle size yielded smoother and more uniform films with less roughness. As a result, the effective contact area between the modified PPy film and the tape would increase with rise in the catechol/Py mole ratio, responsible for the increased adhesion force F_p shown in Figure 5.7b.

5.3.3 Electrical Properties of Functionalized PPy

To investigate the effect of different functional groups on PPy material properties, the electrical conductivity of catechol- and PA-modified PPy with various (DA, CA, DOPA, PA)/Py mole ratios were measured using a standard four-point probe setup. Due to the fact that porosity, density and packing structure may affect the overall conductivity of PPy nanofibers, both compressed pellets and solution-cast film were prepared their conductivities measured to yield the data shown in Figure 5.8.

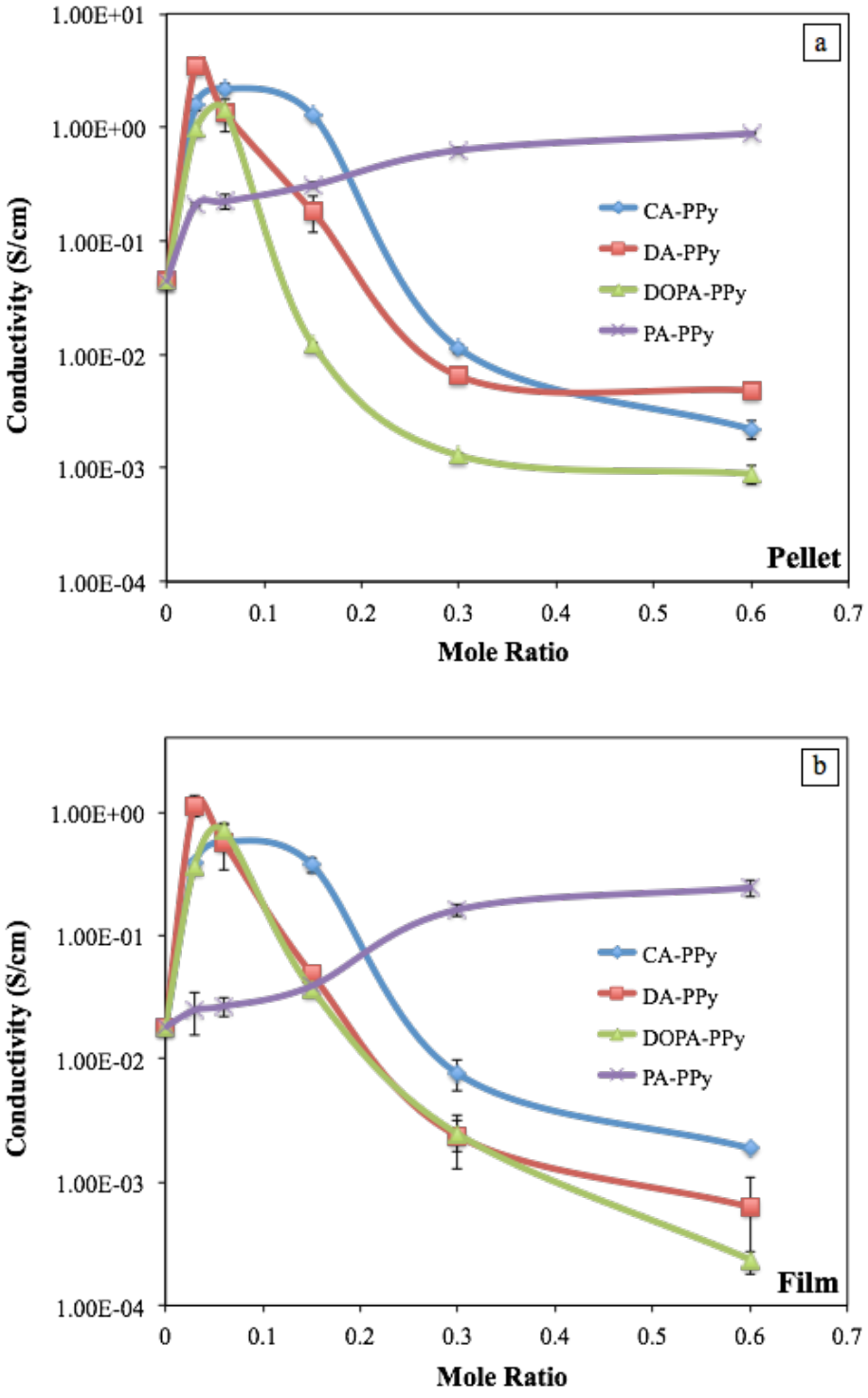

Figure 5.8. Electrical conductivity of DA-, CA-, DOPA- and PA-modified PPy compressed pellets (a) and casted films (b) as a function of (DA, CA, DOPA and PA)/Py mole ratio.

The electrical conductivity of a pristine PPy pellet and film is about 0.04 S/cm and 0.01 S/cm, respectively. For all three catechol derivatives, as the catechol/Py mole ratio increases, the electrical conductivity first increases to a maximum value of 3.8 S/cm for DA-PPy pellet, 1.1 S/cm for DA-PPy film, 2.2 S/cm for CA-PPy pellet, 0.6 S/cm for CA-PPy film, 1.4 S/cm for DOPA-PPy pellet and 0.7 S/cm for DOPA-PPy film. We attributed the conductivity improvement to the following reasons. (1) PPy morphology shifts from globular into fibrous after catechol modification, which is a more effective structure for charge transport. (2) Since catechol derivatives are acidic in water, they may act as a dopant to provide more positive charges on the polymer backbone for electrical conduction. (3) The intrinsic adhesion properties of catechol moieties bring PPy fibers more closely together, increase the contact area among individual fibers and produce a stronger conductive network for electron movement. However, the conductivities of both PPy compressed pellets and films decreased as the catechol/Py mole ratio increased from 0.064 to 0.64. It can be explained by the fact that catechol functional groups may adhere to the PPy surface via covalent bonding, π-π stacking and hydrogen bonding. As a result, the insulating catechol moieties may block the electron transfer between PPy polymer chains at high catechol/Py mole ratio. Moreover, after incorporating catechol derivatives into the PPy chain, especially at high catechol concentration, the PPy chain length was significantly reduced, which may decrease the effective conjugation length and minimize the efficiency of charge hopping to lower the overall conductivity.

For PA-modified PPy, no chemical reactions presumably occur between PA and P. Nevertheless, the conductivity of the PA-PPy composite and film increase when the content of PA is increased as shown in Figure 5.8. One possible explanation is that PA is present where

hydrochloride can dope the system to increase the PPy conductivity. However, it should be noted that DA is also in a form of a hydrochloride salt, but compared with PA-PPy system, acid doping is not the only factor that may affect the DA-PPy conductivity, other reasons including morphology change and DA adhesion property should also be considered to explain the overall DA-PPy conductivity change as discussed above.

Figure 5.9 shows the UV-Vis absorption spectra of the modified PPy at different catechol/Py molar ratios. Note that PA-PPy and pristine PPy cannot be measured by UV-Vis spectroscopy due to their poor dispersion in water. All spectra displayed two distinct peaks close to 350 nm and 700 nm. The first absorption band is associated with the π-π* transition from the valence band to the polaron/bipolaron bands, while the second feature is due to the conduction electrons at the bipolaron state of PPy. For DA-modified PPy, a significant blue-shift of the π-π* transition peak from 450 nm to 351 nm was observed with increasing DA/Py mole ratio. The blue shift of π-π* transition absorption suggests that the conjugation degree of DA-modified PPy is becoming lower. For CA- and DOPA-modified PPy, we found a slight red-shift of the peak with increasing CA/Py and DOPA/Py mole ratio from 0.032 to 0.064. However, when the CA/Py and DOPA/Py mole ratio increased from 0.064 to 0.64, a blue-shift of the peak from 359 nm to 351 nm for CA-PPy and from 377 nm to 349 nm for DOPA-PPy are observed. These observations agree with our four-point probe measurement that the conductivity of DA-PPy decreased with increasing DA/Py ratio from 0.032 to 0.64, while the conductivity of CA-PPy and DA-PPy increased to a maximum value and then decreased with increasing CA/Py and DA/Py mole ratio. It is noted that Wu *et al*. also reported a blue shift in the UV-Vis spectra for PPy-cellulose nanocrystal (CNC) system with increasing Py/CNC mole ratio. They attributed the blue shift into the disorder and

defects introduced to the polymeric chains, resulting in the decrease of overall conductivity.[174]

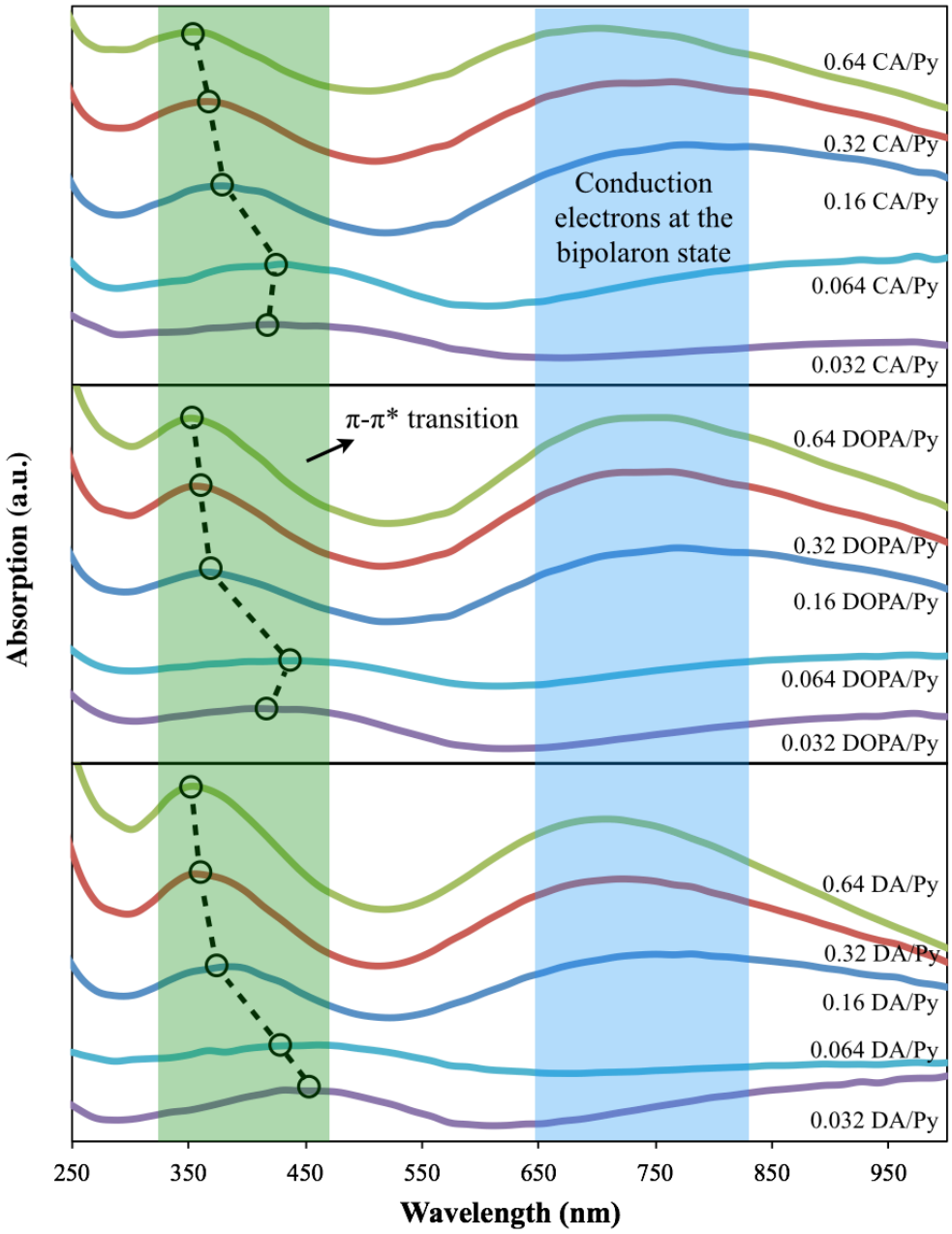

Figure 5.9. UV-Vis spectra of catechol-PPy synthesized with various catechol/Py ratios. The π-π* transition peaks are obtained at local maxima and indicated in black circles.

To further investigate the electrical properties of catechol-modified PPy, their band gap energies (E_g) were calculated from the UV-Vis spectra by the Tauc plot, which is described as:[175]

$$(\alpha h\nu)^n = C\times \left(h\nu - E_g\right) \ (Equation\ 5.2)$$

where α is the absorption coefficient, h is Planck's constant, ν is the frequency of light, C is a proportionality constant, E_g is the band gap and n is the exponent denoting the optical transition process. The values of n can be 1/2, 3/2, 2 and 3, indicating direct allowed, direct forbidden, indirect allowed and indirect forbidden transitions, respectively.[176] The absorption coefficient is defined by the following equation deduced from Beer–Lambert's relation:[177]

$$\alpha = -\frac{1}{t} \times \ln\left(\frac{I_t}{I_0}\right) = \frac{1}{t} \times A \times \log_{10} e \ \ (Equation\ 5.3)$$

where A, t, I_t and I_0 represent the absorbance determined from the UV–visible spectrum, path length of the quartz cuvette, intensity of transmitted light and intensity of incident light, respectively. The band gap E_g can be estimated by extrapolating the straight part of $(\alpha h\nu)^n$ versus $h\nu$ curve to the $h\nu$ axis by linear fitting. Figures 5.10a to 5.10c show plots of $(\alpha h\nu)^2$ versus photon energy ($h\nu$), where n = 2 since the optical transitions for amorphous semiconductors are described as indirect allowed transitions; the linear extrapolated lines are shown as black dash lines. From Tauc plots, the optical band gaps of DA-PPy, CA-PPy and DOPA-PPy at varied catechol/Py reacting mole ratios are summarized in Figure 5.10d. E_g increases from 3.46 eV to 4.94 eV for DA-PPy, indicating that more energy is needed to promote an electron from the valence to the conduction band and the electronic conductivity drops with increasing DA/Py mole ratio. For the CA-PPy and DOPA-PPy systems, E_g value decreases first and then becomes larger with increasing CA/Py and DOPA/Py mole ratio, in agreement with the conductivity results of Figure 5.8.

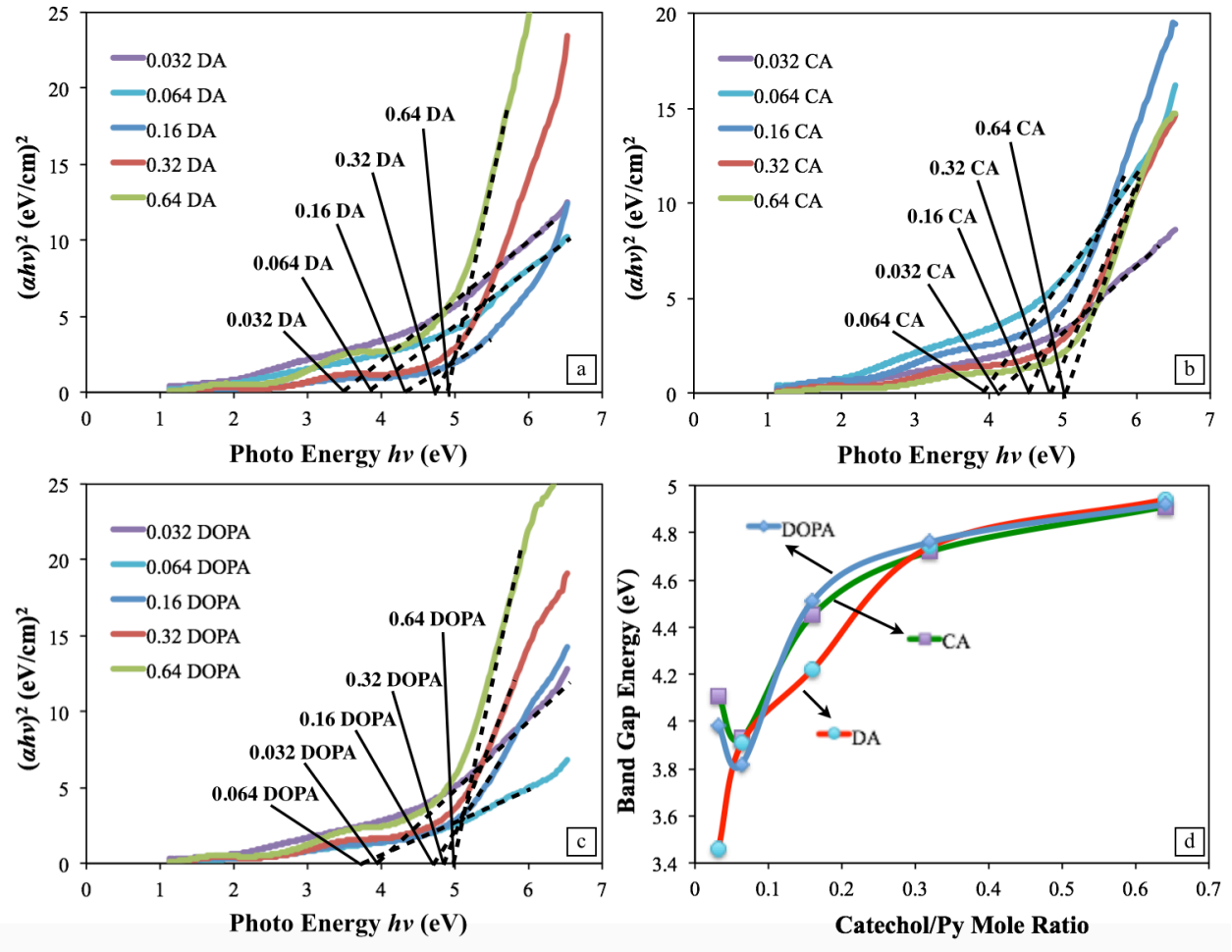

Figure 5.10. Plots of optical band gap of (a) DA-PPy; (b) CA-PPy, and (c) DOPA-PPy. (d) Plot of the band gap energy of DA-PPy, CA-PPy, and DOPA-PPy versus catechol/Py ratios.

5.3.4 Scratch resistances of DA-PPy and its PVA nanocomposite films

Both improved adhesion and conductivity make catechol-PPy a promising candidate for thin coatings in micro-electrical applications, where the durability and mechanical behavior of the coating are almost as important as the function of the thin film itself. As a result, we employed the ASTM standard scratch test to produce and evaluate PPy film surface damage under controlled stress or load.[178] The tests were performed on a DA-PPy film produced at a 0.064 DA/Py mole ratio. We choose this sample because it exhibits the smallest particle size and best

adhesion and electrical conductivity. Figure 5.11a presents a typical scratch track of induced damage on a DA-PPy film as the load is increased under an optical microscope. The critical load - the maximum load that a DA-PPy film can withstand prior to delamination - was determined to obtain the conditions in which the PPy coating can be safely used. As shown in the image, film delamination began almost immediately after scratch started at about 76 g, suggesting a relatively poor scratch resistance.

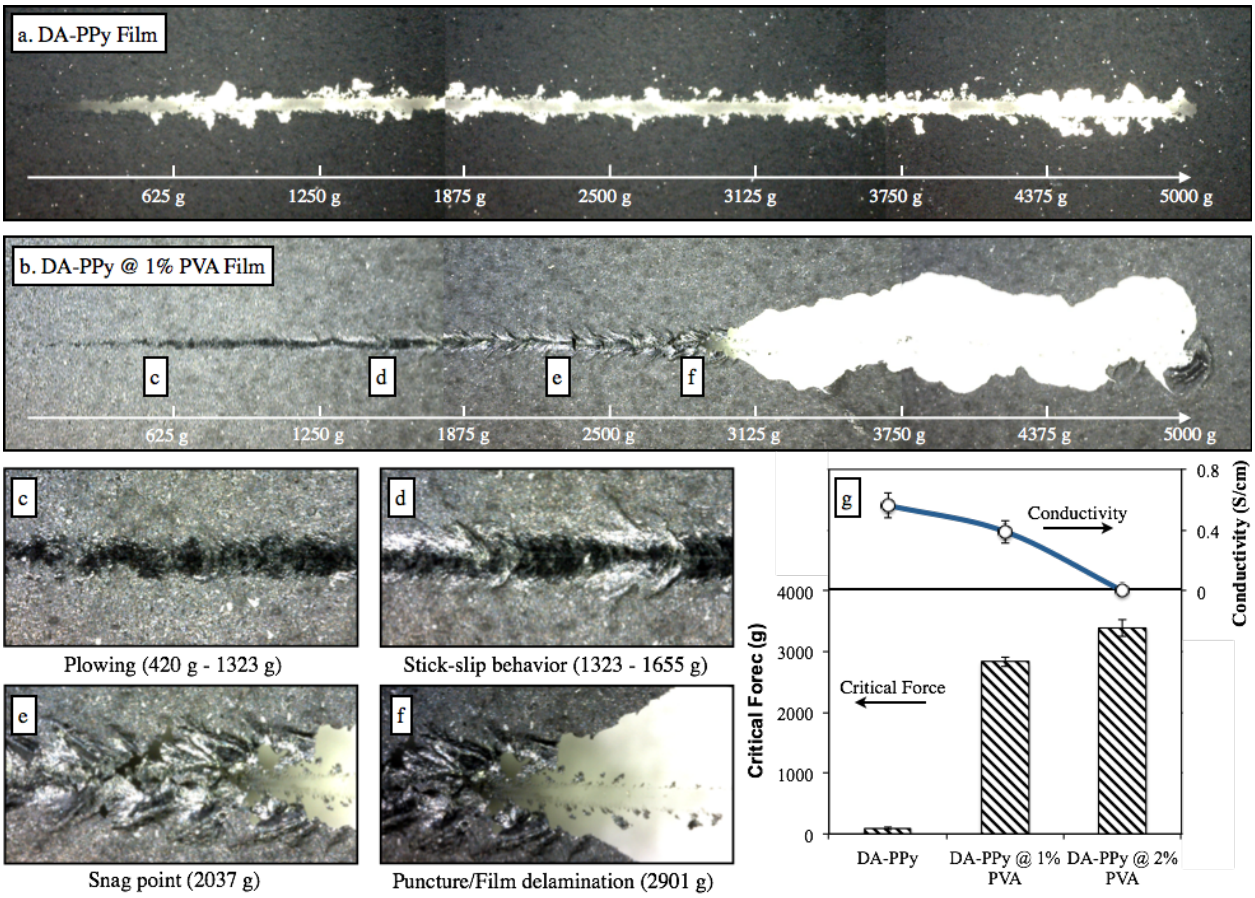

Figure 5.11. Damage observed on test film surface using the scratch test: (a) DA-PPy film, (b) DA-PPy film prepared with 1 wt% PVA solution. Different failures observed on DA-PPy film prepared with 1 wt% PVA solution: (c) plowing, (d) stick-slip behavior, (e) snag point and (f) film delamination. (g) Plot of critical load and conductivity for pure DA-PPy film, DA-PPy film prepared with 1 wt% PVA and DA-PPy film prepared with 2 wt% PVA solutions.

In order to enhance the mechanical properties of the PPy film, we dispersed DA-PPy nanofibers into PVA, which is an excellent polymer binder due to its high water solubility, good

adhesion and biocompatibility. Due to the catechol modification, the hydroxyl groups in PVA could strongly interact with DA-PPy, forming a uniform dispersion that was readily cast into thin films. Two DA-PPy/PVA polymer films were prepared by casting the as-synthesized DA-PPy dispersed in 1 wt% and 2 wt% PVA aqueous solutions. Figure 5.11b displays the optical images of the scratch trace on DA-PPy film prepared with 1 wt% PVA solution deposited on glass substrate. A small amount of deformation, including fully recoverable elastic, time-dependent viscoelastic and non-recoverable plastic deformation, is observed under low loads (0 - 420 g). During the period in which the normal load of the tip is linearly ramped from the minimum to the maximum during sliding, the film damages evolved into plowing (Figure 5.11c, 420 g - 1323 g), stick-slip behavior (Figure 5.11d, 1323 - 1655 g), snag point (Figure 5.11e, 2037 g) and finally film delamination (Figure 5.11f, 2901 g). The critical load and conductivity of the films casted from DA-PPy dispersed in pure water and DA-PPy dispersed in 1 wt% PVA and 2 wt% PVA aqueous solutions are compared in Figure 5.11g. It is clear that the PVA matrix significantly improved the DA-PPy film scratch resistance and maintained high mechanical integrity. Since the film thickness of three samples were measured to be almost identical, this factor has been eliminated. The electrical conductivity of DA-PPy film and DA-PPy film prepared with 1 wt% PVA solution were measured to be 0.056 S/cm and 0.039 S/cm, but the conductivity dropped to 1.6×10^{-5} S/cm for DA-PPy film prepared with 2 wt% PVA solution. It is also informative to notice that film casted by unmodified PPy prepared with 1 wt% PVA solution showed non-uniform dispersibility and almost insulating behavior.

Finally, it would be useful to discuss the technical implications of the DA-PPy combined with PVA for its practical applications. Recently, Hu *et al*. reported that polydopamine (PDA)

itself could be used as a filler to improve the thermal, mechanical and adhesive performance of PVA polymers.[179] Our DA-PPy nanofibers could be used to replace the PDA in order to introduce an additional function of high electrical conductivity to this composite and further widen its potential applications, such as electrical conductive adhesives (ECAs). Traditional ECAs are based on silver-filled polymer composites, which are relatively expensive and not environmentally friendly.[153] Their preparation processes also require the use of solvent, curing agent and stabilizer so that their applications in biotechnology are limited. To achieve better biocompatibility, another conducting polymer polyaniline based PVA composite was prepared, but it suffers from poor conductivity (4.3×10^{-6} S/cm).[180] In this respect, biocompatible DA-PPy/PVA materials with moderate conductivity (0.039 S/cm), could replace traditional ECAs for use in many biological-relevant applications, including artificial muscles, scaffold and biosensors.

5.4 CONCLUSION

In summary, we reported a benign one-step approach to synthesize novel catechol-PPy nanofibers. After comparing the morphology, particle size, dispersibility, adhesion and electrical conductivity of the PPy modified by dopamine hydrochloride (DA), 1,2-dihydroxybenzene (CA), *L*-3,4-dihydroxyphenylalanine (DOPA), and phenylethylamine (PA), respectively, we demonstrated that the di-catechol functional group is responsible for most of the PPy property changes. The catechol moieties can be oxidized into o-quinonimine, which can react with the Py ring to regulate polymer chain growth and form a unique fibrous PPy structure and smaller PPy particle size. The catechol-PPy also exhibited the intrinsic adhesion properties of catechols

whereby the bonding strength between catechol-PPy and glass substrate was significantly enhanced. Due to the strong adhesion and acidic nature of catechol, the electrical conductivity of modified PPy also improved at low catechol/Py mole ratios. Moreover, we found that modified PPy can be uniformly dispersed into a PVA polymer matrix and cast into thin film coating via a convenient solution-cast method. This as-prepared coating exhibited high scratch resistance, biocompatibility and conductivity suitable for broad industrial applications. In addition, this work could open new opportunities of using catechol derivatives to functionalize other conductive polymers for better mechanical and electrical performance.

CHAPTER 6. MODIFICATION OF DOPAMINE FUNCTIONALIZED POLYPYRROLE FOR THE APPLICATIONS OF ADVANCED ELECTRONICS*

6.1 Introduction

With the rapidly growing demand for advanced electronic devices at an ever-small scale, we have witnessed many breakthroughs in electronics miniaturization technology that have provided further strong motivation for developing novel materials and structures approaching the molecular level.[181-184] During the past decade, nanomaterials such as carbon nanotubes (CNTs) and graphene have arisen as promising research subjects in electrical engineering and materials science due to their superior intrinsic properties including mechanical strength, surface area, electrical and thermal conductivity.[185-187] This success suggests that nanomaterials could replace traditional materials in various existing applications ranging from energy harvesting and biochemical sensing to semi-conductors and electronic devices.[188,189] The continuous miniaturization of the electronics sets new standards for material science and engineering and has created challenges in the area of developing functional nanostructures with controllable size, composition, morphology and interface.[190,191] Despite these advantages, the use of CNTs and graphene has some disadvantages such as self-aggregation, non-dispersibility in aqueous media and unchangeable morphology, which significantly limit their potential applications in nanoelectronics and systems.[192-194]

---

* This chapter has been submitted to *Advanced Electronic Materials*.

In recent years, conducting polymers (CPs) have drawn considerable attention in nanomaterials because of their unique properties, such as high conductivity, long-term stability, easy processability and reversible doping-dedoping process.[89,195] In order to successfully transfer these promising materials into practical engineering applications, great effort has been devoted to improving synthetic methods and assembly technologies to better control CP properties.[93,169] For instance, their morphology and shape can be manipulated by physical template-guided synthesis,[104,196] their particle size can be regulated by electro-polymerization or emulsion polymerization,[197,198] their dispersibility can be improved by hydrophilic surface modification[106,199] and their electrical conductivity can be varied based on the choice of dopants.[200] Although extensively investigated, many current techniques have drawbacks for widespread application. Specific examples include the requirement for multi-step procedures, harsh reaction conditions and complicated instrumentation.[157,160] As a result, the development of simple and versatile strategies for facile, efficient and large-scale synthesis of nanostructures of CPs with advanced properties is highly desirable. We have reported a template-free benign method to modify one of the most popular CPs, polypyrrole, with a bio-inspired catechol derivative dopamine, which provided an alternative approach to the facile fabrication of PPy nanomaterials.[10]

Dopamine, with the chemical structure of catecholamine, is a biological neurotransmitter that plays a number of vital roles in the human body.[162,201] It can self-polymerize to form a nanoscale polydopamine film that binds on almost any surface with controllable film thickness and good stability.[1,7] PDA is a dark, insoluble, eumelanin-like pigment material, which has valuable adhesive, electrical conductivity and anti-oxidative properties.[2] Because PDA contains a high

density of reactive functional groups (catechol, amine, and imine), it has the strong ability to modify surfaces.[15] As a consequence of the tremendous potential of PDA as a versatile and multifunctional coating material,[8,21,33] we employed in situ polymerization of pyrrole (Py) with DA. After being functionalized by DA, PPy exhibited fibrous morphology, smaller particle size, better water dispersibility, enhanced adhesion and electrical conductivity.[11] Most importantly, the degree of these modifications can be precisely controlled by the DA/Py mole ratio, which make it stand out as an ideal candidate for a variety of electrical applications. Although DA-PPy has many advantages, its conductivity still requires further improvement, especially at higher DA/Py mole ratio. We found that the maximum conductivity of DA-modified PPy was 3.8 S/cm for compressed pellets, which is not adequate for use in electronics. Also, the maximum conductivity was only obtained at low DA/Py mole ratios, where the dispersibility and particle size of DA-PPy are inferior to that achieved at higher DA concentration. In this regard, it is essential to optimize DA-PPy synthesis to achieve excellent conductivity and dispersibility at the same time.

In this research, we develop new synthetic approaches to the preparation of DA-PPy nanostructures, which have improved both electrical conductivity and water dispersibility compared with the DA-PPy reported in our previous work.[10,11] Moreover, we also explore the suitable application of each as-fabricated nanomaterial depending on the DA/Py mole ratio, as illustrated in Figure 6.1. In particular, DA-PPy produced from a 0.032 DA/Py mole ratio exhibits superior capacitance for supercapacitors; DA-PPy obtained from a 0.064 DA/Py mole ratio can be implemented as a co-filler into the epoxy network in preparation of functional composites for electrically conductive adhesives (ECAs); and DA-PPy synthesized from a 0.64 DA/Py mole ratio can absorb electromagnetic microwaves for electro-magnetic interference (EMI) shielding

applications. This synergetic effect of DA modification, gives PPy unique multifunctional properties, which opens a brand new field in the frontier of nanomaterial synthesis and applications.

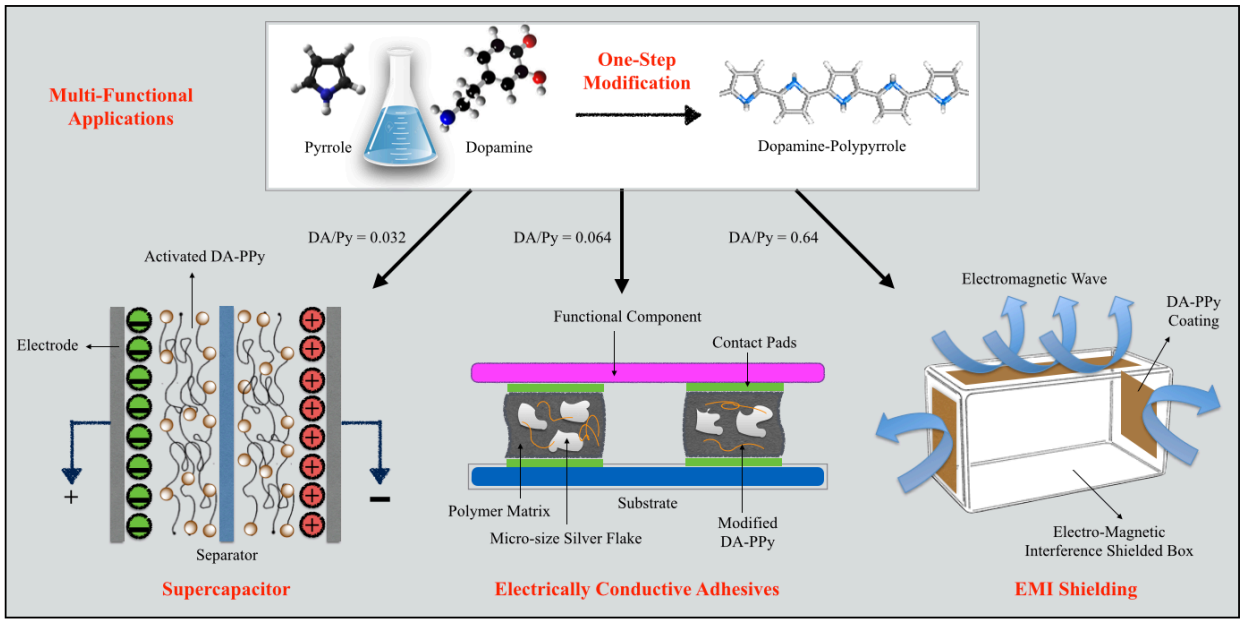

Figure 6.1. Suitable application of each as-fabricated nanomaterials depending on the DA/Py reacting mole ratio.

6.2 Experimental

6.2.1 Synthesis of DA-PPy and its Nanocomposite

Pyrrole (Py, 98%), ferric chloride ($FeCl_3$), dopamine hydrochloride (DA) and silver micro flake (10 μm) were purchased from Sigma-Aldrich and used as-received. Epoxy resin (DER 322) and triethylenetetramine (TETA) containing the crosslinking agent DEH 24 were obtained from Dow Chemical for ECA preparation. The synthesis of dopamine-functionalized polypyrrole was achieved by the following procedure. In a typical experiment to prepare 0.032 DA-PPy, 0.12 ml or 0.116 gram pyrrole monomer and 0.01 g dopamine hydrochloride were dissolved in 20 ml 1 M HCl and cooled down to 8 °C. $FeCl_3$/HCl solution (0.4 g/5 ml) was added to the DA/Py solution

dropwise while stirring vigorously for 12 hr at a reaction temperature of 8 °C. The resulting precipitates were filtered and collected by centrifuging the solution and sequentially washed 5 times with deionized water. The washed precipitates were then freeze-dried for 24 hours to produce a powdered material.

The fabrication of the ECA composite followed our previously established procedure.[153] At first, a small amount of acetone was added to produce a 6 wt% solution. Then 5 mg of synthesized DA-PPy nanofibers along with 200 mg silver flakes were added directly into the epoxy solutions. The composite was agitated for 45 min using a vortex mixer followed by 45 min of sonication. After this mixing, the curing agent TETA was added to the composite and the final mixture was filled into 7 × 7 × 0.5 mm^3 (L×W×D) mold made by adhesive tape on a pre-cleaned microscope glass slide. In order to make a smooth surface with controlled thickness, a clean copper plate was placed on top of the mold to squeeze out extra material. The sample was pre-cured at 60 °C for 30 min and then cured at 150 °C for 2 hrs. After curing, the copper plate and adhesive tape were peeled off. The above procedure was also applied to prepare other pastes at different DA-PPy weight ratios. For all hybrid ECA samples with DA-PPy nanofiber co-fillers, the absolute mass of silver flakes was kept constant, whereas the amount of DA-PPy was varied.

6.2.2 Characterization methods

The morphology of the DA-PPy nanomaterials was examined by scanning electron microscopy (SEM, Zeiss LEO 1550) operating at 5 kV and high-resolution transmission electron microscopy (HRTEM, JEOL 2010F FEG). The electrical resistivity of DA-PPy nanofibers (compressed pellet under 500 MPa pressure) and cured nanocomposites were measured by a

four-point setup that consists of a probe fixture (Cascade Microtech Inc.) and a source meter (Keithley 2440 5A Source Meter, Keithley Instruments Inc.). The conductivity (σ) was calculated by using the following equation:[11]

$$\sigma = F \times \frac{\ln 2}{\pi \times t} \times \frac{I}{V} \quad (Equation\ 6.1)$$

where t, I, V and F represent the sample thickness, applied current, read-out voltage and dimensionless correction factor, respectively. The value of F depends on the ratio of t/s, where s is the probe spacing (s = 0.1 mm). From four-point probe theory, F approaches 1 as t/s approaches 0. Since t/s = 0.1 in our system, we approximate F = 1.

All electrochemical tests were performed on a VSP-300 potentiost at electrochemical station (BioLogic Science Instruments, France) equipped with a three-electrode half-cell configuration. The three electrodes included a platinum counter electrode, a saturated calomel reference electrode (SCE), and a working electrode, which was fabricated by coating DA-PPy (1 mg/mL in 50% water/ethanol dispersion) onto a glassy carbon electrode. The experiments were measured following a 5-cycle cyclic voltammetry (CV) activation between −0.6 and 0.4 V versus SCE in 2M KCl electrolyte. Cyclic voltammetry tests were performed at scan rates of 1, 10, and 100 mV/s. The capacitance can be calculated from Equation 6.2:[174]

$$C_S = \frac{\int idV}{2 \times m \times \Delta V \times S} \quad (Equation\ 6.2)$$

where $\int idV$ is the integrated area under the CV curve, m is the mass of DA-PPy, ΔV is the potential range, S is the scan rate, and C_S is the specific capacitance. Charge and discharge (CD) tests were conducted by applying current densities of 1, 2 and 5 A/g. The cell capacitance determined from CD curves was calculated from equation 6.3:[202]

$$C = \frac{I}{dV/dt} \ (Equation\ 6.3)$$

where I and dV/dt are charge current density (A/g) and the slope of the CD discharge curve.

Indentation measurements of an AISI Type 440-C stainless steel probe (4.63×10^{-4} m) on ECA substrates were performed at room temperature. In each experiment, a probe was brought into contact with a flat ECA surface at 1μm/sec until a preload of 750 g was reached and then separated at the same speed. The associated force and displacement were analyzed in the framework of the Hertzian indentation model. The electro-magnetic parameters were measured with an Agilent HP 8722ES vector network analyzer over the 2-18 GHz range. The samples were prepared by mixing the DA-PPy composites and paraffin wax at 40% weight fraction of each and then pressed into a cylindrical shape with thickness of 2 mm.

6.3 Results and Discussion

6.3.1 Fabrication of DA-PPy Nanostructures with Controllable Morphology

The modified strategy to the synthesis of DA-PPy is illustrated in Figure 6.2a. Compared with our previous method, the reaction was carried out in 1M hydrochloric acid (HCl) instead of Tris-buffer and the oxidant ammonium persulfate (APS) was replaced by $FeCl_3$. HCl acted as a protonic acid to dope PPy for higher electrical conductivity; at the meantime, it also provided low pH environment to prevent DA polymerization, which could form an insulated polydopamine (PDA) layer on PPy surface and decrease the electrical conductivity.[11,158] $FeCl_3$ was applied to improve electromagnetic properties, and potentially influence PPy morphology through chelate interaction between Fe^{3+} and catechol functional groups from DA.[21,203] The surface morphology was characterized by scanning electron microscopy (SEM) (Figure 6.2b-e), which revealed a

striking contrast in DA-PPy nanostructures prepared at different DA/Py reacting mole ratios. Pure PPy showed large, granular particles with a diameter of about 300 nm due to the PPy interchain links (connecting the adjacent PPy backbones) and side chains (connecting to one PPy backbone) during Py polymerization. In the presence of only a small amount of DA, which may minimize the interchain links and side chain formation by chemically reacting with the Py ring, the architecture shifted to a highly interconnected network of nanofibers. As the DA/Py mole ratio continuously increased, PPy polymer chains became much shorter after incorporating more DA and a nanorod morphology developed.

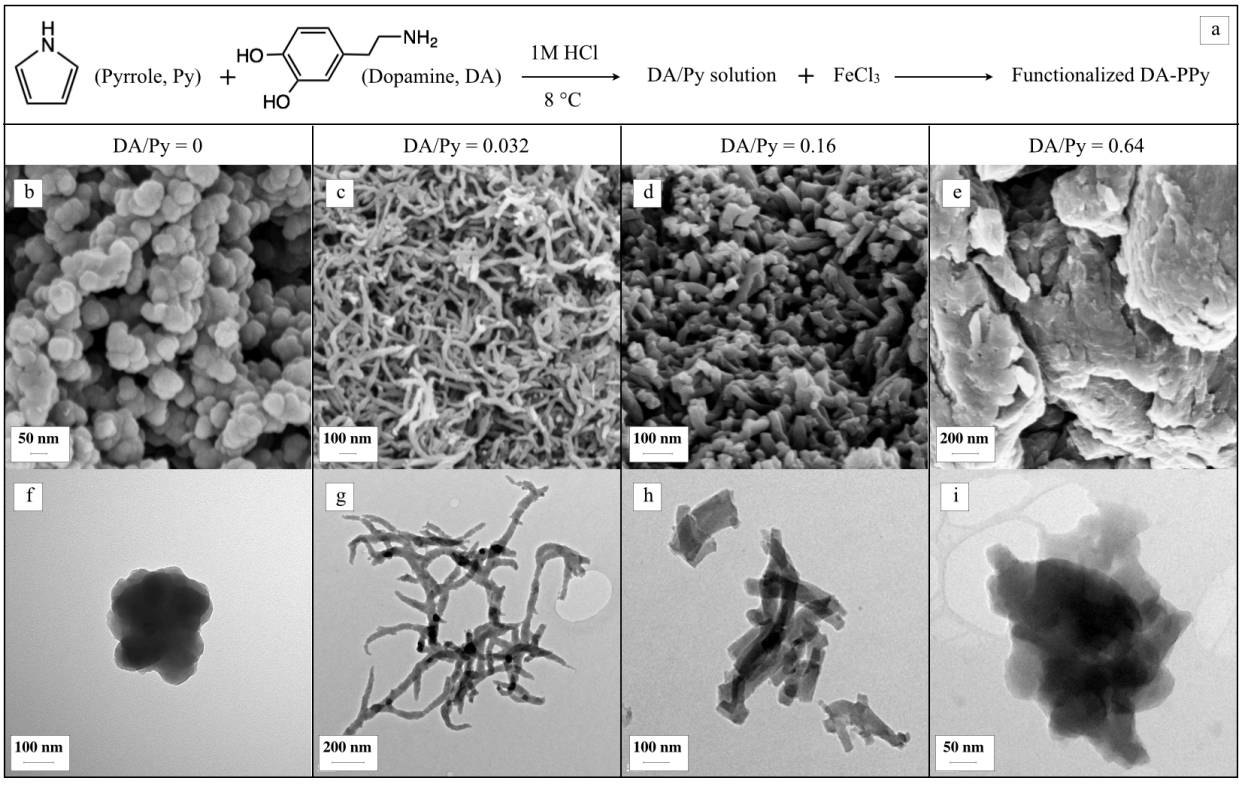

Figure 6.2. (a) The modified strategy to the synthesis of DA-PPy nanostructures; SEM images of DA-PPy with (b) globular morphology; (c) fibrous morphology; (d) nanorod morphology; and (e) nanoflake morphology depending on DA/Py ratio; (f-i) TEM topography images that further confirmed as-prepared nanostructures.

When the DA/Py mole ratio reached 0.64, PPy aggregates formed and merged into flakes due the strong adhesion property of catechol functional groups and the possible formation of $Fe(DA\text{-}PPy)_3$.[6] High-resolution transmission electron microscope (TEM) images presented in Figure 6.2f-i shows similar trends to the SEM images. It was found that nanofibers (Figure 6.2g) with a diameter of 80 nm and a length up to several microns can form at a DA/Py ratio of 0.032, while nanorods (Figure 6.2h) with similar diameter but much shorter length of about 300 nm form when DA/Py = 0.16. Although different PPy morphologies using different methods have been reported in literature,[102,103,204] our versatile approach demonstrated the ability to produce a wide range of PPy nanostrctrues using a single method just by adjusting the DA/PPy molar ratios.

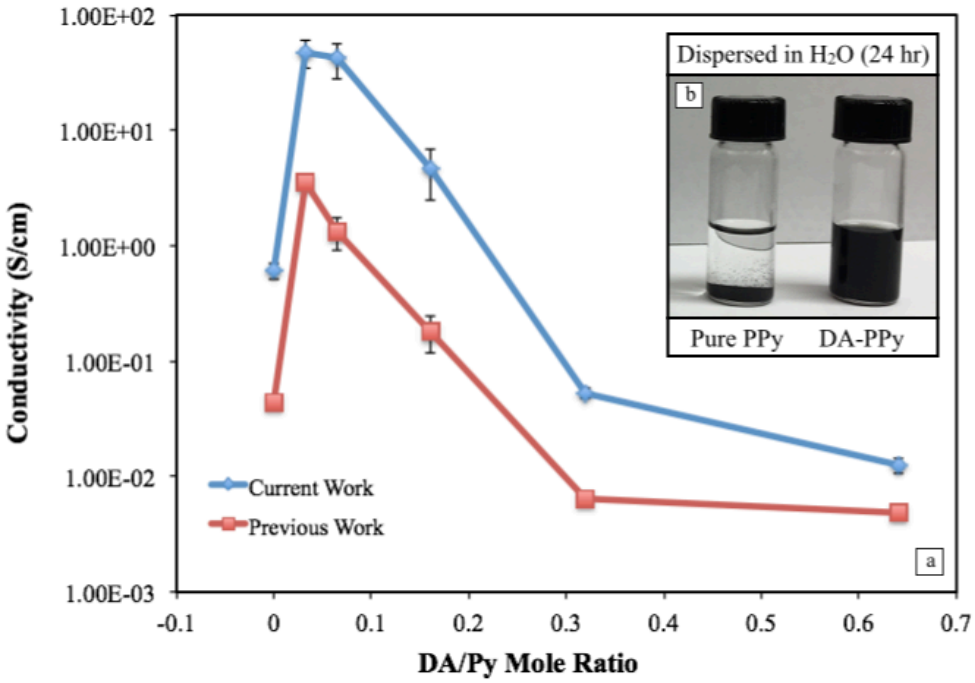

Figure 6.3. (a) Plots of electrical conductivity versus DA/Py mole ratio (Previous work was adapted from Ref.11) and (b) digital photo of vials with 2 mL water-dispersed pure and modified PPy suspension after 24 h.

The electrical conductivities of DA-PPy prepared measure at different DA/Py mole ratios are summarized in Figure 6.3a. The introduction of a small amount of DA significantly improved the

conductivity of PPy from 0.5 S/cm to a peak value of 42 S/cm at a 0.032 DA/Py mole ratio. Therefore, it decreased to as low as 0.05 S/cm at 0.64 DA/Py ratio. It is worthwhile to compare the conductivity results with our previous work. The new synthesis strategy improved the electrical conductivity of DA-PPy by almost one order of magnitude at each DA/Py mole ratio, which can be attributed to the HCl acid doping process. Due to the hydrophilic nature of the catechol groups, modified DA-PPy displayed improved water dispersibility. As shown in Figure 6.3b, a pristine PPy suspension quickly became unstable and precipitated out of the aqueous dispersion within 2 hr. On the other hand, the addition of only a small amount of DA functionalization (0.032 DA/Py mole ratio) gave DA-PPy excellent stability in water for at least 24 hr. Higher DA/Py mole ratio also lead to more stable DA-PPy dispersions because of the abundant amine and hydroxyl groups of DA. These results further indicated that PPy was successfully functionalized by DA to improve both the electrical conductivity and water dispersion at a 0.032 DA/Py mole ratio.

6.3.2 DA-PPy for Supercapacitor Applications

In order to investigate the electrochemical performance of DA-PPy nanomaterials, we have studied their cyclic voltammetry behavior at each DA/Py mole ratio. Figure 6.4a presents the CV curves at scan rates of 0.01, 0.05 and 0.1 V/s of DA-PPy samples prepared from 0.032 DA/Py mole ratio. The quasi-rectangular shape of the CV curves indicates standard capacitance behavior of the electrodes. Also, the integrated charge under the curves is proportional to the scan rate.[205] A higher C_S value is obtained at a slower scan rate, which can be explained by the fact that inner active sites of the DA-PPy cannot complete the redox process at higher scan rates. As a result, a

slower scan rate is preferred in order to better utilize the electrode surface material. Figure 6.4b illustrates the effect of the DA concentration on C_S of DA-PPy at different scan rates. The highest C_S value of 273 F/g was achieved at DA/Py = 0.032 and a scan rate of 0.01 V/s, which was almost 4 times higher than that of the unmodified PPy.

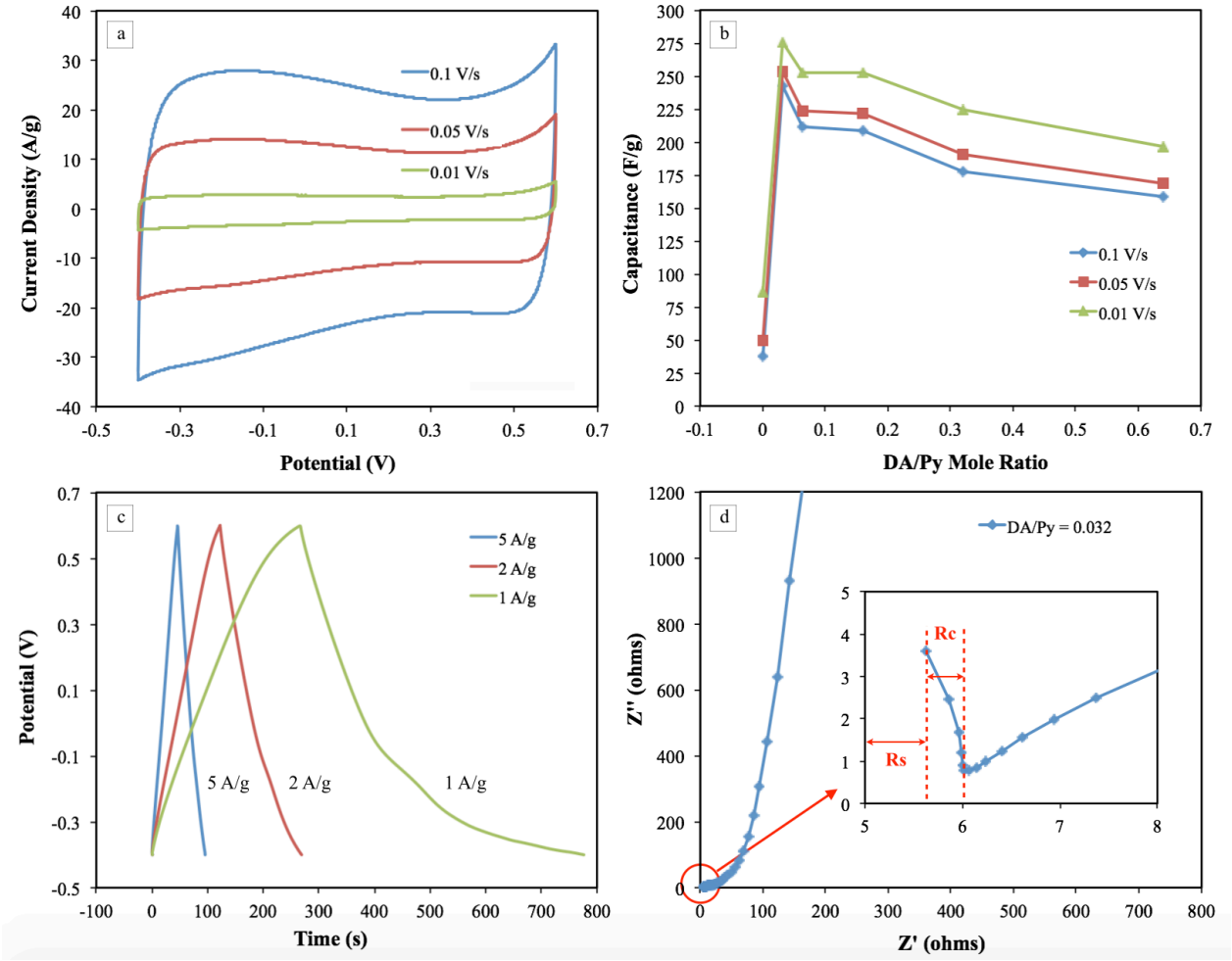

Figure 6.4. (a) CV curves of 0.032 DA-PPy at scan rates of 0.1, 0.05, and 0.01 V/s; (b) effect of DA/Py mole ratio on DA-PPy capacitance; (c) CD curves of 0.032 DA-PPy at 5, 2, and 1 A/g charge currents; and (d) Nyquist plot obtained from EIS for 0.032 DA-PPy.

It is interesting to compare the DA-PPy C_S values with the electrical conductivity data (Figure 6.3a). Both increase to a maximum value at DA/Py = 0.032 and then decrease. The superior DA-PPy C_S can be attributed to the morphology shift from globular to fibrous, which

might provide a larger active surface area for efficient ion diffusion and higher conductivity for electron transport. Moreover, strong interactions such as hydrogen forces or π-π stacking between DA and PPy π-conjugated polymer chains could maintain the structural integrity and facilitate the charge transport within the DA-PPy nanostructure for enhanced capacitance behavior. On the other hand, continuous exchanging of ions and electronic charges during the repeated oxidation and reduction processes of CV, may dramatically influence the unmodified PPy polymer chain structures due to swelling, distortion, or contraction, resulting in the deterioration of electrical performance.[206]

Galvanostatic charge-discharge (CD) process was studied to further characterize the capacitance of the DA-PPy electrodes. Typical CD curves performed on the best DA-PPy electrode (DA/Py = 0.032) with various current densities are presented in Figure 6.4c.It can be seen that the charge curves were almost symmetric to their corresponding discharge counterparts at current densities of 2 and 5 A/g, indicating excellent electrochemical behavior. At the lower rate of 1 A/g, the CD curves were not ideal straight lines and there was an initial voltage drop at the discharging stage caused by internal resistance (IR), resulting the asymmetric shape of the CD curves, which suggested pseudo-capacitive effects of the DA-PPy and the involvement of a faradaic reaction. The calculated capacitance from the discharge slope was 252 F/g at 1 A/g current density, which agreed with the CV results in Figure 6.4b. The improved capacitance performance with the incorporation of DA at 0.032 mole ratio is also evident from electrochemical impedance spectroscopy (EIS). Nyquist plots obtained from EIS (Figure 6.4d), showed a distorted semicircle in the high-frequency region and a steep line in the low-frequency region, indicating an approach to ideal capacitance behaviour.[197] In addition, the semicircle

intercepted the real axis at the bulk solution resistance (R_S = 5.63 Ω) and the charge-transfer resistance (R_C = 0.44 Ω) respectively. On the basis of the above analysis, DA-PPy prepared from 0.032 DA/Py mole ratio yielded a large integrated CV area and small charge-transfer resistance from EIS and so appears to be a promising nanomaterial for supercapacitor applications. It is informative to compare the capacitance of DA-PPy nanomaterial developed in this study with some other similar systems. For example, at the same CV scan rate, the capacitance of MWCNT-PPy prepared by Zhang *et al*. was measured to be 200 F/g.[207] Davies *et al*. reported a graphene-PPy system to have a capacitance of 237 F/g;[208] and Wu *et al*. fabricated CNC-PPy nanocomposite with a capacitance of 248 F/g.[174] It is clear that our DA-PPy system demonstrated better capacitance performance than most of the other PPy-based materials.

6.3.3 DA-PPy for Electrically Conductive Adhesives (ECAs)

Electrically conductive adhesives (ECAs) have attracted considerable attention as robust and environmental-friendly bonding materials for interconnection technologies. They typically consist of a polymer matrix (*e.g.* epoxy) that provides mechanical adhesion and a conductive component (*e.g.* silver flakes) that offers electrical conductivity. In this work, we applied our DA-PPy as a co-filler in the system of epoxy and silver micro-flakes to develop a hybrid nanocomposite adhesive. In order to investigate the effect of DA-PPy on the overall electrical conductivity of their polymer composites, we used conventional ECAs containing 60 wt% silver flakes as a control. Figure 6.5 presents the electrical conductivity versus concentration of different DA-PPy composites made at various DA/Py mole ratios. It was observed that adding pure PPy (DA/Py = 0) decreased the electrical conductivity of the whole composites since

pristine PPy could aggregate easily and block the effect contact among sliver fakes. For all the ECAs containing DA-modified PPy (DA/Py = 0.032, 0.064 and 0.16), the conductivity increased to a peak value when a small amount of DA-PPy was introduced into the epoxy network and then began to decrease as more DA-PPy is added. The maximum conductivity of 2400 S/cm was achieved by adding 3 wt% DA-PPy nanofiber obtained using a 0.064 DA/Py mole ratio.

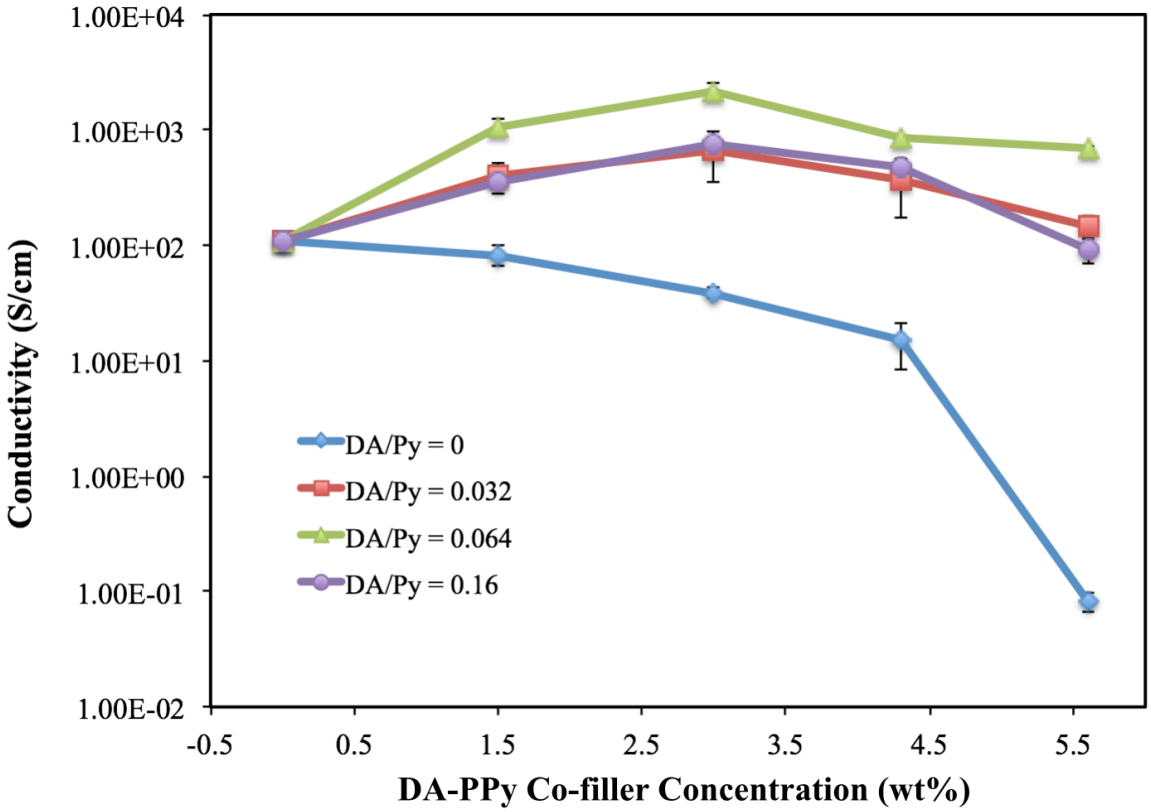

Figure 6.5. Electrical conductivity as a function of DA-PPy filler fraction for hybrid ECAs. DA-PPy made from 0, 0.032, 0.064, 0.16 DA/Py mole ratios were used as the filler.

Compared with conventional ECA 60 wt% silver flake concentration, which exhibited a conductivity of 107 S/cm, our hybrid system improved the electrical conductivity by almost 25 times. Furthermore, the nanocomposite conductivity at 3 wt% DA- PPy nanofiber and 60 wt% silver flakes concentration was similar to the electrical conductivity of conventional ECA with 80

wt% silver flake filler(3000 S/cm). We attribute the synergic effect of DA-PPy to ECAs conductivity to the fact that highly dispersed DA-PPy nanofibers can be uniformly distributed throughout the matrix to bridge the separated silver flakes, providing more electrical paths and as a result, reducing tunneling resistance in the hybrid ECAs. As DA-PPy weight fraction increases further, a large amount of DA-PPy could increase the number of contact points by isolating pre-contacted silver flakes and subsequently increase the constriction resistance among the fillers, which was detrimental to the overall conductivity of the filler network. Although the electrical conductivity of DA-PPy prepared at 0.032 DA/Py mole ratio was larger than that obtained at DA/Py = 0.064, the latter exhibited better water dispersibility because of the higher DA content, which has been considered as the dominant factor affecting the overall ECA conductivity in this case. It is important to note that the electrical resistivity of the base ECAs (60 wt% silver flakes) incorporated with DA-PPy made from 0.32 and 0.64 DA/Py mole ratios were higher than the upper limit of our four-point probe electrometer (1 x 10^9) so are not discussed here.

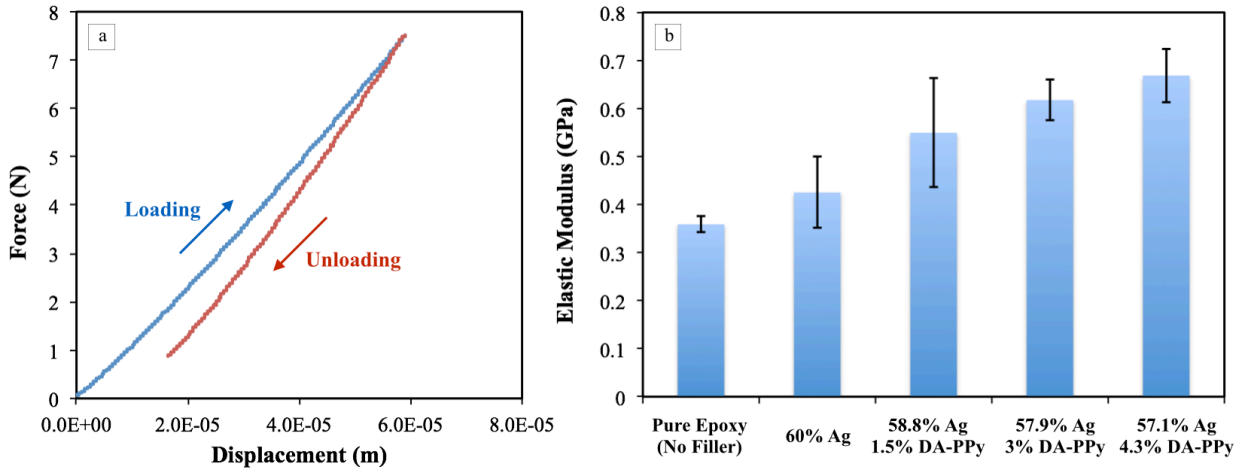

Figure 6.6. (a) Indentation curves of a hybrid ECA with 60 wt% silver flakes and 3 wt% 0.064 DA-PPy co-filler; and (b) illustration of the elastic modulus of different types of ECAs.

Reinforcement of functional composites with short or long fibers has been a significant

success in both thermo-plastics and elastomers.[209,210] In this regard, we applied Hertzian theory to evaluate the mechanical properties of DA-PPy nanofiber-reinforced ECAs. Since the best electrical conductivity of ECAs was achieved by adding 0.064 DA/Py mole ratio resulted DA-PPy nanofiber, they have been added into conventional ECAs with 60 wt% silver flakes at different weight percentages (1.5%, 3%, and 4.3%). The mechanical properties of these ECA samples were investigated by microindentation during the compressive loading and the unloading processes. Figure 6.6a showed a typical plot of the compressive force versus displacement during the loading and unloading processes of the measurements on an ECA sample with 1.5 wt% DA-PPy and 60 wt% silver flakes. The normal force increases at an approximately linear rate once the probe contacted with the ECA sample. It was also found that the loading curve and the unloading curve were not reversible, indicating a significant amount of loading−unloading hysteresis, which was possibly consumed by the thermodynamic free energy. We analyzed all data in the framework of the classic Hertzian contact mechanics. When a spherical probe of radius *R* indents a flat surface, the applied force *F* is related to the displacement d by Equation 6.4:[211]

$$F = \frac{4}{3}E^{*}\times R^{\frac{1}{2}}\times d^{\frac{3}{2}} \ (Equation\ 6.4)$$

where *E** is the effective elastic modulus. During the experiments, *F* and *d* were recorded by the UMT tribological instrument and elastic modulus (*E**) was estimated from the loading curve using the Hertzianmodel (Figure 6.6b). The elastic module of pure epoxy and ECA with 60 wt% silver flakes were measured as the controls and found to be 0.36 GPa and 0.42 GPa, respectively. For the DA-PPy-reinforced ECAs, the modulus increased almost linearly with the DA-PPy content from 0.55 GPa for the 1.5 wt% composite to 0.67 GPa for the 4.3 wt%. The highly

dispersed DA-PPy nanofibers within the polymer matrix provided a significant surface area for the fiber-epoxy interaction. Also, a large amount of amine (primary or secondary) functional groups from DA may further strengthen the epoxy network by cross-linking fiber molecules with the resins, affording a nanocomposite with exceptional mechanical properties. As proposed in Figure 6.7a, the ring opening reaction was first achieved between the aliphatic amines and epoxy groups to form a hydroxyl group and a secondary amine, which can further react with epoxide to yield a tertiary amine and an additional hydroxyl group. Thereafter, epoxide-(DA-PPy) is obtained to conduct the polymerization to form a pronounced cross-linked polymer matrix mainly through the hydrogen bonding among catechol/quinone functional groups (Figure 6.7b). It is noted that primary amines are also one of the most important components of commercial epoxy curing agents/hardeners. Mechanically reinforced polymer composites with electrical conductivities as high as 2400 S/cm were prepared by simply incorporating DA-PPy nanofibers (DA/Py = 0.064) into the composite formulation, which clearly demonstrated the advantage and multifunctionality of such material in ECA applications.

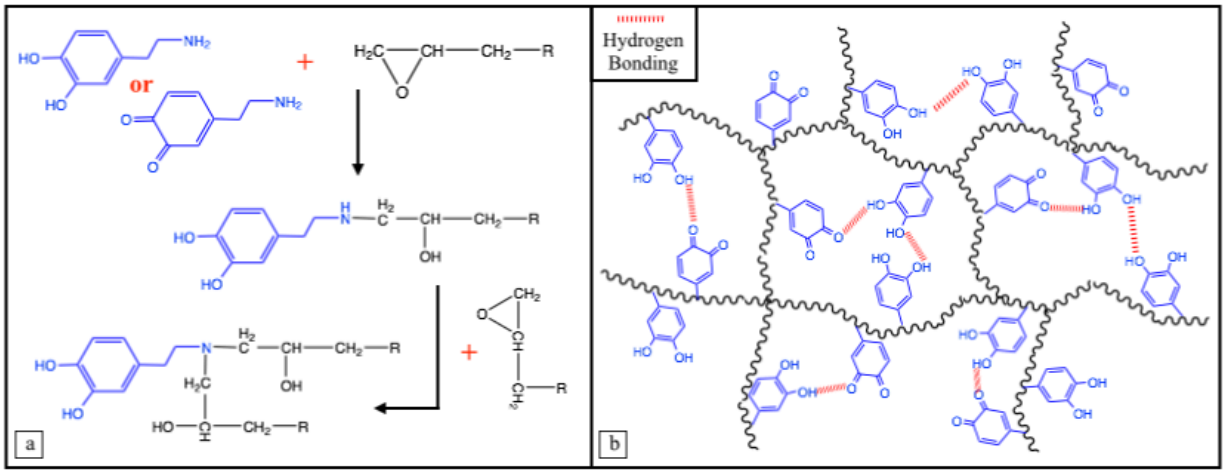

Figure 6.7. (a) Possible chemical reactions between epoxy and dopamine, and (b) a schematic illustration of DA-PPy reinforced epoxy network.

6.3.4 DA-PPy for Electro-Magnetic Interference (EMI) Shielding Application

With the continuously increasing DA/Py mole ratio, the resulting DA-PPy became less electrically conductive and its morphology emerged as nanoflakes at DA/Py = 0.64. Although this type of DA-PPy displayed relatively low electrical conductivity, it exhibited an impressive capability of absorbing electromagnetic microwaves making it potentially useful for electro-magnetic interference shielding. The complex permittivity ($\varepsilon r = \varepsilon' - j\varepsilon''$) and complex permeability ($\mu r = \mu' - j\mu''$) are two factors that significantly influence the microwave absorption properties of an absorber.[212] The real permittivity (ε') and real permeability (μ') represent the energy storage ability of electric and magnetic fields, while the imaginary parts of the permittivity (ε'') and permeability (μ'') symbolize the energy dissipation ability of electric and magnetic fields.[213] Within an electrically conductive material, conduction and displacement currents can be generated when exposed to an electromagnetic wave. The first one is induced by the free electrons and provides electric loss (imaginary permittivity ε''), the latter is caused by polarization of localized charges (real permittivity ε').[214] Figure 6.8(a, b) presents the variation of the complex permittivity (ε' and ε'') for DA-PPy nanomaterials synthesized from different DA/Py mole ratios. The real (ε') and imaginary (ε'') permittivity decreased as the frequency increased in the 2 to 18 GHz range. The real permittivity (ε') was improved dramatically by introducing small amount of DA (DA/Py = 0.032 and 0.064) on PPy, indicating the polarization degree of the materials were increased by the hydrophilic functional groups of DA. Moreover, DA-PPy at the same concentrations also exhibited large imaginary (ε'') permittivity values, suggesting their

strong electric energy loss capability owing to the enhanced electrical conductivity. At the highest DA/Py = 0.64 mole ratio, the values of both real and imaginary parts of permittivity were small and almost independent of the frequencies, which is related to its relatively low conductivity. The complex permeability (μ′ and μ″) of different DA-PPy samples are demonstrated in Figure 6.8(c, d). The real parts of permeability remained constant with a little fluctuation in the measured frequency range, showing there was almost no magnetic loss during the microwave absorption. The imaginary permeability slightly decreased with the frequency, attributed to the decrease of wavelength in the microwave absorber material.

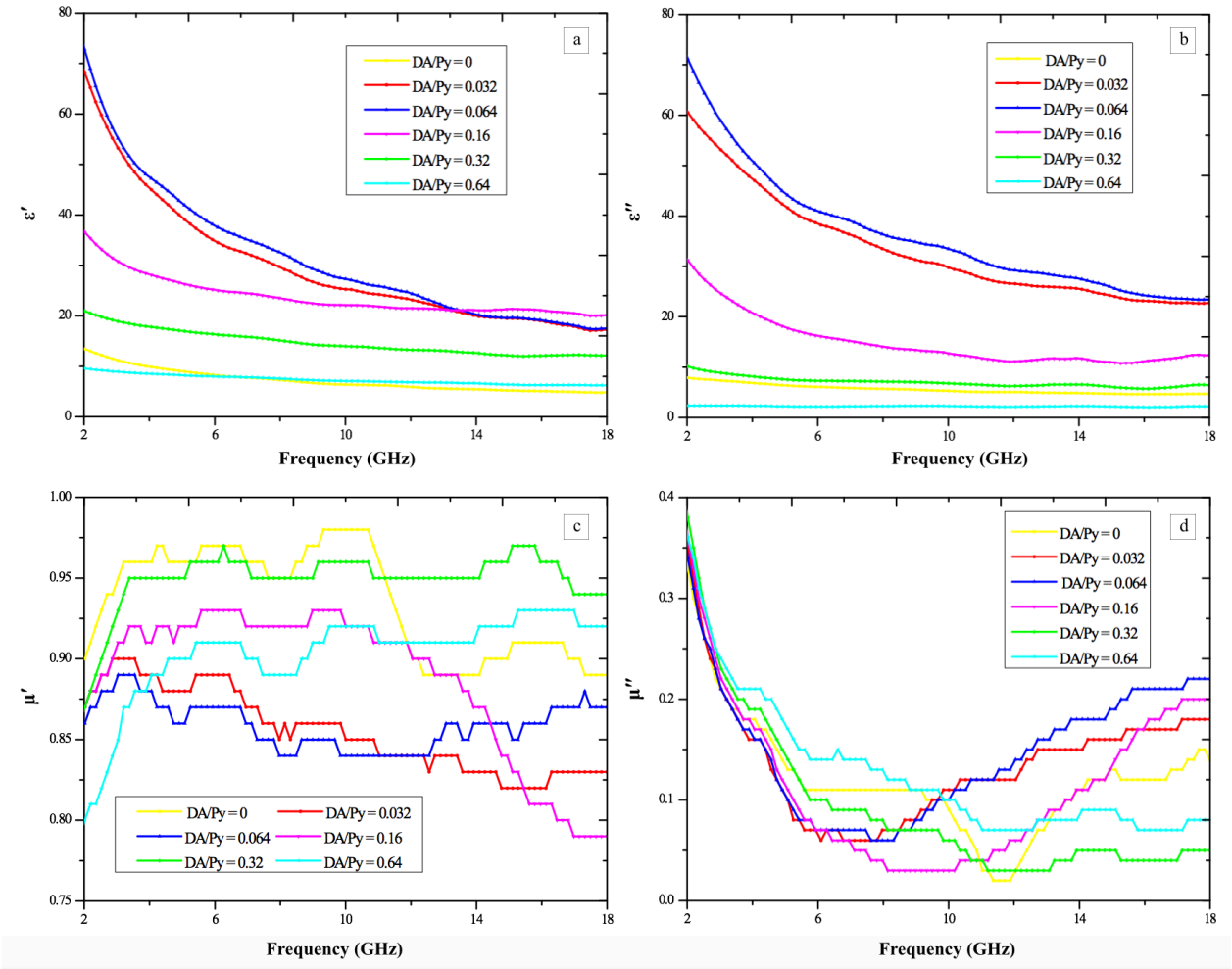

Figure 6.8. Electromagnetic properties of DA-PPy nanomaterials in the range of 2-18 GHz (a) real permittivity (ε′); (b) imaginary permittivity (ε″); (c) real permeability (μ′); and (d) imaginary permeability (μ″).

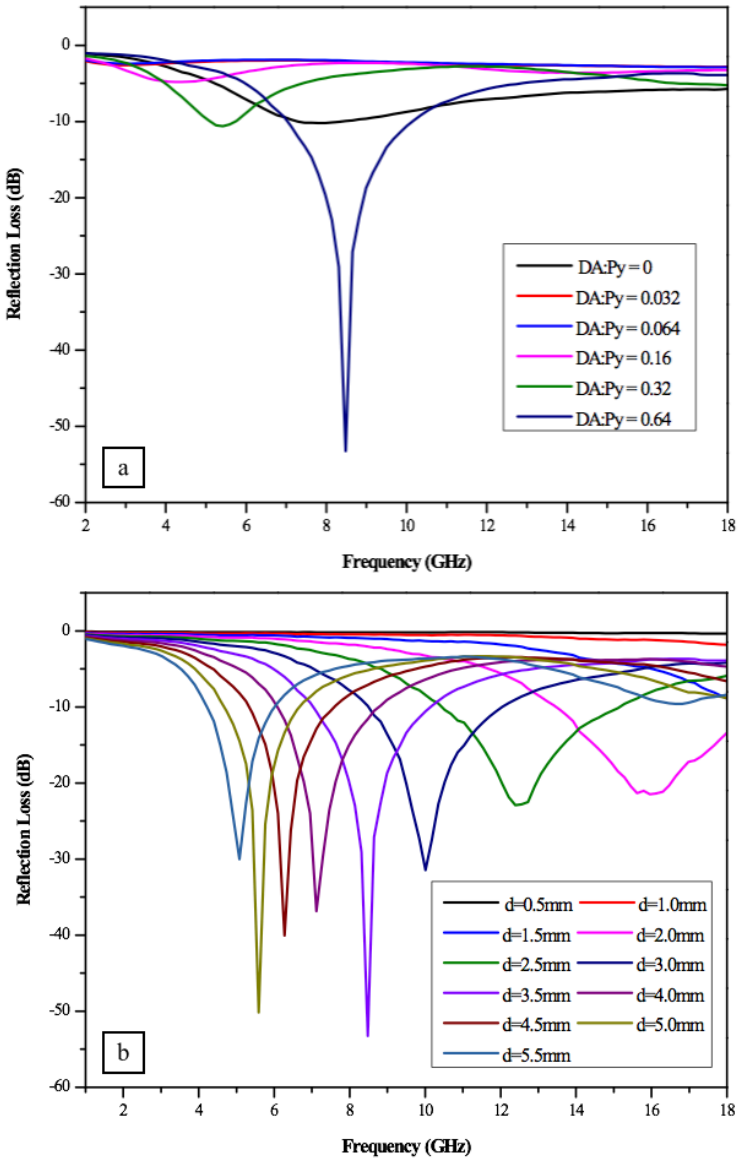

Figure 6.9. (a) Frequency dependence of the reflection loss of DA-PPy samples with a thickness of 3.5 mm in 2-18 GHz; (b) reflection loss of 0.64 DA-PPy by varying the thickness of the absorbent.

The reflection loss (R_L) values of the DA-PPy nanocomposites, which represented the microwave absorbing ability of the materials, were calculated by the following equations:

$$R(dB) = 20 \lg \left| \frac{Z_{in} - 1}{Z_{in} + 1} \right| \quad (Equation\ 6.5)$$

$$Z_{in} = \left(\frac{\varepsilon}{\mu}\right)^{1/2} \tanh\left[j\left(\frac{2\pi f d}{c}\right)(\mu\varepsilon)^{1/2}\right] \quad (Equation\ 6.6)$$

where Z_{in}, f, d and c signify the input impedance of the absorber, frequency of the electromagnetic waves, thickness of the absorber and velocity of light in free space, respectively. Figure 6.9a presents the reflection loss characteristics curve of DA-PPy prepared a different mole ratio with a absorber thicknesses of 3.5 mm. It was found that 0.64 DA-PPy exhibited the best microwave absorbing ability and the maximum R_L reached −54 dB at 8.5 GHz and the absorption bandwidth exceeding −10 dB was 4 GHz (from 7 GHz to 11 GHz). Figure 6.9b showed the reflection loss of the DA-PPy prepared from 0.64 DA/Py mole ratio at different thicknesses. The absorbing peaks shifted toward lower frequency with increasing thickness and the composites with the thickness of 3.5 mm achieved the maximum absorbing value. We ascribed such excellent microwave absorption performance to the unique DA-PPy core-shell interfaces, which could improve dielectric loss through interface polarization and relaxation effects. In addition, the good dispersion of DA-PPy at high DA/Py mole ratio in epoxy, as well as the excellent dielectric properties of DA-PPy, may also be beneficial to enhance the electromagnetic absorption. For microwave absorption materials, R_L = −50.0 dB implies 99.999% attenuation of the electromagnetic wave, therefore the DA-PPy prepared at DA/Py = 0.64 was demonstrated to be a promising candidate as a microwave absorber material in X-band frequencies.

6.4 Conclusions

In summary, we have prepared a series of DA-PPy nanomaterials with various morphologies including nanospheres, nanofibers, nanorods and nanoflakes, which can be precisely controlled by simply varying the DA/Py reacting mole ratio. Moreover, these nanostructures also possessed

tunable electrical properties. To be specific, 0.032 DA-PPy fabricated electrodes displayed outstanding supercapacitor behavior with a capacitance of 182 F/g; 0.064 DA-PPy dramatically improved the electrical conductivity and mechanical properties of conventional ECAs at only 3 wt% loading; and 0.64 DA-PPy displayed excellent electromagnetic microwave absorption ability and can be applied effectively for shielding purposes. Overall, all of these extreme properties can be combined in one type of material - DA-PPy. We believe our approach could develop a promising system for the future technical innovations.

CHAPTER 7. CONCLUSION AND FUTURE WORK

7.1 Summary of Contributions and Concluding Remarks

This research program aims to investigate polydopamine thin film properties and develop novel hybrid conductive functional polydopamine-polypyrrole nanocomposites with desired properties. To achieve the objectives of this project, research on the nature, morphology, chemical and physical properties of the PDA and DA-PPy has been divided into four sections:

(1) **Fundamental Investigations of PDA films**

A series of experimental studies were carried out to characterize the PDA thin films coated on three typical well-defined substrates - glass, polydimethylsiloxane (PDMS) and epoxy - to investigate their material behavior under a mechanical stress/strain field and the effects of coating substrates. Micro-indentation measurements combined with Johnson–Kendall–Roberts (JKR) contact mechanics theory were also used to systematically study the tribological properties of PDA thin films in both dry and wet conditions. This work first reported different properties including adhesion, friction and cracking of PDA thin film in water and revealed the material properties of hydrated PDA films are significantly different from those of dehydrated ones. This work also benefits PDA thin film applications in bioengineering where water is the medium. We published this work in *Biomacromolecules* **2013**, *14*, 349-405.

(2) Dopamine functionalization of PPy and its potential application

Systematic studies of PDA films provide insights into their stability, mechanical and adhesive properties. Based on these results, we combined DA with a conducting polymer

polypyrrole (PPy). We found that DA-modified PPy exhibited different morphology, enhanced adhesion, higher electrical conductivity and smaller particle size. All of these new features made DA-PPy stand out as a promising candidate for many commercial applications. In this work, we have developed an effective synthetic approach to the preparation of DA-PPy nanocomposites. Methods for fabricating these materials were unknown prior to this work. We published this work in *Macromolecular Rapid Communications* **2014**, *35*, 350-354.

(3) Mechanism Study

DA surface modification of PPy introduces new functional groups and properties for further reactions without limiting its biocompatibility. This has been shown to provide additional chemical and physical properties for PPy commercial applications. However, much effort is still necessary to explain the mechanisms involved in their synthesis. With this regard, we performed a detailed and systematic investigation using three types of bio-inspired catechol derivatives - simple catechol (CA), DOPA and dopamine - and 2-phenylethylamine (PA) in the synthesis of PPy. These studies have provided strong evidence that catechol modification of PPy by a one-step, template-free and benign in-situ procedure as a general protocol to functionalize conducting polymers to overcome the problems of poor water dispersibility and low interfacial adhesion of PPy. We published this work in *Advanced Functional Materials* **2015**, *25*, 1588-1597.

(4) Modification of PDA functionalized PPy

After understanding the mechanism of the effect of PDA on the adhesion and conductivity properties of PPy, further modification of the synthesis of polydopamine

functionalized polypyrrole was achieved by using a different dopant and oxidizing agent. The modified DA-PPy exhibited various morphologies including nanospheres, nanofibers, nanorods, and nanoflakes. All of these nanostructures can be achieved by simply varying the DA/Py reaction mole ratio. Furthermore, we also explored suitable applications of each as-fabricated DA-PPy depending on their unique properties. In particular, DA-PPy obtained at a 0.032 dopamine/pyrrole (DA/Py) mole ratio demonstrated superior capacitance for supercapacitors; at DA/Py = 0.064, DA-PPy can be implemented as a co-filler into the epoxy network to prepare hybrid electrically conductive adhesives (ECAs); and DA-PPy synthesized from 0.64 DA/Py mole ratio revealed impressive electromagnetic microwave absorption ability, which can be used for electro-magnetic interference (EMI) shielding applications. Due to the synergistic effect of DA modification, this one-step procedure for PPy functionalization is able to produce all of these different properties in one type of material, and open the possibility of using DA to modify other functional materials. We have submitted this work to *Advanced Electronic Materials*.

7.2 List of Peer-reviewed Publications

- **Wei Zhang**, Zihe Pan, Fut K. Yang, Boxin Zhao. A Facile In-Situ Approach to Polypyrrole Functionalization through Bio-Inspired Catechols. *Advanced Functional Materials*. **2015**, *25*, 1588-1597.
- **Wei Zhang**, Fut K. Yang, Zihe Pan, Jian Zhang, Boxin Zhao. Bio-inspired Dopamine Functionalization of Polypyrrole for Improved Adhesion and Conductivity.

Macromolecular Rapid Communication. **2014**, *35*, 350-354.

- **Wei Zhang**, Fut K. Yang, Yougun Han, Ravi Gaikwad, Zoya Leonenko, Boxin Zhao. Surface and Tribological Behaviors of the Bioinspired Polydopamine Thin Films Under Dry and Wet Conditions. *Biomacromolecules*. **2013**, *14*, 394-405.
- **Wei Zhang**, Behnam Meschi Amoli, Jeffrey d'Eon, Alex Chen, Boxin Zhao. Development of Novel Polydopamine-Polypyrrole Nanofibers for Electrically Conductive Adhesive Applications. *Journal of Surface Mount Technology*. Feb 2nd, **2015**.
- **Wei Zhang**, Yikang Zhou, Kun Feng, Josh Trinidad, Boxin Zhao. Morphologically Controlled Bio-Inspired Dopamine-Polypyrrole Nanostructures With Tunable Electrical Properties. *Advanced Functional Materials*. **2015**, submitted.
- Fut K. Yang, **Wei Zhang**, Yougun Han, Serge Yoffe, Yungchi Cho, Boxin Zhao. "Contact" of Nanoscale Stiff Films. *Langmuir*. **2012**, *28*, 9562-9572.
- Dhamodaran Arunbabu, Hamed Shahsavan, **Wei Zhang**, Boxin Zhao. Poly(AAc-co-MBA) Hydrogel Films: Adhesive and Mechanical Properties in Aqueous Medium. *Journal of Physical Chemistry B*. **2013**, *117*, 441-449.
- Juntao Tang, Micky Fu Xiang Lee, **Wei Zhang**, Boxin Zhao, Richard M Berry, Kam C. Tam. Dual Responsive Pickering Emulsion Stabilized by PDMAEMA Grafted Cellulose Nanocrystals. *Biomacromolecules*. **2014**, *15*, 3052-3060.
- Zihe Pan; Hamed Shahsavan; **Wei Zhang**; Fut K Yang, Boxin Zhao. Superhydro-oleophobic Bio-inspired Polydimethylsiloxane Micropillared Surface via FDTS Coating/Blending Approaches. *Applied Surface Science*, **2015**, *324*, 612-620.

7.3 Future Work

This work successfully demonstrated the potential of DA-PPy nanomaterials in a range of technical areas. However, several additional questions can be answered in future work, which would broaden the understanding of their potential applications as well as the performance in the next generation of advanced electronics.

(1) We have proposed several possible DA and PPy reaction models; it is still necessary to confirm our hypothesis. Molecular weights, molecular weight distributions and chemical structures of modified PPy are useful information that could help understand the effect of the presence of dopamine on PPy polymerization and its physical properties. It is not feasible to perform solution NMR on PPy and PDA since neither of them can be dissolved in any known organic solvent. Solid stage C^{13} NMR and N^{15} NMR are two options that can be performed in the future to determine the chemical structure of DA-PPy. Elemental analysis may give the C, N and H composition of DA-PPy samples, which could be used to identify the final ratio of DA to PPy in the product. High temperature gel permeation chromatography (GPC) experiment of DA-PPy composites, which may yield the polymer molecular weight and distribution, are also worth investigation.

(2) Since the thermal stability of DA-PPy is essential to its application in ECAs, TGA and DSC should be conducted on ECAs containing pure PDA, pure PPy, PDA functionalized PPy and DA-PPy. By examining the decomposition temperatures and transition states of each sample, we may be able to identify whether DA is covalently linked to Py or non-covalently by van der Waals forces in either polymeric or oligomeric form. We have demonstrated that a large amount of amine (primary or secondary) functional groups from

DA-PPy could further strengthen the epoxy network by cross-linking fiber molecules with the resins and afford nanocomposites with exceptional mechanical properties. Thus, systematic TGA and DSC investigations could reveal much useful information regarding the interaction of DA-PPy with epoxy resin. For example, does the epoxy curing temperature change after adding different amounts of DA-PPy co-fillers? Could DA-PPy potentially replace the curing agent in the composite? Does the addition of DA-PPy into the epoxy/silver system shorten the epoxy curing time or lower epoxy curing temperature? All of these fundamental questions are extremely helpful for the development of novel ECA systems.

(3) Although we have characterized the electrical properties of DA-PPy when they were applied in specific applications, the intrinsic DA-PPy electrical properties are still unexplored. For example, the electrical conductivity was measured when DA-PPy was compressed into pellets; the electrochemical properties were characterized when DA-PPy was fabricated on the electrodes as thin films; the electro-magnetic properties were investigated when DA-PPy was dispersed into wax. Nevertheless, since the contact of the individual nanoparticles varies under different pressures and forms, the packaging effect may have certain influences on the electrical properties of DA-PPy nanomaterial. As a result, we believe the intrinsic DA-PPy electrical properties, as well as the influence of sample packaging to their properties and the surface area of each type of the nanostructures, are worthwhile to investigate in the future.

(4) We hope that by better understanding the effect of DA on the adhesion and conductivity properties of PPy, it can be applied to functionalize other conducting polymers, such as

polyaniline. Polyaniline and PPy are both π-conjugated polymers that can be prepared by chemical oxidative polymerization of the corresponding monomers in an aqueous medium. Similar to PPy, the physical form of polyaniline is usually an insoluble powder, which requires further modification before industrial use. Thus, the DA functionalization strategy may also be applied to polyaniline synthesis to broaden its potential applications.

References

(1) Lee, H.; Dellatore, S. M.; Miller, W. M.; Messersmith, P. B. Mussel-inspired surface chemistry for multifunctional coatings. *Science***2007**, *318*, 426-430.

(2) Waite, J. H. Surface chemistry: Mussel power. *Nat. Mater.***2008**, *7*, 8-9.

(3) Lee, H.; Lee, Y.; Statz, A. R.; Rho, J.; Park, T. G.; Messersmith, P. B. Substrate-independent layer-by-layer assembly by using mussel-adhesive-inspired polymers. *Adv. Mater.***2008**, *20*, 1619-1623.

(4) Lee, H.; Rho, J.;Messersmith, P. B. Facile conjugation of biomolecules onto surfaces via mussel adhesive protein inspired coatings. *Adv. Mater.***2009**, *21*, 431-434.

(5) Liu, Y.; Ai, K.; Lu, L. Polydopamine and its derivative materials: Synthesis and promising applications in energy, environmental, and biomedical fields. *Chem. Rev.***2014**.*114*, 5057-5115.

(6) Waite, J. H. Mussel-inspired wet adhesives and coatings. *Annu. Rev. Mater. Res.***2011**, *41*, 99-132.

(7) Zhang, W.; Yang, F. K.; Han, Y.; Gaikwad, R.; Leonenko, Z.; Zhao, B. Surface and tribological behaviors of the bioinspired polydopamine thin films under dry and wet conditions. *Biomacromolecules***2013**, *14*, 394-405.

(8) Yang, F. K.; Zhang, W.; Han, Y.; Yoffe, S.; Cho, Y.; Zhao, B. Contact of nanoscale stiff films. *Langmuir***2012**, *28*, 9562-9572.

(9) Ball, V.; Del Frari, D.; Toniazzo, V.; Ruch, D. Kinetics of polydopamine film deposition as a function of pH and dopamine concentration: insights in the polydopamine deposition mechanism. *J. Colloid Interface Sci.***2012**, *386*, 366-372.

(10) Zhang, W.; Yang, F. K.; Pan, Z.; Zhang, J.; Zhao, B. Bio-inspired dopamine

functionalization of polypyrrole for improved adhesion and conductivity. *Macromol. Rapid Commun.***2014**, *35*, 350-354.

(11) Zhang, W.; Pan, Z.; Yang, F. K.; Zhao, B. A facile in situ approach to polypyrrole functionalization through bioinspired catechols.*Adv. Funct. Mater.***2015**, *25*, 1588-1597.

(12) You, Z.; Wang, Y. A versatile synthetic platform for a wide range of functionalized biomaterials. *Adv. Funct. Mater.***2012**, *22*, 2812-2820.

(13) Darder, M.; Aranda, P.; Ruiz-Hitzky, E. Bionanocomposites: a new concept of ecological, bioinspired, and functional hybrid materials. *Adv. Mater.***2007**, *19*, 1309-1319.

(14) Varenberg, M.;Gorb, S. A beetle-inspired solution for underwater adhesion.*J. R. Soc. Interface***2008**, *5*, 383-385.

(15) Lee, H.; Lee, B. P.; Messersmith, P. B. A reversible wet/dry adhesive inspired by mussels and geckos.*Nature***2007**, *448*, 338-341.

(16) Waite, J. H. Nature's underwater adhesive specialist. *Int. J. Adhes. Adhes***1987**, *7*, 9-14.

(17) Kinloch, A. J. The science of adhesion.*J. Mater. Sci.***1980**, *15*, 2141-2166.

(18) Johnson, K. L. Mechanics of adhesion. *Tribol. Int.***1998**, *31*, 413-418.

(19) Bowditch, M. R. The durability of adhesive joints in the presence of water.*Int. J. Adhes. Adhes.***1996**, *16*, 73-79.

(20) Clint, J. H.; Wicks, A. C. Adhesion under water: surface energy considerations. *Int. J. Adhes. Adhes.***2001**, *21*, 267-273.

(21) Wilker, J. J. Marine bioinorganic materials: mussels pumping iron. *Curr.Opin.Chem. Biol.***2010**, *14*, 276-283.

(22) Sever, M. J.; Weisser, J. T.; Monahan, J.; Srinivasan, S.; Wilker, J. J. Metal-mediated

cross-linking in the generation of a marine-mussel adhesive. *Angew. Chem. Int. Ed.***2004**, *43*, 448-450.

(23) Liu, X.; Cao, J.; Li, H.; Li, J.; Jin, Q.; Ren, K.; Ji, J. Mussel-inspired polydopamine: a biocompatible and ultrastable coating for nanoparticles in vivo. *ACS Nano***2013**, *7*, 9384-9395.

(24) Lee, B. P.; Dalsin, J. L.; Messersmith, P. B. Synthesis and gelation of DOPA-modified poly (ethylene glycol) hydrogels. *Biomacromolecules***2002**, *3*, 1038-1047.

(25) Lee, H.; Scherer, N. F.; Messersmith, P. B. Single-molecule mechanics of mussel adhesion. *Proc. Natl. Acad. Sci. U.S.A.***2006**, *103*, 12999-13003.

(26) Zeng, H.; Hwang, D. S.; Israelachvili, J. N.; Waite, J. H. Strong reversible Fe^{3+}-mediated bridging between dopa-containing protein films in water. *Proc. Natl. Acad. Sci. U.S.A.***2010**, *107*, 12850-12853.

(27) Waite, J. H.; Qin, X. Polyphosphoprotein from the adhesive pads of Mytilusedulis. *Biochemistry***2001**, *40*, 2887-2893.

(28) White, J. D.;Wilker, J. J. Underwater bonding with charged polymer mimics of marine mussel adhesive proteins. *Macromolecules***2011**, *44*, 5085-5088.

(29) Yu, M.; Hwang, J.; Deming, T. J. Role of *L*-3, 4-dihydroxyphenylalanine in mussel adhesive proteins. *J. Am. Chem. Soc.***1999**, *121*, 5825-5826.

(30) Ye, Q.; Zhou, F.; Liu, W. Bioinspired catecholic chemistry for surface modification. *Chem. Soc. Rev.***2011**, *40*, 4244-4258.

(31) Westwood, G.; Horton, T. N.; Wilker, J. J. Simplified polymer mimics of cross-linking adhesive proteins. *Macromolecules***2007**, *40*, 3960-3964.

(32) Yu, M.; Deming, T. J. Synthetic polypeptide mimics of marine adhesives.

*Macromolecules***1998**, *31*, 4739-4745.

(33) Sedó, J.; Saiz-Poseu, J.; Busqué, F.; Ruiz-Molina, D. Catechol-based biomimetic functional materials. *Adv. Mater.***2013**, *25*, 653-701.

(34) Faure, E.; Falentin-Daudré, C.; Jérôme, C.; Lyskawa, J.; Fournier, D.; Woisel, P.; Detrembleur, C. Catechols as versatile platforms in polymer chemistry. *Prog. Polym.Sci.***2013**,*38*, 236-270.

(35) Zangmeister, R. A.; Morris, T. A.; Tarlov, M. J. Characterization of polydopamine thin films deposited at short times by autoxidation of dopamine. *Langmuir***2013**, *29*, 8619-8628.

(36) Yang, H. C.; Wu, Q. Y.; Wan, L. S.; Xu, Z. K. Polydopamine gradients by oxygen diffusion controlled autoxidation. *Chem. Commun.***2013**, *49*, 10522-10524.

(37) Du, X.; Li, L.; Li, J.; Yang, C.; Frenkel, N.; Welle, A.; Heissler, S.; Nefedov, A.; Grunze, M.; Levkin, P. A. UV-Triggered dopamine polymerization: control of polymerization, surface coating, and photopatterning. *Adv. Mater.***2014**. *26*, 8029-8033.

(38) dIschia, M.; Napolitano, A.; Ball, V.; Chen, C. -T.; Buehler, M. J. Polydopamine and eumelanin: from structure-property relationships to a unified tailoring strategy. *Acc.Chem. Res.***2014**.*47*, 3541-3550.

(39) Arzillo, M.; Mangiapia, G.; Pezzella, A.; Heenan, R. K.; Radulescu, A.; Paduano, L.; dIschia, M. Eumelanin buildup on the nanoscale: aggregate growth/assembly and visible absorption development in biomimetic 5, 6-dihydroxyindole polymerization. *Biomacromolecules***2012**, *13*, 2379-2390.

(40) Dreyer, D. R.; Miller, D. J.; Freeman, B. D.; Paul, D. R.; Bielawski, C. W. Elucidating the structure of poly(dopamine). *Langmuir***2012**, *28*, 6428-6435.

(41) Lin, S.; Chen, C. -T.; Bdikin, I.; Ball, V.; Grácio, J.; Buehler, M. J. Tuning heterogeneous poly(dopamine) structures and mechanics: in silico covalent cross-linking and thin film nanoindentation. *Soft Matter***2014**, *10*, 457-466.

(42) Liebscher, J. R.; Mrowczyn ski, R.; Scheidt, H. A.; Filip, C.; Ha dade, N. D.; Turcu, R.; Bende, A.; Beck, S. Structure of polydopamine: a never-ending story? *Langmuir***2013**, *29*, 10539-10548.

(43) Hong, S.; Na, Y. S.; Choi, S.; Song, I. T.; Kim, W. Y.; Lee, H. Non-covalent self-Assembly and covalent polymerization co-contribute to polydopamine formation. *Adv. Funct. Mater.***2012**, *22*, 4711-4717.

(44) Dimitrakopoulos, C. D.;Malenfant, P. R. L. Organic thin film transistors for large area electronics. *Adv. Mater.***2002**, *14*, 99-117.

(45) Peterson, I. R. Langmuir-blodgett films. *J. Phys. D: Appl. Phys.***1990**, *23*, 379-395.

(46) Chen, W.; McCarthy, T. J. Layer-by-layer deposition: a tool for polymer surface modification. *Macromolecules***1997**, *30*, 78-86.

(47) Zhou, J.; Ellis, A. V.; Voelcker, N. H. Recent developments in PDMS surface modification for microfluidic devices. *Electrophoresis***2010**, *31*, 2-16.

(48) Ambrico, M.; Ambrico, P. F.; Cardone, A.; Della Vecchia, N. F.; Ligonzo, T.; Cicco, S. R.; Talamo, M. M.; Napolitano, A.; Augelli, V.; Farinola, G. M.; d'Ischia, M. Engineering polydopamine films with tailored behaviour for next-generation eumelanin-related hybrid devices. *J. Mater. Chem. C***2013**, *1*, 1018-1026.

(49) Lynge, M. E.; van der Westen, R.; Postma, A.; Städler, B. Polydopamine-a nature-inspired polymer coating for biomedical science. *Nanoscale***2011**, *3*, 4916-4928.

(50) Jiang, J. H.; Zhu, L. P.; Zhu, L. J.; Zhu, B. K.; Xu, Y. Y. Surface characteristics of self-polymerized dopamine coating deposited on hydrophobic polymer films. *Langmuir***2011**, *27*, 14180-14187.

(51) Kim, H. W.; McCloskey, B. D.; Choi, T. H.; Lee, C.; Kim, M. -J.; Freeman, B. D.; Park, H. B. Oxygen concentration control of dopamine-induced high uniformity surface coating chemistry. *ACS Appl. Mater. Interfaces***2013**, *5*, 233-238.

(52) Ku, S. H.; Ryu, J.; Hong, S. K.; Lee, H.; Park, C. B. General functionalization route for cell adhesion on non-wetting surfaces. *Biomaterials***2010**, *31*, 2535-2541.

(53) Zhang, L.; Shi, J.; Jiang, Z.; Jiang, Y.; Qiao, S.; Li, J.; Wang, R.; Meng, R.; Zhu, Y.; Zheng, Y. Bioinspired preparation of polydopamine microcapsule for multienzyme system construction. *Green Chem.***2011**, *13*, 300-306.

(54) Yang, F. K.; Zhao, B. Adhesion properties of self-polymerized dopamine thin film. *Open Surf. Sci. J.***2011**, *3*, 115-122.

(55) Bernsmann, F.; Ponche, A.; Ringwald, C.; Hemmerle, J.; Raya, J.; Bechinger, B.; Voegel, J. C.; Schaaf, P.; Ball, V. Characterization of dopamine-melanin growth on silicon oxide. *J. Phys. Chem. C***2009**, *113*, 8234-8242.

(56) Bernsmann, F.; Ball, V.; Addiego, F.; Ponche, A.; Michel, M.; Gracio, J. J. A.; Toniazzo, V.; Ruch, D. Dopamine-melanin film deposition depends on the used oxidant and buffer solution. *Langmuir***2011**, *27*, 2819-2825.

(57) Bothma, J. P.; de Boor, J.; Divakar, U.; Schwenn, P. E.; Meredith, P. Device-quality electrically conducting melanin thin films. *Adv. Mater.***2008**, *20*, 3539-3542.

(58) Ball, V.; Frari, D.; Michel, M.; Buehler, M. J.; Toniazzo, V.; Singh, M. K.; Gracio, J.; Ruch,

D. Deposition mechanism and properties of thin polydopamine films for high added value applications in surface science at the nanoscale. *BioNanoScience***2012**, *2*, 16-34.

(59) Wei, Q.; Zhang, F.; Li, J.; Li, B.; Zhao, C. Oxidant-induced dopamine polymerization for multifunctional coatings. *Polym. Chem.***2010**, *1*, 1430-1433.

(60) You, I.; Kang, S. M.; Byun, Y.; Lee, H. Enhancement of blood compatibility of poly(urethane) Substrates by Mussel-inspired adhesive heparin coating. *Bioconjugate Chem.***2011**, *22*, 1264-1269.

(61) Kang, S. M.; Hwang, N. S.; Yeom, J.; Park, S. Y.; Messersmith, P. B.; Choi, I. S.; Langer, R.; Anderson, D. G.; Lee, H. One-step multipurpose surface functionalization by adhesive catecholamine. *Adv. Funct Mater.***2012**, *22*, 2949-2955.

(62) Kang, S. M.; You, I.; Cho, W. K.; Shon, H. K.; Lee, T. G.; Choi, I. S.; Karp, J. M.; Lee, H. One-step modification of superhydrophobic surfaces by a mussel-inspired polymer coating. *Angew. Chem. Int. Ed.***2010**, *49*, 9401-9404.

(63) Sileika, T. S.; Kim, H. D.; Maniak, P.; Messersmith, P. B. Antibacterial performance of polydopamine modified polymer surfaces containing passive and active components. *ACS Appl. Mater.Interfaces***2011**, 3, 4602-4610.

(64) Kang, S.;Elimelech, M. Bioinspired single bacterial cell force spectroscopy. *Langmuir***2009**, *25*, 9656-9659.

(65) Chao, C.; Xiang, X.; Zhai, R.; Zhang, B.; Liu, J.; Chen, R. Natural nanotube-based biomimetic porous microspheres for significantly enhanced biomolecule immobilization. *ACS Sustainable Chem. Eng.***2013**, *2*, 396-403.

(66) Ryu, J.; Ku, S. H.; Lee, H.; Park, C. B. Mussel-inspired polydopamine coating as a universal

route to hydroxyapatite crystallization. *Adv. Funct. Mater.***2010**, *20*, 2132-2139.

(67) Ku, S. H.; Lee, J. S.; Park, C. B. Spatial control of cell adhesion and patterning through mussel-inspired surface modification by polydopamine. *Langmuir***2010**, *26*, 15104-15108.

(68) Yang, S. H.; Kang, S. M.; Lee, K. -B.; Chung, T. D.; Lee, H.; Choi, I. S. Mussel-inspired encapsulation and functionalization of individual yeast cells. *J. Am. Chem. Soc.***2011**, *133*, 2795-2797.

(69) Yu, B.; Wang, D. A.; Ye, Q.; Zhou, F.; Liu, W. Robust polydopamine nano/microcapsules and their loading and release behavior. *Chem. Commun.***2009**, *44*, 6789-6791.

(70) Zhang, L.; Shi, J.; Jiang, Z.; Jiang, Y.; Meng, R.; Zhu, Y.; Liang, Y.; Zheng, Y. Facile preparation of robust microcapsules by manipulating metal-coordination interaction between biomineral layer and bioadhesive layer. *ACS Appl. Mater. Interfaces***2011**, *3*, 597-605.

(71) Postma, A.; Yan, Y.; Wang, Y.; Zelikin, A. N.; Tjipto, E.; Caruso, F. Self-polymerization of dopamine as a versatile and robust technique to prepare polymer capsules. *Chem. Mater.***2009**, *21*, 3042-3044.

(72) Ochs, C. J.; Hong, T.; Such, G. K.; Cui, J.; Postma, A.; Caruso, F. Dopamine-mediated continuous assembly of biodegradable capsules. *Chem. Mater.***2011**, *23*, 3141-3143.

(73) Cui, J.; Wang, Y.; Postma, A.; Hao, J.; Hosta-Rigau, L.; Caruso, F. Monodisperse polymer capsules: tailoring size, shell thickness, and hydrophobic cargo loading via emulsion templating. *Adv. Funct. Mater.***2010**, *20*, 1625-1631.

(74) Cui, J.; Yan, Y.; Such, G. K.; Liang, K.; Ochs, C. J.; Postma, A.; Caruso, F. Immobilization and intracellular delivery of an anticancer drug using mussel-inspired polydopamine capsules. *Biomacromolecules***2012**, *13*, 2225-2228.

(75) Ryou, M. H.; Lee, Y. M.; Park, J. K.; Choi, J. W. Mussel-inspired polydopamine-treated polyethylene separators for high-power Li-ion batteries. *Adv. Mater.***2011**, *23*, 3066-3070.

(76) Zhang, L.; Wu, J.; Wang, Y.; Long, Y.; Zhao, N.; Xu, J. Combination of bio-inspiration: a general route to superhydrophobic particles. *J. Am. Chem. Soc.***2012**, *134*, 9879-9881.

(77) Fouineau, J.; Brymora, K.; Ourry, L.; Mammeri, F.; Yaacoub, N.; Calvayrac, F.; Ammar, S.; Greneche, J. -M. Synthesis, Mössbauer characterization, and ab initio modelling of iron oxide nanoparticles of medical interest functionalized by dopamine. *J. Phys. Chem. C***2013**, *117*, 14925-14302.

(78) Shukoor, M. I.; Natalio, F.; Therese, H. A.; Tahir, M. N.; Ksenofontov, V.; Panthofer, M.; Eberhardt, M.; Theato, P.; Schro der, H. C.; Mu ller, W. E. Fabrication of a silica coating on magnetic γ-Fe_2O_3 nanoparticles by an immobilized enzyme. *Chem. Mater.***2008**, *20*, 3567-3573.

(79) Fei, B.; Qian, B.; Yang, Z.; Wang, R.; Liu, W.; Mak, C.; Xin, J. Coating carbon nanotubes by spontaneous oxidative polymerization of dopamine. *Carbon***2008**, *46*, 1795-1797.

(80) Hu, H.; Yu, B.; Ye, Q.; Gu, Y.; Zhou, F. Modification of carbon nanotubes with a nanothin polydopamine layer and polydimethylamino-ethyl methacrylate brushes. *Carbon***2010**, *48*, 2347-2353.

(81) Shi, J.; Yang, C.; Zhang, S.; Wang, X.; Jiang, Z.; Zhang, W.; Song, X.; Ai, Q.; Tian, C. Polydopamine microcapsules with different wall structures prepared by a template-mediated method for enzyme immobilization. *ACS Appl. Mater. Interfaces***2013**, *5*, 9991-9997.

(82) Kaminska, I.; Das, M. R.; Coffinier, Y.; Niedziolka-Jonsson, J.; Sobczak, J.; Woisel, P.; Lyskawa, J.; Opallo, M.; Boukherroub, R.; Szunerits, S. Reduction and functionalization of graphene oxide sheets using biomimetic dopamine derivatives in one step. *ACS Appl. Mater.*

*Interfaces***2012**, *4*, 1016-1020.

(83) Cheng, C.; Li, S.; Nie, S.; Zhao, W.; Yang, H.; Sun, S.; Zhao, C. A general and biomimetic approach to biopolymer functionalized graphene oxide nanosheet through adhesive dopamine. *Biomacromolecules***2012**, *13*, 4236-4246.

(84) Xu, L. Q.; Yang, W. J.; Neoh, K. -G.; Kang, E. -T.; Fu, G. D. Dopamine-induced reduction and functionalization of graphene oxide nanosheets. *Macromolecules***2010**, *43*, 8336-8339.

(85) Kang, S. M.; Park, S.; Kim, D.; Park, S. Y.; Ruoff, R. S.; Lee, H. Simultaneous reduction and surface functionalization of graphene oxide by mussel-inspired chemistry. *Adv. Funct. Mater.***2011**, *21*, 108-112.

(86) Mi, Y.; Wang, Z.; Liu, X.; Yang, S.; Wang, H.; Ou, J.; Li, Z.; Wang, J. A simple and feasible in-situ reduction route for preparation of graphene lubricant films applied to a variety of substrates. *J. Mater. Chem.***2012**, *22*, 8036-8042.

(87) Street, G. B.; Clarke, T. C. Conducting polymers: a review of recent work. *IBM J. Res. Dev.***1981**, *25*, 51-57.

(88) Pfluger, P.; Street, B. Chemical, electronic, and structural properties of conducting heterocyclic polymers: a view by XPS. *J. Chem. Phys.***1984**, *80*, 544-552.

(89) Kane-Maguire, L. A.; Wallace, G. G. Chiral conducting polymers. *Chem. Soc. Rev.***2010**, *39*, 2545-2576.

(90) Das, T. K.;Prusty, S. Review on conducting polymers and their applications. *Polym-Plast. Technol.***2012**, *51*, 1487-1500.

(91) Ravichandran, S.; Nagarajan, S.; Kokil, A.; Ponrathnam, T.; Bouldin, R. M.; Bruno, F. F.; Samuelson, L.; Kumar, J.; Nagarajan, R. Micellarnanoreactors for hematin catalyzed synthesis of

electrically conducting polypyrrole. *Langmuir***2012**, *28*, 13380-13386.

(92) Efimov, O. N. Polypyrrole: a conducting polymer; its synthesis, properties and applications. *Russ. Chem. Rev.***1997**, *66*, 443-453.

(93) Janata, J.;Josowicz, M. Conducting polymers in electronic chemical sensors. *Nat. Mater.***2003**, *2*, 19-24.

(94) Ateh, D. D.; Navsaria, H. A.; Vadgama, P. Polypyrrole-based conducting polymers and interactions with biological tissues. *J. R. Soc. Interface***2006**, *3*, 741-752.

(95) Ansari, R. Polypyrrole conducting electroactive polymers: synthesis and stability studies. *J. Chem.***2006**, *3*, 186-201.

(96) Sasso, C.; Beneventi, D.; Zeno, E.; Chaussy, D.; Petit-Conil, M.; Belgacem, N. Polypyrrole and polypyrrole/wood-derived materials conducting composites: a review. *BioResources***2011**, *6*, 3585-3620.

(97) Park, B. -W.; Yang, L.; Johansson, E. M.; Vlachopoulos, N.; Chams, A.; Perruchot, C.; Jouini, M.; Boschloo, G.; Hagfeldt, A. Neutral, polaron, and bipolaron states in PEDOT prepared by photoelectrochemical polymerization and the effect on charge generation mechanism in the solid-state dye-sensitized solar cell.*J. Phys. Chem. C***2013**, *117*, 22484-22491.

(98) Sabouraud, G.; Sadki, S.; Brodie, N. The mechanisms of pyrrole electropolymerization.*Chem. Soc. Rev.***2000**, *29*, 283-293.

(99) Tan, Y.;Ghandi, K. Kinetics and mechanism of pyrrole chemical polymerization. *Synth.Met.***2013**, *175*, 183-191.

(100) Oh, E. J.; Jang, K. S.; MacDiarmid, A. G. High molecular weight soluble polypyrrole. *Synth. Met.***2001**, *125*, 267-272.

(101) Lendlein, A.; Langer, R. Biodegradable, elastic shape-memory polymers for potential biomedical applications.*Science***2002**, *296*, 1673-1676.

(102) Carswell, A. D.; O'Rear, E. A.; Grady, B. P. Adsorbed surfactants as templates for the synthesis of morphologically controlled polyaniline and polypyrrole nanostructures on flat surfaces: from spheres to wires to flat films. *J. Am. Chem. Soc.***2003**, *125*, 14793-14800.

(103) Zhang, X.; Zhang, J.; Liu, Z.; Robinson, C. Inorganic/organic mesostructure directed synthesis of wire/ribbon-like polypyrrole nanostructures. *Chem. Commun.***2004**, *16*, 1852-1853.

(104) Zhang, X.;Manohar, S. K. Narrow pore-diameter polypyrrole nanotubes.*J. Am. Chem. Soc.***2005**, *127*, 14156-14157.

(105) Zhang, X.; Zhang, J.; Song, W.; Liu, Z. Controllable synthesis of conducting polypyrrole nanostructures.*J. Phys. Chem. B***2006**, *110*, 1158-1165.

(106) Shen, Y.; Wan, M. Soluble conductive polypyrrole synthesized by in situ doping with *β*-naphthalene sulphonic acid. *J. Polym. Sci., Part A: Polym. Chem.* **1997**, *35*, 3689-3695.

(107) Lim, K.; Lee, O.; Song, J.; Kim, G.; Kim, H. Synthesis and properties of soluble polypyrrole doped with dodecylbenzenesulfonate and combined with polymeric additive poly(ethylene glycol). *J. Appl. Polym. Sci.***2005**, *97*, 1170-1175.

(108) Schnoor, T. I.; Smith, G.; Eder, D.; Koziol, K. K.; Tim Burstein, G.; Windle, A. H.; Schulte, K. The production of aligned MWCNT/polypyrrole composite films. *Carbon***2013**, *60*, 229-235.

(109) Chen, L.; Guo, C. X.; Zhang, Q.; Lei, Y.; Xie, J.; Ee, S.; Guai, G.; Song, Q.; Li, C. M. Graphene quantum-dot-doped polypyrrole counter electrode for high-performance dye-sensitized solar cells. *ACS Appl. Mater.Interfaces***2013**, *5*, 2047-2052.

(110) Zhang, Y.; Qi, S.; Duan, G.; Wu, X. Preparation and characterization of high electrically

conductive polypyrrole/nickel plating graphite nanosheets composites. *Synth. Met.***2012**, *162*, 1386-1391.

(111) Nan, A.; Craciunescu, I.; Turcu, R.; Reichert, D.; Liebscher, J. Synthesis and characterization of new functionalised pyrrole copolymers. *J. Optoelectron. Adv. Mater.***2008**, *10*, 2265-2270.

(112) Kim, J.; Sohn, D.; Sung, Y.; Kim, E. -R. Fabrication and characterization of conductive polypyrrole thin film prepared by in situ vapor-phase polymerization. *Synth. Met.***2003**, *132*, 309-313.

(113) Hsu, F. -H.; Wu, T. -M.In situ synthesis and characterization of conductive polypyrrole/graphene composites with improved solubility and conductivity.*Synth. Met.***2012**, *162*, 682-687.

(114) Ozaydin-Ince, G.; Coclite, A. M.; Gleason, K. K. CVD of polymeric thin films: applications in sensors, biotechnology, microelectronics/organic electronics, microfluidics, MEMS, composites and membranes. *Rep. Prog. Phys.***2012**, *75*, 1-40.

(115) Caruso, F.; Caruso, R. A.;Möhwald, H. Nanoengineering of inorganic and hybrid hollow spheres by colloidal templating. *Science***1998**, *282*, 1111-1114.

(116) Chapman, B. N. Thin-film adhesion.*J. Vac. Sci. Technol.***1974**, *11*, 106-113.

(117) Klauk, H.; Gundlach, D. J.; Nichols, J. A.; Jackson, T. N. Pentacene organic thin-film transistors for circuit and display applications. *IEEE Trans. Electron.Devices***1999**, *46*, 1258-1263.

(118) Lee, J. K.; Char, K.; Rhee, H. W.; Ro, H. W.; Yoo, D. Y.; Yoon, D. Y. Synthetic control of molecular weight and microstructure of processiblepoly(methylsilsesquioxane)s for

low-dielectric thin film applications. *Polymer***2001**, *42*, 9085-9089.

(119) Pop-Georgievski, O.; Popelka, T. P. N.; Houska, M.; Chvostov, D.; Proks, V.; Rypacek, F. Poly(ethylene oxide) layers grafted to dopamine-melanin anchoring layer: stability and resistance to protein adsorption. *Biomacromolecules***2011**, *12*, 3232-3242.

(120) Kim, S.; Park, C. B. Dopamine-induced mineralization of calcium carbonate vaterite microspheres. *Langmuir***2010**, *26*, 14730-14736.

(121) Mueller, M.;Keler, B. Deposition from dopamine solutions at Ge substrates: an in-situ ATR-FTIR study. *Langmuir***2011**, *27*, 12499-12505.

(122) Jin, G.; Yu, M. Kim.;Herna, C.; Blaine, Z.; Barbara, S.; Yadong, W.A neuroinductive biomaterial based on dopamine. *Proc. Natl. Acad. Sci. U.S.A.***2006**, *103*, 16681-16686.

(123) Falk, B.; Ludovic, R.; Bernard, S.; Philippe, L.; Jean-Claude, V.; Pierre, S.; Vincent, B. Use of dopamine polymerisation to produce free-standing membranes from (PLL-HA)n exponentially growing multilayer films.*Soft Matter***2008***, 4,* 1621-1624.

(124) Paul, G.; Hoyong, C.; Newell, R. W.; Metin, S.Enhanced reversible adhesion of dopamine methacrylamide-coated elastomer microfibrillarstructures under wet conditions.*Langmuir* **2009***, 25,* 6607-6612.

(125) Harihara, S. S.; Xia, H.; Ann, K. N.; Jean-Rene, E.; Collin; W.; Patrick, M.; Kris, S.; Shaoyi, J.One-step dip coating of zwitterionicsulfobetaine polymers on hydrophobic and hydrophilic surface.*ACS Appl. Mater. Interfaces* **2014***, 6,* 6664−6671.

(126) Beuth, J. L. Cracking of thin bonded films in residual tension. *Int. J. Solids Struct.***1992**, *29*, 1657-1675.

(127) Tsui, T. Y.; McKerrow, A. J.; Vlassak, J. J. Constraint effects on thin film channel cracking

behavior. *J. Mater. Res.***2005**, *20*, 2266-2273.

(128) Tsui, T. Y.; Griffin, J.; Fields, R.; Jacques, J. M.; McKerrow, A. J.; Vlassak, J. J. The effect of elastic modulus on channel crack propagation in organosilicate glass films. *Thin Solid Films***2006**, *515*, 2257-2261.

(129) Dundurs, J. Edged-bonded dissimilar orthogonal elastic wedges under normal ail shear loading. *J. Appl. Mech.***1969**, *36*, 650-652.

(130) Vlassak, J. J. Channel cracking in thin films on substrates of finite thickness. *Int. J. Fract.***2003**, *119*, 299-323.

(131) Chai, H. Channel cracking in inelastic film/substrate systems. *Int. J. Solids Struct.***2011**, *48*, 1092-1100.

(132) Owens, D. K.; Wendt, R. C. Estimation of the surface free energy of polymers.*J. Appl. Polym. Sci***1969**, *13*, 1741-1747.

(133) Pinto, S.; Alves, P.; Matos, C. M.; Santos, A. C.; Rodrigues, L. R.; Teixeira, J. A.; Gil, M. H. Poly(dimethyl siloxane) surface modification by low pressure plasma to improve its characteristics towards biomedical applications. *Colloids Surf.B***2010**, *81*, 20-26.

(134) Hallab, N. J.; Bundy, K. J.; O'Connor, K.; Moses, R. L.; Jacobs, J. J. Evaluation of metallic and polymeric biomaterial surface energy and surface roughness characteristics for directed cell adhesion. *Tissue Eng.***2001**, *7*, 55-71.

(135) Johnson, K. L.; Kendall, K.; Roberts, A. D. Surface energy and the contact of elastic solids.*Proc. R. Soc. London, Ser. A***1971**, *324*, 301-313.

(136) Homola, A. M.; Israelachvili, J. N.; McGuiggan, P. M.; Gee, M. L. Fundamental experimental studies in tribology: the transition from “interfacial” friction of undamaged

molecularly smooth surface to “normal” friction with wear. *Wear***1990**, *136*, 65-83.

(137) Liu, X.; Nanao, H.; Li, T.; Mori, S.A study on the friction properties of PAAc hydrogel under low loads in air and water.*Wear***2004**, *257*, 665-670.

(138) Berman, A.; Drummond, C.; Israelachvili, J. Amontons' law at the molecular level.*Tribol. Lett.***1998**, *4*, 95-101.

(139) Wu-Bavouzet, F.; Cayer-Barrioz, J.; Le Bot, A.; Brochard-Wyart, F.; Buguin, A. Effect of surface pattern on the adhesive friction of elastomers. *Phys. Rev. E***2010**, *82*, 031806.

(140) Li, L.; Lizzul, C.; Kim, H.; Sacolick, I.; Morris, J. E. Electrical, structural and processing properties of electrically conductive adhesives. *IEEE Trans. Compon., Hybrids, Manuf. Technol.***1993**, *16*, 843-851.

(141) Jagt, J. C.; Beris, P. J. M.; Lijten, G. Electrically conductive adhesives: A prospective alternative for SMD soldering? *IEEE Trans. Compon.Packag. Manuf. Technol. Part B: Adv. Packag.***1995**, *18*, 292-298.

(142) Wong, C. P.; Lu, D.; Meyers, L.; VonaJr, S. A.; Tong, Q. K. Fundamental study of electrically conductive adhesives (ECAs). *Polym. Electron.Packag, 1997.Proceedings, IEEE Int. Symp.on*. 80-85.

(143) Lu, D.; Wong, C. P. Novel conductive adhesives for surface mount applications.*Adv.Packag. Mater. 1999. Proceedings. Int. Symp.on*. 288-294.

(144) Lu, D.; Wong, C. P. Development of conductive adhesives for solder replacement.*IEEE Trans. Compon.Packag. Technol.* **2000**, *23*, 620-626.

(145) Jagt, J. C. Reliability of electrically conductive adhesive joints for surface mount applications: a summary of the state of the art. *IEEE Trans. Compon.Packag. Manuf. Technol.*

*Part A***1998**, *21*, 215-225.

(146) Kang, S. K.; Rai, R. S.; Purushothaman, S. Development of high conductivity lead (Pb)-free conducting adhesives. *IEEE Trans. Compon.Packag. Manuf. Technol. Part A***1998**, *21*, 18-22.

(147) Klosterman, D.; Li, L.; Morris, J. E. Materials characterization, conduction development, and curing effects on reliability of isotropically conductive adhesives.*IEEE Trans. Compon.Packag. Manuf. Technol. Part A***1998**, *21*, 23-31.

(148) Lu, D.; Tong, Q. K.; Wong, C. P. A study of lubricants on silver flakes for microelectronics conductive adhesives. *IEEE Trans. Compon.Packag. Technol.***1999**, *22*, 365-371.

(149) Kang, S. K.;Purushothaman, S. Development of conducting adhesive materials for microelectronic applications. *J. Electron. Mater.***1999**, *28*, 1314-1318.

(150) Li, Y.; Moon, K. S.; Wong, C. P. Materials science. Electronics without lead. *Science***2005**, *308*, 1419-1420.

(151) Tan, F.; Qiao, X.; Chen, J.; Wang, H. Effects of coupling agents on the properties of epoxy-based electrically conductive adhesives.*Int. J. Adhes. Adhes.***2006**, *26*, 406-413.

(152) Li, Y.; Wong, C. P. Recent advances of conductive adhesives as a lead-free alternative in electronic packaging: Materials, processing, reliability and applications. *Mater. Sci. Eng., R.***2006**, *51*, 1-35.

(153) Amoli, B. M.; Gumfekar, S.; Hu, A.; Zhou, Y. N.; Zhao, B. Thiocarboxylate functionalization of silver nanoparticles: effect of chain length on the electrical conductivity of nanoparticles and their polymer composites. *J. Mater. Chem.***2012**, *22*, 20048-20056.

(154) Voss, D. Cheap and cheerful circuits.*Nature***2000**, *407*, 442-444.

(155) Faverolle, F.; Attias, A. J.; Bloch, B.; Audebert, P.; Andrieux, C. P. Highly conducting and strongly adhering polypyrrole coating layers deposited on glass substrates by a chemical process. *Chem. Mater.***1998**, *10*, 740-752.

(156) Pyo, M.; Bohn, C. C.; Smela, E.; Reynolds, J. R.; Brennan, A. B. Direct strain measurement of polypyrrole actuators controlled by the polymer/gold interface. *Chem. Mater.***2003**, *15*, 916-922.

(157) Buitrago-Sierra, R.; García-Fernández, M. J.; Pastor-Blas, M. M.; Sepúlveda-Escribano, A. Environmentally friendly reduction of a platinum catalyst precursor supported on polypyrrole. *Green Chem.***2013**, *15*, 1981-1985.

(158) Dreyer, D. R.; Miller, D. J.; Freeman, B. D.; Paul, D. R.; Bielawski, C. W. Perspectives on poly(dopamine). *Chem. Sci.***2013**, *4*, 3796-3802.

(159) Jang, J.; Oh, H. Fabrication of a highly transparent conductive thin film from polypyrrole/poly(methyl methacrylate) core/shell nanospheres. *Adv. Funct. Mater.***2005**, *15*, 494-502.

(160) Yuan, L.; Yao, B.; Hu, B.; Huo, K.; Chen, W.; Zhou, J. Polypyrrole-coated paper for flexible solid-state energy storage. *Energy Environ. Sci.***2013**, *6*, 470-476.

(161) Xu, L. Q.; Jiang, H.; Neoh, K. -G.; Kang, E. -T.; Fu, G. D. Poly(dopamine acrylamide)-co-poly(propargyl acrylamide)-modified titanium surfaces for ‘click’ functionalization. *Polym. Chem.***2012**, *3*, 920-927.

(162) Wise, R. A. Dopamine, learning and motivation.*Nat. Rev.Neurosci.***2004**, *5*, 483-494.

(163) Saiz-Poseu, J.; Sedó, J.; García, B.; Benaiges, C.; Parella, T.; Alibés, R.; Hernando, J.; Busqué, F.; Ruiz-Molina, D. Versatile nanostructured materials via direct reaction of

functionalized catechols. *Adv. Mater.***2013**, *25*, 2066-2070.

(164) Kaneko, D.; Matsumoto, K.; Kinugawa, S.; Tateyama, S.; Kaneko, T. Effects of adhesive characteristics of the catechol group on fiber-reinforced plastics. *Polym. J.***2011**, *43*, 944-947.

(165) Moulay, S. Dopa/catechol-tethered polymers: bioadhesives and biomimetic adhesive materials. *Polym. Rev.***2014**, *54*, 436-513.

(166) Karabulut, E.; Pettersson, T.; Ankerfors, M.; Wågberg, L. Adhesive layer-by-layer films of carboxymethylated cellulose nanofibril-dopamine covalent bioconjugates inspired by marine mussel threads. *ACS Nano***2012**, *6*, 4731-4739.

(167) Liu, A.; Zhao, L.; Bai, H.; Zhao, H.; Xing, X.; Shi, G. Polypyrrole actuator with a bioadhesive surface for accumulating bacteria from physiological media. *ACS Appl. Mater.Interfaces***2009**, *1*, 951-955.

(168) Gomez, N.; Lee, J. Y.; Nickels, J. D.; Schmidt, C. E. Micropatterned polypyrrole: acombination of electrical and topographical characteristics for the stimulation of cells. *Adv.Funct. Mater.***2007**, *17*, 1645-1653.

(169) Hardy, J. G.; Lee, J. Y.; Schmidt, C. E. Biomimetic conducting polymer-based tissue scaffolds. *Curr.Opin.Biotechnol.***2013**, *24*, 1-8.

(170) Pu, N. -W.; Peng, Y. -Y.; Wang, P. -C.; Chen, C. -Y.; Shi, J. -N.; Liu, Y. -M.; Ger, M. -D.; Chang, C. -L. Application of nitrogen-doped graphene nanosheets in electrically conductive adhesives. *Carbon***2014**, *67*, 449-456.

(171) De Vito, S.; Martin, C. R. Toward colloidal dispersions of template-synthesized polypyrrole nanotubules. *Chem. Mater.***1998**, *10*, 1738-1741.

(172) Zhang, J.; Liu, X.; Zhang, L.; Cao, B.; Wu, S. Reactive template synthesis of polypyrrole

nanotubes for fabricating metal/conducting polymer nanocomposites. *Macromol. Rapid Commun.***2013**, *34*, 528-532.

(173) Joo, J.; Lee, J. K.; Baeck, J. S.; Kim, K. H.; Oh, E. J.; Epstein, J. Electrical, magnetic, and structural properties of chemically and electrochemically synthesized polypyrroles. *Synth.Met.***2001**, *117*, 45-51.

(174) Wu, X.; Chabot, V. L.; Kim, B. K.; Yu, A.; Berry, R. M.; Tam, K. C. Cost-effective and scalable chemical synthesis of conductive cellulose nanocrystals for high-performance supercapacitors. *Electrochim.Acta***2014**, *138*, 139-147.

(175) Tauc, J. Optical properties and electronic structure of amorphous Ge and Si.*Mater. Res. Bull.***1968**, *3*, 37-46.

(176) Buchholz, D. B.; Liu, J.; Marks, T. J.; Zhang, M.; Chang, R. P. Control and characterization of the structural, electrical, and optical properties of amorphous zinc-indium-tin oxide thin films. *ACS Appl. Mater.Interfaces***2009**, *1*, 2147-2153.

(177) Khan, Z.; Khannam, M.; Vinothkumar, N.; De, M.; Qureshi, M. Hierarchical 3D NiO–CdSheteroarchitecture for efficient visible light photocatalytic hydrogen generation. *J.Mater. Chem.***2012**, *22*, 12090-12095.

(178) Borrero-López, O.; Hoffman, M.; Bendavid, A.; Martin, P. J.The use of the scratch test to measure the fracture strength of brittle thin films.*Thin Solid Films***2010**, *518*, 4911-4917.

(179) Xiong, S.; Wang, Y.; Yu, J.; Chen, L.; Zhu, J.; Hu, Z. Polydopamine particles for next-generation multifunctional biocomposites. *J. Mater. Chem.A***2014**, *2*, 7578-7587.

(180) Gumfekar, S. P.; Wang, W.; Zhao, B. In situ doped polyaniline nanotubes for applications in flexible conductive coatings. *Macromol. Mater. Eng.***2014**, *8*, 966-976.

(181) Arico, A. S.; Bruce, P.; Scrosati, B.; Tarascon, J. M.; Van Schalkwijk, W. Nanostructured materials for advanced energy conversion and storage devices. *Nat. Mater.***2005**, *4*, 366-377.

(182) Martin, C. R.; Baker, L. A. Materials science. Expanding the molecular electronics toolbox. *Science***2005**, *309*, 67-68.

(183) Menard, E.; Meitl, M. A.; Sun, Y.; Park, J. U.; Shir, D. J.; Nam, Y. S.; Jeon, S.; Rogers, J. A. Micro- and nanopatterning techniques for organic electronic and optoelectronic systems. *Chem. Rev.***2007**, *107*, 1117-1160.

(184) Akinwande, D.; Petrone, N.; Hone, J. Two-dimensional flexible nanoelectronics.*Nat.Commun***2014**, *5*, 5678-5682.

(185) Torrisi, F.; Hasan, T.; Wu, W.; Sun, Z.; Lombardo, A.; Kulmala, T. S.; Hsieh, G. W.; Jung, S.; Bonaccorso, F.; Paul, P. J.; Chu, D.; Ferrari, A. C. Inkjet-printed graphene electronics. *ACS Nano***2012**, *6*, 2992-3006.

(186) De Volder, M. F.; Tawfick, S. H.; Baughman, R. H.; Hart, A. J. Carbon nanotubes: present and future commercial applications. *Science***2013**, *339*, 535-539.

(187) Dreyer, D. R.; Park, S.; Bielawski, C. W.; Ruoff, R. S.The chemistry of graphene oxide.*Chem. Soc. Rev.***2010**, *39*, 228-240.

(188) Zhu, Y.; Murali, S.; Cai, W.; Li, X.; Suk, J. W.; Potts, J. R.; Ruoff, R. S. Graphene and graphene oxide: synthesis, properties, and applications. *Adv. Mater.***2010**, *22*, 3906-3924.

(189) Dai, L.; Chang, D. W.; Baek, J. B.; Lu, W. Carbon nanomaterials for advanced energy conversion and storage. *Small***2012**, *8*, 1130-1166.

(190) Rojas, J. P.; Torres Sevilla, G. A.; Ghoneim, M. T.; Inayat, S. B.; Ahmed, S. M.; Hussain, A. M.; Hussain, M. M. Transformational silicon electronics. *ACS Nano***2014**, *8*, 1468-1474.

(191) Rogers, J. A.; Someya, T.; Huang, Y. Materials and mechanics for stretchable electronics.*Science***2010**, *327*, 1603-1607.

(192) Becerril, H. A.; Mao, J.; Liu, Z.; Stoltenberg, R. M.; Bao, Z.; Chen, Y. Evaluation of solution-processed reduced graphene oxide films as transparent conductors. *ACS Nano***2008**, *2*, 463-470.

(193) Hwang, S. H.; Kang, D.; Ruoff, R. S.; Shin, H. S.; Park, Y. B. Poly(vinyl alcohol) reinforced and toughened with poly(dopamine)-treated graphene oxide, and its use for humidity sensing. *ACS Nano***2014**, *8*, 6739-6747.

(194) Si, Y.;Samulski, E. T. Synthesis of water soluble graphene. *Nano Lett.***2008**, *8*, 1679-1682.

(195) Long, Y. -Z.; Li, M. -M.; Gu, C.; Wan, M.; Duvail, J. -L.; Liu, Z.; Fan, Z. Recent advances in synthesis, physical properties and applications of conducting polymer nanotubes and nanofibers. *Prog. Polym.Sci.***2011**, *36*, 1415-1442.

(196) Zhang, X.;Manohar, S. K. Bulk synthesis of polypyrrole nanofibers by a seeding approach.*J. Am. Chem. Soc.***2004**, *126*, 12714-12715.

(197) Dubal, D. P.; Lee, S. H.; Kim, J. G.; Kim, W. B.; Lokhande, C. D. Porous polypyrrole clusters prepared by electropolymerization for a high performance supercapacitor. *J. Mater. Chem.***2012**, *22*, 3044-3052.

(198) Reung-U-Rai, A.; Prom-Jun, A.; Prissanaroon-Ouajai, W.; Ouajai, S. Synthesis of highly conductive polypyrrole nanoparticles via microemulsion polymerization.*J. Met. Mater. Miner.***2008**, *18*, 27-31.

(199) Rivers, T. J.; Hudson, T. W.; Schmidt, C. E. Synthesis of a novel, biodegradable electrically conducting polymer for biomedical applications. *Adv. Funct. Mater.***2002**, *12*, 33-37.

(200) Wang, D.; Ye, Q.; Yu, B.; Zhou, F. Towards chemically bonded p–n heterojunctions through surface initiated electrodeposition of p-type conducting polymer inside TiO_2 nanotubes. *J. Mater. Chem.***2010**, *20*, 6910-6916.

(201) LaVoie, M. J.; Ostaszewski, B. L.; Weihofen, A.; Schlossmacher, M. G.; Selkoe, D. J. Dopamine covalently modifies and functionally inactivates parkin. *Nat. Med.***2005**, *11*, 1214-1221.

(202) Wu, X.; Tang, J.; Duan, Y.; Yu, A.; Berry, R. M.; Tam, K. C. Conductive cellulose nanocrystals with high cycling stability for supercapacitor applications. *J. Mater. Chem.A***2014**, *2*, 19268-19274.

(203) Krogsgaard, M.; Behrens, M. A.; Pedersen, J. S.; and Birkedal, H. Self-healing mussel-inspired multi-pH-responsive hydrogels.*Biomacromolecules***2013**, *14*, 297-301.

(204) Carrasco, P. M.; Grande, H. J.; Cortazar, M.; Alberdi, J. M.; Areizaga, J.; Pomposo, J. A. Structure–conductivity relationships in chemical polypyrroles of low, medium and high conductivity. *Synth. Met.***2006**, *156*, 420-425.

(205) Fan, L. -Z.; Maier, J. High-performance polypyrrole electrode materials for redox supercapacitors.*Electrochem. Commun.***2006**, *8*, 937-940.

(206) Zang, J.; Li, X. In situ synthesis of ultrafine *β*-MnO_2/polypyrrole nanorod composites for high-performance supercapacitors.*J. Mater. Chem.***2011**, *21*, 10965-10969.

(207) Zhang, B.; Xu, Y.; Zheng, Y.; Dai, L.; Zhang, M.; Yang, J.; Chen, Y.; Chen, X.; Zhou, J. A facile synthesis of polypyrrole/carbon nanotube composites with ultrathin, uniform and thickness-tunable polypyrrole shells.*Nanoscale Res.Lett.***2011**, *6*, 431-440.

(208) Davies, A.; Audette, P.; Farrow, B.; Hassan, F.; Chen, Z.; Choi, J. -Y.; Yu, A.

Graphene-based flexible supercapacitors: pulse-electropolymerization of polypyrrole on free-standing graphene films. *J. Phys. Chem. C***2011**, *115*, 17612-17620.

(209) Eitan, A.; Fisher, F. T.; Andrews, R.; Brinson, L. C.; Schadler, L. S. Reinforcement mechanisms in MWCNT-filled polycarbonate. *Compos. Sci. Technol.***2006**, *66*, 1162-1173.

(210) Rafiee, M. A.; Rafiee, J.; Wang, Z.; Song, H.; Yu, Z. Z.; Koratkar, N. Enhanced mechanical properties of nanocomposites at low graphene content. *ACS Nano***2009**, *3*, 3884-3890.

(211) Zeng, K.; Breder, K.; Rowcliffe, D. J.; Herrström, C. Elastic modulus determined by Hertzian indentation. *J. Mater.Sci.***1992**, *27*, 3789-3792.

(212) Li, N.; Huang, Y.; Du, F.; He, X.; Lin, X.; Gao, H.; Ma, Y.; Li, F.; Chen, Y.; Eklund, P. C. Electromagnetic interference (EMI) shielding of single-walled carbon nanotube epoxy composites. *Nano Lett.***2006**, *6*, 1141-1145.

(213) Geetha, S.; Satheesh Kumar, K. K.; Rao, C. R. K.; Vijayan, M.; Trivedi, D. C. EMI shielding: methods and materials-a review. *J. Appl. Polym.Sci.***2009**, *112*, 2073-2086.

(214) Varshney, S.; Ohlan, A.; Jain, V. K.; Dutta, V. P.; Dhawan, S. K. In situ synthesis of polypyrrole-γ-Fe_2O_3-fly ash nanocomposites for protection against EMI pollution.*Ind. Eng. Chem. Res.***2014**, *53*, 14282-14290.